AD NUMBER

ADB023408

LIMITATION CHANGES

TO:

Approved for public release; distribution is unlimited.

FROM:

Distribution authorized to U.S. Gov't. agencies only; Test and Evaluation; 06 DEC 1977. Other requests shall be referred to Rome Air Development Center, Attn: ESM, Hanscom AFB, MA 01731.

AUTHORITY

RADC ltr, 11 Mar 1982

AD B023408

AUTHORITY: RADC USAF
ltr, 11, MAR 82

DISCLAIMER NOTICE

THIS DOCUMENT IS THE BEST QUALITY AVAILABLE.

COPY FURNISHED CONTAINED A SIGNIFICANT NUMBER OF PAGES WHICH DO NOT REPRODUCE LEGIBLY.

RADC-TR-77-286
Interim Technical Report
August 1977

LASER WINDOW MATERIALS AND OPTICAL COATING SCIENCE

Hughes Research Laboratories

Sponsored By
DEFENSE ADVANCED RESEARCH PROJECTS AGENCY (DOD)
ARPA Order No. 2415

Monitored By
ROME AIR DEVELOPMENT CENTER
Air Force Systems Command
Griffiss Air Force Base, NY 13441

ARPA Order No. 2415

Program Code No. 1E50

Contractor:
Hughes Research Laboratories

Effective Date of Contract:
19 September 1976

Contract No. F19628-76-C-0309

Principal Investigator: M. Braunstein
Phone No. (213) 456-6411

AFSC Project Scientist: H. Posen
Phone No. (617) 861-3532

Contract Expiration Date:
19 December 1977

The views and conclusions contained in this document are those of the authors and should not be interpreted as necessarily representing the official policies, either expressed or implied, of the Defense Advanced Research Projects Agency or the U.S. Government.

Distribution limited to U.S. Government agencies only; Test and Evaluation of Military Equipment August 1977. Other requests for this document must be referred to RADC/ETSR, Hanscom AFB, MA 01731.

This report has been reviewed and is approved for publication.

APPROVED: Harold Posen
HAROLD POSEN
Contract Monitor

APPROVED: Robert M. Barrett
ROBERT M. BARRETT
Director
Solid State Sciences Division

John P. Kuss

UNCLASSIFIED

SECURITY CLASSIFICATION OF THIS PAGE (When Data Entered)

REPORT DOCUMENTATION PAGE	READ INSTRUCTIONS BEFORE COMPLETING FORM
1. REPORT NUMBER: RADC-TR-77-286	2. GOVT ACCESSION NO. / 3. RECIPIENT'S CATALOG NUMBER
4. TITLE (and Subtitle): LASER WINDOW MATERIALS AND OPTICAL COATING SCIENCE.	5. TYPE OF REPORT & PERIOD COVERED: Interim Tech. Report 19 Sept 1976-19 Mar 1977
	6. PERFORMING ORG. REPORT NUMBER: Semiannual Tech No. 1
7. AUTHOR(s): M. Braunstein, I.J. D'Haenens, S.D. Allen, A.A. Harrington, M.E. Pedinoff, J.E. Rudisill, R.R. Turk, R.C. Pastor, D.E. Zuccaro	8. CONTRACT OR GRANT NUMBER(s): F19628-76-C-0309
9. PERFORMING ORGANIZATION NAME AND ADDRESS: Hughes Research Laboratories, 3011 Malibu Canyon Road, Malibu, California 90265	10. PROGRAM ELEMENT, PROJECT, TASK AREA & WORK UNIT NUMBERS: ARPA Order No. 2415, Program Code No. 1E50
11. CONTROLLING OFFICE NAME AND ADDRESS: Defense Advanced Projects Agency, 1400 Wilson Blvd., Arlington, VA 22209	12. REPORT DATE: August 1977
	13. NUMBER OF PAGES: 149
14. MONITORING AGENCY NAME & ADDRESS (if different from Controlling Office): Deputy for Electronic Technology (RADC/ESM), Hanscom AFB, MA 01731, Contract Monitor: Harold Posen	15. SECURITY CLASS (of this report): Unclassified
	15a. DECLASSIFICATION DOWNGRADING SCHEDULE

16. DISTRIBUTION STATEMENT (of this Report) — 6 DEC 1977

Distribution limited to U.S. Government Agencies only; test and evaluation. Other requests for this document must be referred to RADC/ESM, Hanscom AFB, MA 01731.

17. DISTRIBUTION STATEMENT (of the abstract entered in Block 20, if different from Report)

Semiannual technical rept. no. 1, 19 Sep 76 - 19 Mar 77, 143 p.

18. SUPPLEMENTARY NOTES

Sponsored by Defense Advanced Research Projects Agency, DoD, ARPA Order No. 2415.

19. KEY WORDS (Continue on reverse side if necessary and identify by block number)

Infrared laser windows, surface finishing, thin films, antireflection-coatings, surface characterization, optical evaluations and laser calorimetry at 10.6 μm, 5.3 μm, 3.8 μm, and 2.8 μm, infrared ellipsometry, modulated light ellipsometer, potassium chloride.

20. ABSTRACT (Continue on reverse side if necessary and identify by block number)

We report on the objectives and the progress achieved in a program to establish a definitive correlation between preparation procedures and optical performance of antireflective coated windows for high-power infrared lasers: HF (2.7 μm), DF (3.8 μm), CO (5.3 μm), and CO_2 (9.27 and 10.6 μm). The window materials that are under investigation include selected alkali halides and alkaline earth fluorides, in both

DD FORM 1 JAN 73 1473 EDITION OF 1 NOV 65 IS OBSOLETE

UNCLASSIFIED

SECURITY CLASSIFICATION OF THIS PAGE (When Data Entered)

172600 LB

single and polycrystalline form and of alloyed and unalloyed composition. The reactive atmosphere processing (RAP) of metal halide crystals in the presence of hydrogen halide gas does not efficiently exclude oxide and hydroxide anions; an additional RAP agent being needed to overcome the hydrolytic action of H_2C which outgasses during the metal halide crystal growth process. CF_4, which has been used as the second RAP agent to HF for growth of the alkaline earth fluorides, has been found to be highly corrosive to carbon at the high processing temperatures and long soak times characteristic of production scale up for fluoride windows. (The insulation, heating elements, and crucible of the growth apparatus are all made of carbon.) BF_3, which is four times less corrosive than CF_4 at 1500°C and 10 Torr pressure, is presently the favored alternative RAP agent. Comparison studies of optical coatings prepared under conventional high vacuum (HV) and under ultra-high vacuum (UHV) conditions were contained. Antireflection coated KCl windows produced under UHV conditions continued to have 1/2 to 1/5 lower optical absorption at 10.6 μm than did those produced under HV conditions. Excellent low absorption (0.02% per surface) results were achieved for As_2Se_3/KCl/As_2Se_3 coatings on polycrystalline KCl. Single layer coatings of As_2Se_3 were deposited on KCl, CaF_2, and SrF_2 to evaluate the deposition and material parameters for coatings for use at 3.5 μm. Laser calorimetric measurements for windows and coatings are now a routine evaluation procedure at 2.8 μm, 3.8 μm, 5.3 μm, 4.27 4.27 μm, and 10.6 μm wavelengths. The IR Ellipsometer is operating at 10.6 μm; it is used to measure the refractive index of laser window materials and films, the thickness of films, and the effect of strain on the refractive index of IR materials. The stability of the ellipsometer system has been improved during this report period from ± 4% per hour to ±1% per hour by installing a dual-channel 0.9 μm modulator drive monitoring system. This has improved the system significantly, but not to our ultimate goal of 0.1%.

TABLE OF CONTENTS

LIST OF ILLUSTRATIONS

SECTION 1

INTRODUCTION AND SUMMARY

This is the first semiannual technical report of the "Laser Window Materials and Optical Coating Science" program (Contract F19628-76-C-0309), which is being conducted by the Hughes Research Laboratories (HRL) under the technical monitorship of Rome Air Development Center (RADC/ESM). The ultimate objective of this program is to establish a correlation between preparation procedures and the optical performance of anti-reflective (AR) coated windows for high-powered infrared lasers: HF (2.7 μm), DF (3.8 μm), CO (5.3 μm), and CO_2 (9.27 and 10.6 μm). The window materials to be investigated include selected alkali halides and alkaline earth fluorides. These window materials will be both single and polycrystalline and of alloyed and unalloyed composition.

Under preparation procedures, we have included specification of window substrate growth (RAP or conventional) and treatment (forging, polishing) parameters and, in addition, the vacuum (uv or conventional) conditions under which a variety of AR coatings (film material and coating designs) have been applied. The optical performance parameters are the resultant transmission and absorption of the AR-coated high-power infrared laser windows.

The tasks under this program are organized into seven broad categories. First, the application of reactive atmosphere processing (RAP) chemistry techniques to the growth, polishing, grain growth stabilization, and AR coating passivation of poly- and single-crystal KCl and of alkaline earth fluorides. Second, the application of press forging to RAP materials to enhance yield strength, and a study of the grain growth kinetics in such press forged materials. Third, a study of chemical-mechanical surface finishing techniques for the preparation of laser window materials. Fourth, a characterization of substrate and coating surface finishing using (1) scanning electron microscopy and X-ray diffraction, and (2) structural and chemical analysis

using low-energy electron diffraction (LEED), Auger electron spectroscopy (AES), and microprobe techniques. Fifth, a comparison of AR coatings prepared under ultrahigh vacuum ($<10^{-9}$ Torr) and conventional (10^{-6} to 10^{-9} Torr) conditions and by ion beam sputtering techniques. Sixth, an optical evaluation of the AR-coated windows using infrared spectrophotometry, absorption calorimetry, ellipsometry, and scattering measurements. And seventh, a selection of substrate materials and AR-coated window specimens for study of laser damage mechanisms (this will be performed by Dr. M. Bass of the USC Center for Laser Studies).

Coordination is being maintained between this research program and (1) the programs conducted by Dr. M. Bass at the University of Southern California on laser damage to windows, (2) Dr. M. Shen's program at the University of California on organic polymer coatings, and (3) Dr. H. Bennett's program at the Naval Weapons Center, China Lake, California.

The remainder of this section is a summary of the progress reported on in the body of the report.

A. REACTIVE ATMOSPHERE PROCESSING AND PRESS FORGING OF WINDOW MATERIALS

We used RAP to produce alloyed KCl crystals with 1.8 at. % Rb^+ and 20 atoms per million cation (apm) Sr^{+2}. Press forging these crystals at 300°C to 86% reduction produced an increase in yield strength from 2900 to 4100 psi.

The growth of metal halide crystals in the presence of hydrogen halide gas does not efficiently exclude oxide and hydroxide anions; an additional RAP agent is needed to overcome the hydrolytic action caused by the H_2O which outgasses during the metal halide crystal growth process.

For growing the alkaline earth fluorides, CF_4 serves as the second RAP agent to HF. We have found that, at the high processing temperatures and long soak times characteristic of production scale up

for fluor[illegible] windows, CF_4 is highly corrosive to carbon (the insulation, heating e[illegible]nts, and crucible of the growth apparatus are all made of carbon). BF_3, which is four times less corrosive than CF_4 at 1500°C and 10 Torr pressure, is the presently favored alternative RAP agent.

B. SURFACE FINISHING

The previously reported polishing recipe for producing low surface absorption at 10.6 μm in alloyed KCl (1.8 at. % Rb) by using black rouge (Fe_3O_4) in glycol on a pitch lap has been modified. It now includes an HCl etch to remove grinding damage, with a final surface wipe on isopropanol-moistened Texwipe Absorbond paper. This modification was found necessary to minimize surface scratches and attendant 10.6 μm surface absorption.

C. WINDOW COATINGS

Comparison studies of optical coatings prepared under conventional high vacuum (HV) and under ultrahigh-vacuum (UHV) conditions were continued to verify our previous observations that significantly lower absorption can be achieved in UHV-deposited films. In addition to the three-layer AR coatings, single-layer coatings were prepared for material evaluation. Optical coatings were prepared under UHV conditions for refractive index evaluation using our 10.6 μm modulated light ellipsometer and for 10.6 μm pulsed laser damage studies by Dr. M. Bass at USC.

AR-coated KCl windows produced under UHV conditions continued to have 1/2 to 1/5 lower optical absorption at 10.6 μm than did those produced under HV conditions. Excellent low absorption (0.02% per surface) results were achieved for an $As_2Se_3/KCl/As_2Se_3$ coating on polycrystalline KCl.

UHV deposition of single layer As_2S_3 films using Atomergic Chemical Corporation (ACC) material was accompanied by the evolution of a large amount of water vapor, a significant amount of petroleum ether, and a trace of acetic acid. The As_2S_3 was subsequently

reacted with CS_2 for two hours to remove the impurities and then deposited in single-layer samples. These films exhibited a 5% decrease in transmission at 9 μm and a threefold increase in the 9.27 μm optical absorption band. In contrast, the deposition of single-layer films of ACC's As_2Se_3 was not accompanied by any significant outgassing. The first film had a 4% dip in transmission at 9 μm, while the remaining films did not show any absorption band.

Absorption bands in As_2Se_3 glasses correlated to oxide impurities have been reported previously. We prepared three batches of As_2Se_3 for starting material by different techniques. If H_2O vapor was present and oxidized arsenic was used, strong 9.5 μm and 9 μm absorption bands were observed in the glass. When oxide-free arsenic was used and water vapor excluded by loading under dry N_2, the material was free of these absorption bands. Using the latter as starting material, single-layer coatings of As_2Se_3 have been deposited on KCl, CaF_2, and SrF_2 to evaluate the deposition and the material parameters for 3.8 μm coatings.

D. OPTICAL EVALUATION

1. Calorimetric Absorption Measurements

Crystals of NdF_3 and ThF_4 material grown under another contract (F33615-76-C-5449) were measured calorimetrically to have absorption coefficients of 2.9 and 1.2 cm^{-1}, respectively. Absorption in RAP cast NaF was measured to be 0.62 and 0.11 cm^{-1} at 10.6 and 9.27 μm, respectively. RAP cast LiF gave 0.14 cm^{-1} absorption at 5.1 μm, measured spectrophotometrically. For comparison, the AFCRL Compendium on IR Laser Window Materials gives $\beta = 0.77\ cm^{-1}$ at 10.5 μm for NaF.

RAP grown NaCl was evaluated at three different wavelengths: 10.6, 9.27, and 5.3 μm. The results on four samples of approximately 4 cm length were β (10.6 μm) = 0.0010 ± 0.0001, β (9.27 μm) = 0.0003 ± 0.0001, and β (5.3 μm) = 0.00004 ± 0.00002 cm^{-1}. Additional measurements will be made at 5.3, 3.8, and 2.8 μm on these four samples.

Three KCl bars grown in different RAP atmospheres were measured at 10.6 μm as a check on the growth conditions. Bulk absorption in the samples grown in N_2/CCl_4 and $He/CO_2/CCl_4$ was less than 10^{-4} cm^{-1} ($\beta = 8 \times 10^{-5}$ and 6×10^{-5} cm^{-1}, respectively). The samples grown in He/CCl_4 had a bulk absorption coefficient of 1.0×10^{-4} cm^{-1}. These measurements imply that the cost of RAP processing could be lowered considerably, since N_2 and perhaps even dry air could be used instead of He for the carrier medium.

Several comparison checks were made on the CO calorimeter during this report period. SrF_2 samples supplied and measured by UDRI (material supplied by Raytheon) were measured at HRL. Initial results on the samples as received were approximately a factor of two higher than the UDRI values. Careful cleaning of the substrates brought the HRL measurements into agreement with the UDRI results. HRL also participated in the CO Round Robin sponsored by UDRI. The results were presented and discussed at the LWTVP meeting in Annapolis, 20 April 1977. An apparent increase in measured absorption with time was observed in the CaF_2 samples. Another series of measurements on the substrates is planned by UDRI, and the complete results will be discussed in a subsequent report.

The DF/HF chemical laser was placed in operation for calorimetric studies of the absorption coefficient of windows and coatings at 3.8 and 2.7 μm. An air calorimeter was used initially while a specially designed vacuum calorimeter head was being constructed. The materials studies at the chemical laser wavelengths included CaF_2 (both single and polycrystalline), SrF_2, KCl (polycrystalline, Rb doped), ThF_4, and NdF_3. The absorption coefficients (β's) measured for the alkaline earth fluorides ranged from 3 to 30×10^{-4} cm^{-1} at 3.8 μm, with most being near 6×10^{-4} cm^{-1}; at 2.7 μm the situation was decidedly worse as most materials exhibited β's near 2.5×10^{-3} cm^{-1}. KCl showed a similar range of absorption values. Single-layer coatings of fluorides, oxides, and semiconductors were deposited on CaF_2 and measured at both DF and HF wavelengths. The fluoride and As_2S_3 or As_2Se_3 films had average film absorptions of about 0.1%/surface while the oxides had about 10 times this amount.

2. IR Ellipsometry Measurements

The objective of this phase of the program is to measure the refractive index of laser window materials and films, the thickness of films, and the effect of strain on the refractive index of these materials.

The stability of the ellipsometer system has been improved during this report period. The stability of the modulator system was improved from ±4% per hour to ±1% per hour by installing a dual channel 0.9 μm modulator drive monitoring system. One of these channels, modified by the addition of a Mica quarter-wave plate, generates a large amplitude reference signal at the ultrasonic drive frequency; the other channel generates a modulation signal at twice the ultrasonic drive frequency, which goes to zero at the appropriate drive amplitude. These signals are processed in a phase-sensitive detector to yield the modulator drive servo error signal. This has improved the system significantly, but not to our ultimate goal of 0.1%. This goal should be attained when the modulator medium is changed from polycrystalline ZnSe to single-crystal Ge. Although this modification is being made, a low priority has been given it because of the need to take ellipsometric data on currently available samples.

Data was taken on a single crystal of ThF_4. The measured index was 1.302 ± 1%. This result is preliminary because it is only a single sample measurement and surface finish effects can alter the results. Data was also taken on an As_2Se_3 film deposited on KCl. The selection of the data runs showing the smallest spread leads to the results

$$\overline{N} = 2.84 \pm 2.5\%$$
$$\overline{T} = 3.25\ \mu m \pm 0.5\% \ .$$

These results will be checked against measurements to be made in the next report period on films of different thickness. N and T were also measured independently in a spectrometer and a Tolansky interferometer with the following results:

$$N = 2.8 \pm 5\%$$

$$T = 3.313 \pm 5\% \quad .$$

The ellipsometer program, which simultaneously extracts N and T from the data, assumes that K is zero or small. If K values are also important, it will be necessary to obtain thickness values to better than 1% by some other technique (e.g., Tolansky) and to process the data in a program that yields N and K when given T and the delta, psi data.

The N, T ellipsometer program is being revised to facilitate processing an entire measurement run instead of just single data entries. The revision is proving non-trivial, but it is essential to the facilitation of data handling.

SECTION 2

TECHNICAL DISCUSSION – PROGRAM TASKS

In this section, we discuss in order the technical approach being pursued and the progress to date in the program task areas.

A. RAP CHEMISTRY AND PRESS FORGING OF WINDOW MATERIALS

Window materials for high-energy infrared lasers must have sufficient strength to resist (1) deformation caused by differential laser gas pressures and (2) thermal stresses resulting from the passage of the laser beam. Distortion of the flat window faces causes lensing and resultant beam dispersion.

KCl windows exhibit low absorption at the 10.6 μm CO_2 laser wavelength. By forging single-crystal KCl into a fine-grained structure the yield strength is raised almost an order of magnitude, from 300 psi to 2800 psi. This structure is unstable in the presence of water vapor, undergoing exaggerated grain growth with time, so that grains of 1 cm and larger are formed.[1] This process reduces the forged strength to values approaching that of the original single crystal.

Grain growth, which occurs at relative humidities above 40% (Ref. 1), is prevented or greatly reduced by: (1) decreasing the forging reduction to below 60%, (2) maintaining a dry environment, (3) using RAP-grown original crystals, and (4) adding alloy or dopant ions such as Rb^{+} or Sr^{++} during growth of the original crystals. At Hughes, RAP crystal growth and dopant addition are used to give a material most resistant to grain growth, even when forged to maximum structural uniformity by high reduction.

Rubidium-doped RAP KCl boules were forged at 1% min^{-1} to about 70% reduction in height (Table 1). Since doped boules tend to crack during room-temperature forging, the samples were forged at 300°C. Grain size averaged 10 μm, with a spread from 3 to 30 μm.

Table 1. Forging RAP-Grown KCl[a]

Sample	Dopant	Reduction, %
B156-8	1.75% Rb^+	60
B157-4	1.75% Rb^+	72
B164-2	1.75% Rb^+	67
B164-5A	1.75% Rb^+	70
B167-2	1.75% Rb^+	67
B167-4	1.75% Rb^+	69
B167-6	1.75% Rb^+	68
B169-5	1.75% Rb^+	77
B169-6	1.75% Rb^+	70
B171	1.8% Rb^+, 550 apm Sr^{++}	71
B174-2	1.8% Rb^+, 20 apm Sr^{++}	51
B174-5	1.8% Rb^+, 20 apm Sr^{++}	60
B174-6	1.8% Rb^+, 20 apm Sr^{++}	68
B174-8	1.8% Rb^+, 20 apm Sr^{++}	86

[a]All forging done at 300°C.

No exaggerated grain growth was found on examination of forged specimens. Nine of the forged specimens were doped with Rb alone, while one had an additional 550 apm Sr and four had an additional 20 apm Sr. Figure 1 shows sectioning and forged pieces from a typical boule of RAP-doped KCl.

KCl doped with both Rb^{++} and Sr^{++} was forged at reductions increasing from 51 to 86%, and flexure strength was measured versus reduction (Table 2). Strength appeared to increase with deformation, unlike undoped KCl, which remains constant at about 2800 psi (Ref. 1). Grain size decreased with increasing deformation, confirming the petch relationship of strength versus grain size. The sample that was forged to 86% reduction was stronger, and showed a smaller spread in values (five pieces were tested from each forging). This indicates that high deformation produces a more uniform structure.

Analysis of dopant in boules after crystal growth is shown in Table 3. In most boules, the amount found on analysis seems close (within the limits of analytical accuracy) to the amount added. But the analytical figure given is a summation of values along each boule; it does not reflect the variation in amounts of dopant throughout the crystal.

Differences of over 60% were found along the length or from center to circumference of the crystal. However, scatter of 50% is reported by our vendor, so these differences could well be due to variables in analytical procedure, rather than in the boule. No consistent trend toward dopant segregation was seen, either between the axis of the boule and its circumference or along the boule axis from cone to heel. Typical values are shown for boule B156 in Figure 2.

We introduced RAP conditions during forging by immersing the deforming boule under Cereclor 42P, a chlorinated paraffin. This viscous, honey-colored liquid is 41% chlorine by weight, and loses 0.5% chlorine every 4 hr at 175°C. Our runs, at 200°C, caused formation of chlorine throughout the press chamber. Undoped KCl was used for this experiment to ascertain the full effect of RAP

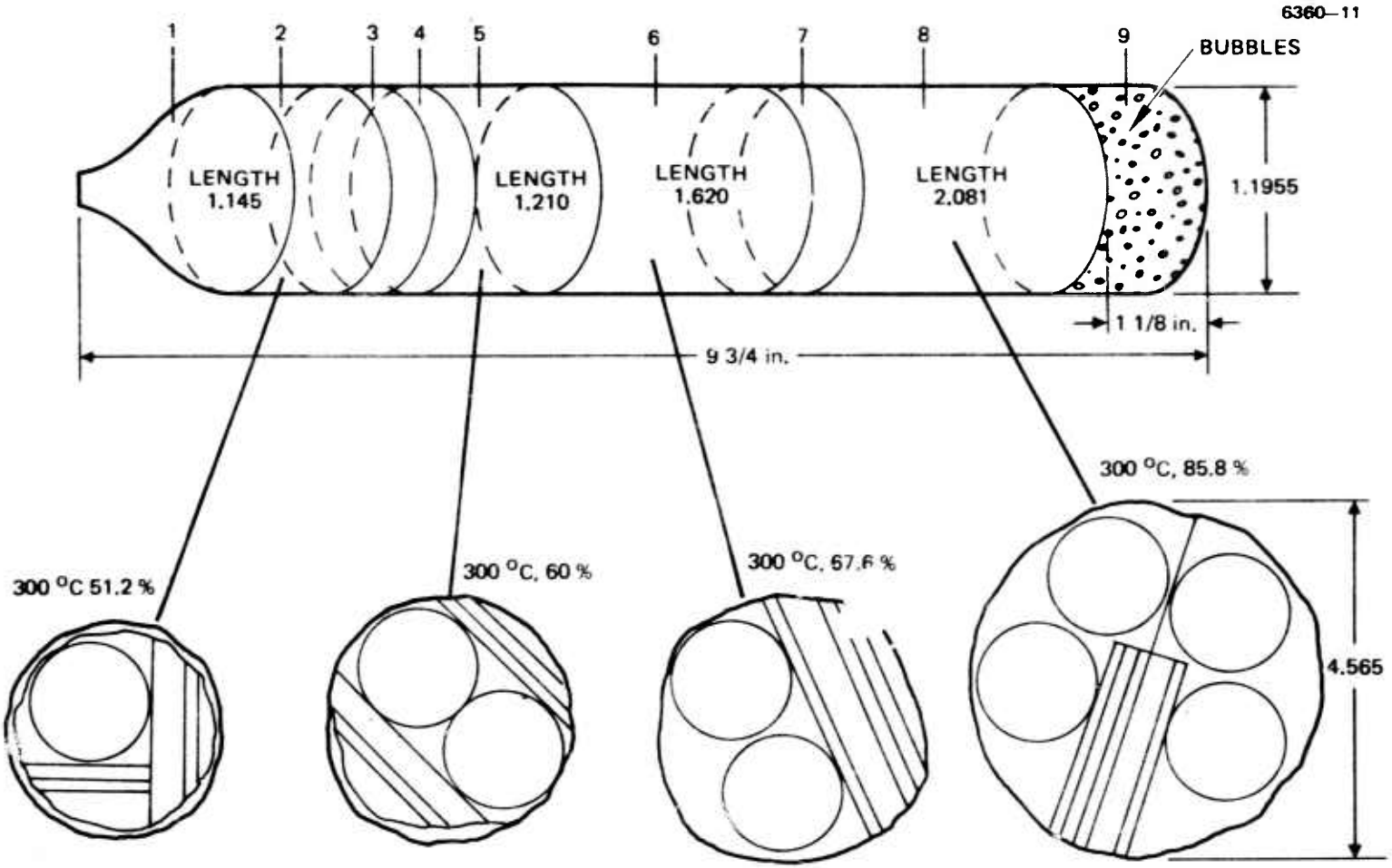

Figure 1. Sectioning and forged pieces from a typical boule of RAP-doped KCl.

Table 2. Strength versus Reduction, RAP KCl 1.8% Rb^{+}, 20 apm Sr^{++}[a]

Sample	Reduction, %	Yield Strength, psi	Average Grain Size, μm
B174-2	51	2862 ± 446	17
B174-5	60	3366 ± 414	14
B174-6	68	3316 ± 515	12
B174-8	86	4116 ± 249	10

[a] All forging done at 300°C.

Table 3. Analyses of Dopant in RAP-Grown KCl Boules

Boule	Mol % RbCl	
	Added	Analyzed
B156	1.73	1.75 ± 0.58 (11 tests)
B157	1.75	1.96 ± 0.97 (5 tests)
B158	1.75	1.90 ± 0.45 (5 tests)
B159	1.75	2.22 ± 0.08 (2 tests)
B164	1.75	1.64 ± 0.22 (2 tests)
B167	1.75	1.90 ± 0.66 (4 tests)
B169	1.80	1.11 ± 0.26 (4 tests)
B174	1.80[a]	1.15 ± 0.39 (4 tests)

[a] Boule B174 also was doped with 20 apm Sr^{++}, but this was too small an amount to analyze.

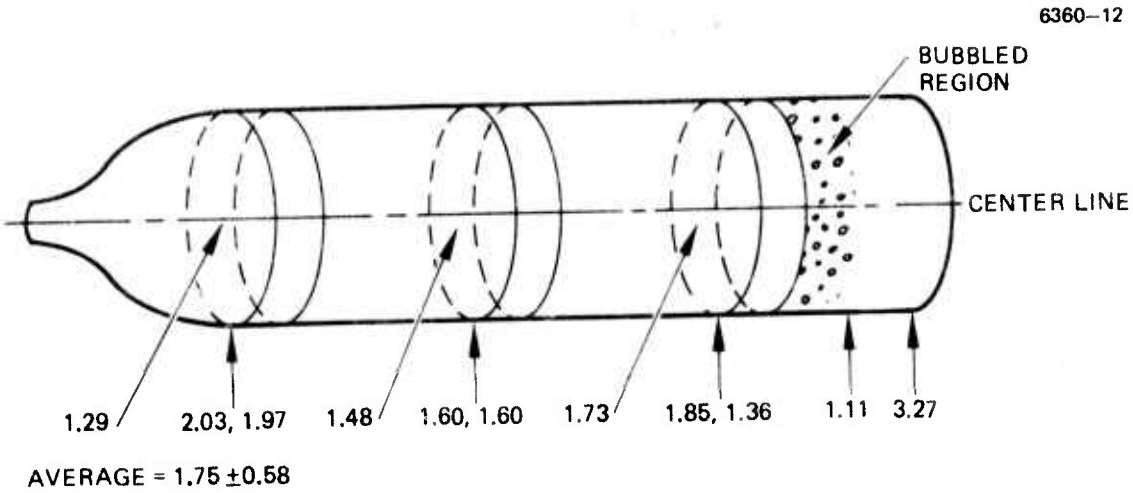

Figure 2. Analyses of RbCl-doped KCl boule B 156, mole percent RbCl.

processing in the absence of dopant. The initial run was made at 68% reduction, 200°C, with no graphite foil lubricant (considered to be a contaminant source). This yielded a highly cracked, rectangular-shaped forging, indicating that the steel plungers permitted very little surface slippage for the deforming boule. The second run, a 76% reduction at 200°C, was made with foil lubricant. This requires less pressure and gave a good, uncracked forging. No difference was visible in the forged blank compared to standard forging runs without cereclor. Grain size averaged 12 μm, yield strength 2908 psi (Table 4).

Absorption of the RAP-doped KCl after forging was measured on discs which had been ground and polished, then thoroughly etched for 2 min in concentrated HCl. This gives baseline values that can be used to evaluate the material without the effect of polishing variables, since all disturbed surface is removed, both from forging and from polishing. The results (Table 5) show typical values of 2 to 3 x 10^{-4} cm^{-1} for discs 1 cm thick. Values for unforged KCl are given for comparison. Forging appears to increase absorption very little, judging by boule B169, which was checked before and after forging.

Grain growth was tested versus time in 67% humidity at 24°C. Rubidium-doped forgings grew grains up to about 3.5 mm long in 1500 hr, after which growth almost stopped (Table 6). This is similar to the limited growth found in RAP undoped KCl and similarly occurs at localized points of high local deformation or polishing damage. No large overall growth up to 1 cm was found like that which occurs in non-RAP forged KCl.

A boule of NaCl, prepared by RAP growth, was tested for calorimetric absorption at 10.6 μm and 9.28 μm. Values were, respectively, 1.1 x 10^{-3} and 6.0 x 10^{-4} cm^{-1}. Figure 3 shows absorption related to position in the boule. The value of 1 x 10^{-3} cm^{-1} at 10.6 μm agrees with Ref. 2 and is close to intrinsic for NaCl. Strength of RAP NaCl boule B20, forged 69.6% at 300°C, averaged 5,400 psi yield, 7000 psi rupture. This yield strength is 2 to 3 times that of the single crystal, as measured at HRL[2] and by Armington, et al.[3]

Table 4. RAP Forging of Undoped KCl under Cereclor, a Chlorinated Paraffin[a]

Sample	Reduction, %	Yield Strength, psi	Remarks
B93	68	3122 ± 32 (3 tests)	No lube, cracked
B89-2	76	2908 ± 375 (5 tests)	With lube, good

[a]All forging done at 200°C.

Table 5. Calorimetric Absorption Values at 10.6 μm for RAP-doped KCl, Forged and Non-Forged

Sample	Condition	Absorption, cm^{-1}
B156	Single crystal	1.2×10^{-4}[a]
B155[b]	Single crystal	8.8×10^{-5}[a]
B169	Single crystal	1.7×10^{-4}
B164-5A	Forged	3.1×10^{-4}
B167-6	Forged	2.0×10^{-4}
B169-6	Forged	2.7×10^{-4}

[a]These are total boule absorptions, ≈1 in. long.

[b]This boule was not doped.

1. RAP Chemistry

In the RAP growth of metal fluorides, HF is the primary reactive agent. This agent converts oxide and hydroxide anions to fluoride.[4] However, the concentration limit to the ratio of $OH^-:F^-$ during growth depends on the existing ratio of the partial pressures, $P(H_2O):P(HF)$. This is seen in the following reaction,

$$F^-(c) + H_2O(g) \rightleftharpoons OH^-(c) + HF(g) \quad , \qquad (1)$$

where (c) and (g) are the condensed and gas phases, respectively. The oxide impurity is just a derivative of the hydroxide,

$$2OH^-(c) \rightleftharpoons O^=(c) + H_2O(g) \quad . \tag{2}$$

Therefore, to obtain a lower ratio of $OH^-:F^-$ in the crystal, a secondary RAP agent is employed to cope with $H_2O(g)$ from HF(g) and outgas. We find that CF_4 is adequate, since it converts H_2O to HF at temperatures as low as 900 C (Ref. 5):

$$CF_4(g) + 2H_2O(g) \rightleftharpoons 4HF(g) + CO_2(g) \quad . \tag{3}$$

Table 6. Grain Growth in Rb-Doped Forgings after 1500 Hours in 67% Relative Humidity at 24°C

Sample	Forging Conditions	Maximum Grain Length, mm
164-2	300°C, 67%	3.8
164-5A	300°C, 70%	3.3
169-3	300°C, 70%	1.0
169-2	300°C, 69%	2.2
174-2	300°C, 51%	0.03
174-5	300°C, 60%	0.02
174-6	300°C, 68%	1.2[a]
174-8	300°C, 86%	3.3

[a]One grain only, at a local deformation point.

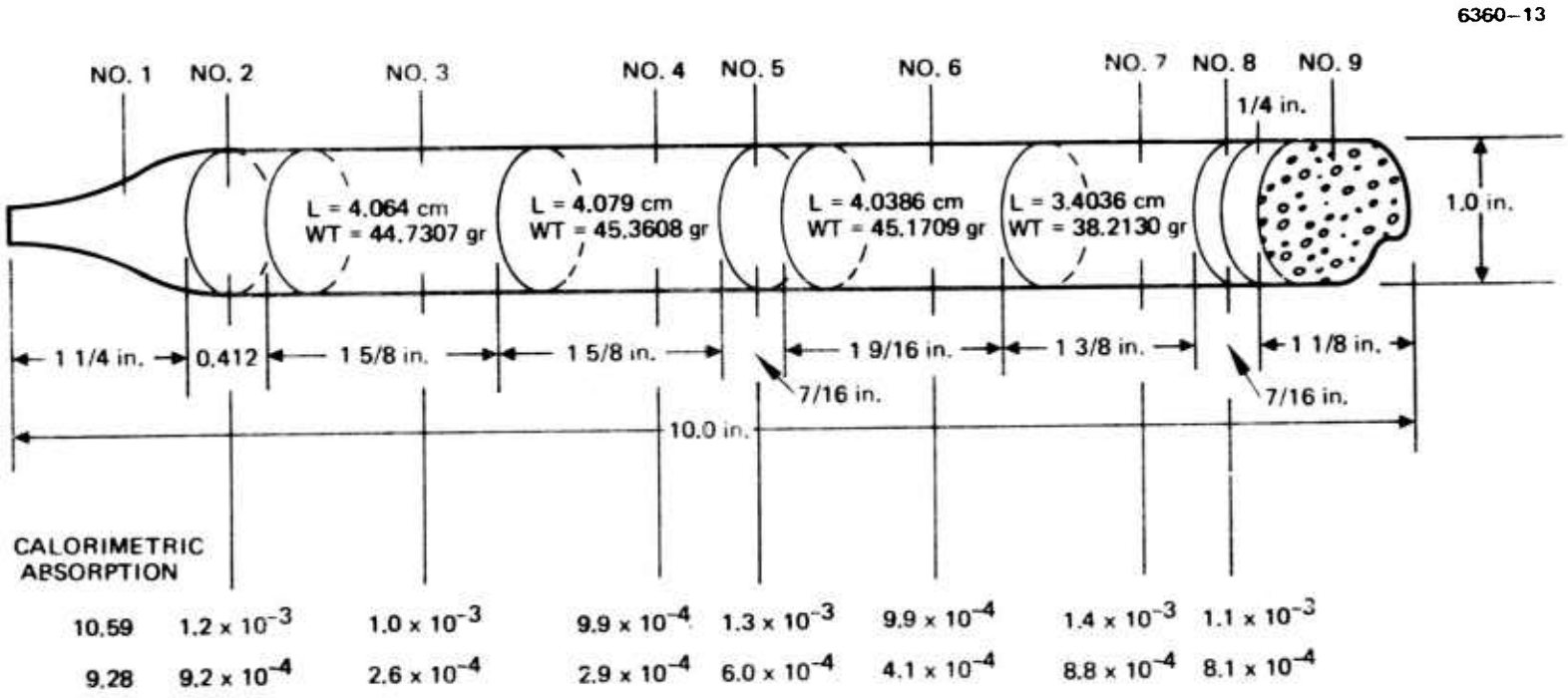

Figure 3. Absorption related to position in the boule for RAP-grown NaCl.

The objective in fluoride RAP growth is to achieve a low $OH^-:F^-$ ratio. This is done through a balance in CF_4 and HF. The CF_4 takes care of $H_2O(g)$. Together with a high value of P(HF), they favor the reverse direction of Eq. 1. However, the value of P(HF) is limited by its melt solubility. The latter must be below the value that leads to trapped bubbles, i.e., HF exsolved in the process of crystallization. With the apparatus air-tight and the gases of low humidity, outgas is the main source of H_2O. The latter depends on the working temperature, which, in turn, depends on the melting point of the metal fluoride. Calculations in the case of CaF_2 show that outgas H_2O determines the RAP-index, $P(H_2O):P(HF) \approx 10^{-3}$ (Ref. 4).

2. Accomplishments

A comparison of alkaline-earth fluorides (CaF_2, SrF_2, and BaF_2) grown by HF/He with similar crystals grown in (HF, CF_4)/He shows that the latter processing easily removes extrinsic absorption bands in the 3 to 10 μm region.[4, 5] Thus, (HF, CF_4)/He provides the lower RAP index during growth. The improvement in infrared optical transparency with the use of (HF, CF_4)/He encouraged us to search for an ultrapure source of CF_4. Our studies show that the much cheaper polytetrafluoroethylene (PTFE), or Teflon, depolymerized to its basic molecular unit, C_2F_4, serves as a good source for generating CF_4 by pyrolysis:[6]

$$C_2F_4(g) \rightleftharpoons C(c) + CF_4(g) \quad . \tag{4}$$

In the joint study with Raytheon on an AFML-funded program on scale-up fusion casting of CaF_2 and SrF_2, we RAP treated and compacted the materials in (HF, CF_4)/He. These compacts were then fusion cast at Raytheon under a CF_4 bleed of 10 to 20 Torr against a roughing pump. We soon discovered that, under the high temperature and long soak period characteristic of scale up, CF_4 is significantly corrosive to carbon. And carbon makes up the insulation, heating element, and crucible. The corrosion rate increased with the porosity of the sample and the temperature, thus creating a corrosion-runaway situation with time at the hotter section of the heating element.

For instance, the corrosion flux for graphitite-G, the material used at Hughes, is 1.68×10^{-4} mg cm^{-2} min^{-1} $Torr^{-1}$, independent of $P(CF_4) \leq 80$ Torr, for virgin samples. Repeating the runs three times with two used samples gave an average value of 10.0×10^{-4} mg cm^{-2} min^{-1} $Torr^{-1}$ with a deviation within 5%. Virgin samples of the more porous Great Lakes carbon, the material used at Raytheon, yielded the value of 12.9×10^{-4} mg cm^{-2} min^{-1} $Torr^{-1}$. Vitreous carbon was no better than graphitite-G in its resistance to corrosion.

Thermalization of CF_4 by the carrier gas influenced corrosion. At the same value of $P(CF_4)$, CF_4/Ar is three times more corrosive than CF_4/He.

We also discovered that the corrosion reaction was so efficient that it was still limited by the CF_4 inflow: at a CF_4 partial pressure of 20 Torr and exposure at 1500°C/95 min, a more than 100% increase in corrosion rate was observed for a 33% increase in flow rate.

These difficulties in using CF_4 for scale up caused us to extend the current study of fluoride RAP chemistry to other secondary agents. We chose $SF_6(g)$ and $BF_3(g)$ as alternative secondary RAP agents — these have, respectively, smaller and larger fluorine bond strengths than that of CF_4. (Bond strengths: S-F > 80 kcal, C-F ≈ 21 kcal, and B-F ≈ 133 kcal.)

An evaluation of carbon corrosion at 1500°C showed that corrosion is magnified if the fluorine bond breaks easily. Thus, SF_6 is 57 times more corrosive than CF_4, while BF_3 is about four times less corrosive than CF_4.

3. Future Plans

Boron trifluoride is much more reactive with $H_2O(g)$ than is $CF_4(g)$,

$$2BF_3(g) + 3H_2O(g) \rightleftharpoons 6HF(g) + B_2O_3(c) \quad . \qquad (5)$$

It reacts vigorously with $H_2O(g)$ even at room temperature; presumably, a lower concentration of BF_3 will be required to lower the RAP index. Carbon attacked directly by BF_3 leads to the formation of the refractory boron carbide:

$$4BF_3(g) + 6C(c) \rightleftharpoons 3CF_4(g) + B_4C_3(c) \quad . \qquad (6)$$

This reaction will probably lead to surface passivation of the carbon ware.

In the next period, we will verify whether such passivation occurs. Also, we will carry out the RAP growth of CaF_2 or SrF_2 under (HF, BF_3)/He and optically evaluate the resulting crystal.

Using undoped KCl as the test material, we showed that a carrier gas much cheaper than He can be used in RAP crystal growth. The bulk absorption at 10.6 μm versus carrier gas went as follows:

10×10^{-5} cm^{-1} for KCl grown in CCl_4/He
8×10^{-5} cm^{-1} for KCl grown in CCl_4/N_2
6×10^{-5} cm^{-1} for KCl grown in CCl_4/(He, CO_2).

These results tell us that (N_2, CO_2) is a satisfactory carrier for CCl_4 in the scale-up crystal growth of NaCl. NaCl grown in CCl_4/He showed intrinsic optical absorption: 1×10^{-3} cm^{-1} at 10.6 μm and 6×10^{-4} cm^{-1} at 0.27 μm.

B. SURFACE FINISHING

Infrared laser windows for high-power applications must be finished flat and parallel to pass an undistorted laser beam. At 2.8 and 3.8 μm, CaF_2 and SrF_2 are favored; KCl is a prime candidate for 10.6 μm. Polycrystalline substrates are desired for increased cleavage resistance and strength.

Optical finishing requires removing the material from the window surfaces by progressive grinding and polishing steps. This process leaves damaged layers, which exhibit high absorption. A combination of chemical and mechanical surface removal offers the best chance of obtaining flat, reasonably damage-free surfaces.

Recent program emphasis has been on the finishing of CaF_2 and SrF_2 windows. These materials, which are harder than KCl and less sensitive to water, are more easily polished and handled than is KCl. However, there are some problems in using polycrystalline materials

for these windows: although their strength is higher and catastrophic cleavage is minimized, micro-cleavage on (111) planes during grinding and polishing can cause extensive damage to grains oriented so as to expose a (111) surface. This was recognized for single crystal windows,[7] and orientations have been specified that are insensitive to cleavage. The grinding of a polycrystalline surface, however, usually reveals many poorly oriented grains that can damage deeply. In addition, CaF_2 and SrF_2 are resistant to chemical attack by most etchant materials. Therefore, lengthy mechanical polishing techniques are usually used to remove preliminary grinding damage. Our objective is to develop chemical-mechanical polishing techniques that give the lowest possible final absorption for flat and parallel window surfaces.

In the previous period, we reported on the polishing recipe and the low 10.6 μm absorption that it is capable of yielding in forged KCl doped with 1.8 at.% Rb^+. However, this finishing of forged KCl on pitch with black rouge (Fe_3O_4) in ethanediol (glycol) has produced inconsistent results. Pitch polishing does not cause increased absorption; it results from grinding damage and from the final cleanup on a flannel buff. We remove grinding damage with an HCl etch and follow polishing with a wipe on isopropanol moistened Texwipe Absorbond paper. This neither scratches the surface nor appreciably increases absorption at 10.6 μm.

1. Calcium Fluoride

Preliminary grinding and polishing experiments with CaF_2 revealed that, in polycrystalline windows, deep grinding damage was found in specific grains in the form of craters which only appeared after final polishing with Linde A 0.3 μm Al_2O_3 abrasive (Figure 4). This damage is caused by a combination of two circumstances. First, orientation of certain grains is such that cleavage can easily occur when high local stress is applied. Second, use of a coarse grinding abrasive on a hard lap provides the high local stress conducive to cleavage. All grains must be ground regardless of orientation, and

Figure 4. Nomarski photograph at 165X—craters in polished CaF_2 that were caused by coarse grinding abrasive on a hard lap.

coarse grit must be used for initial grinding. Therefore, we searched for a lap soft enough to allow coarse abrasive to sink in and relieve high impressed stresses, but firm enough to allow surface removal by the abrasive. Politex Super S polishing pads have this property, and, using abrasives sized from 5 μm down to 0.3 μm, they polished with no craters. Figure 5 compares a commercial finish (hidden craters) with Super S finish. For optical surfaces, soft pitch (No. 73 Swiss) gave the requisite yielding for grinding, and is used for grinding with garnet of 18 μm, 8 μm, and 4 μm sizes, followed by 1 μm Al_2O_3. Initial polishing is also done on soft pitch, starting with a charge of 2 μm cerium oxide, which breaks down to finer abrasive with re-use and is constantly fed back to the lap. This procedure gives us a surface free of craters and should minimize deep damage (see Figure 6).

For removal of final small scratches and surface damage, a chemical-mechanical finish polish is required. Chelate-type solvents such as EDTA were tried, along with combinations of nitric, sulphuric, and acetic acids, but attack was too slow or insufficient. Finally, a mixture of nitric and hydrochloric acids was found to etch both CaF_2 and SrF_2 at a satisfactory rate; it is now being used in the proportion of $3HCl:1HNO_3$ (aqua regia) plus 3 parts of H_2O. This etchant, as a vehicle for Linde B (0.05 μm Al_2O_3) on a pitch lap, is now being used for final surface polishing.

This work has just started, but results to date are encouraging (Figure 7). Freedom from craters and most scratches is being obtained, and studies of polishing time versus absorption are underway.

CaF_2 and SrF_2 are anisotropic with respect to polishing damage and also to etch rate. We found that height differences resulting from variations in the etching rate of various grains are eliminated during polishing. It is expected that highly damaged surfaces are attacked most rapidly by etching. However, we will continue searching for an etchant combination that will etch all orientations uniformly. In either case, we expect that the technique of chemical-mechanical polishing will reduce the time required to attain lowest absorption values at 2.8 and 3.8 μm.

6360–15

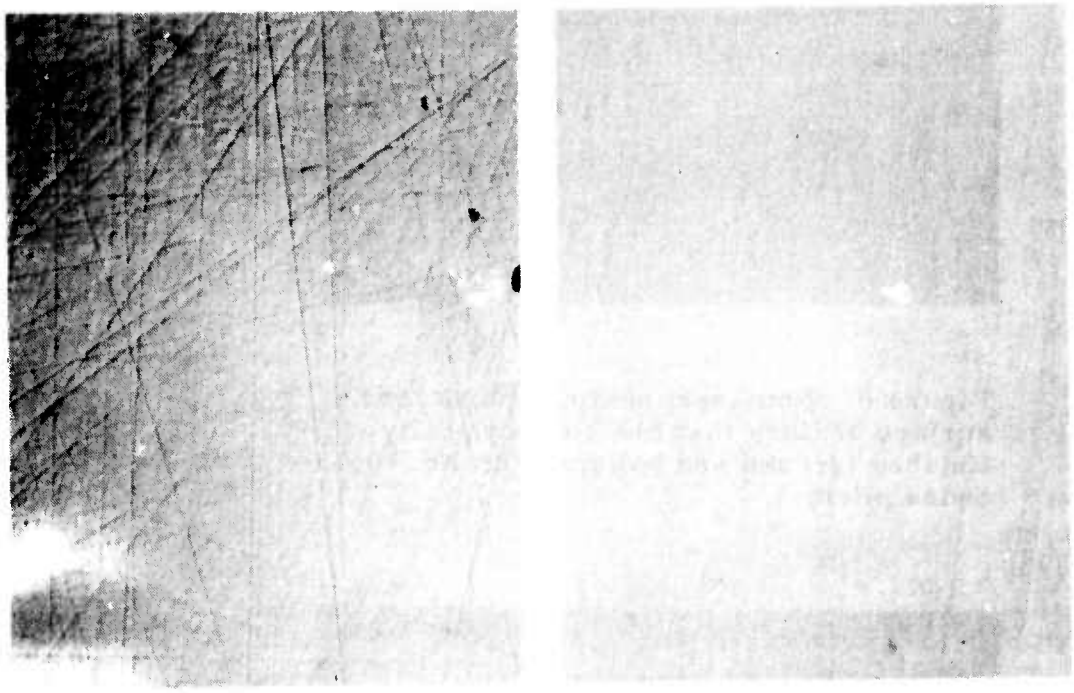

AS RECEIVED COMMERCIAL FINISH HUGHES'S SUPER-S FINISH

Figure 5. Comparison photographs of commercially finished CaF_2 (hidden craters) and Nomarski photographs at 165X—CaF_2 ground and polished on Politex Super 5 pad with decreasing abrasive size from 5 to 0.3 μm.

6360-16

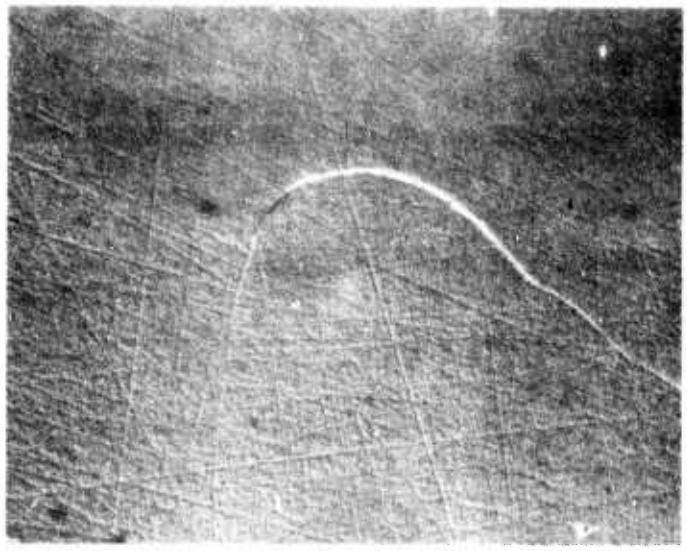

Figure 6. Nomarski photograph at 165X— surface of CaF_2 that has been optically finished (ground and polished) on No. 73 Swiss pitch.

6360-17

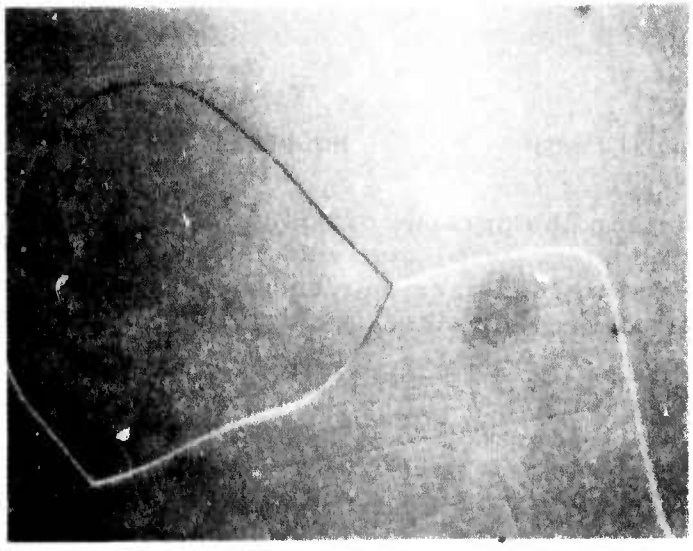

Figure 7. Nomarski photograph at 165X— CaF_2 surface which has been optically polished using chemical-mechanical methods. Note the polish/etch anisotropy of the different grains.

2. Potassium Chloride

Previous work on finishing of KCl resulted in a chemical-mechanical polishing technique giving 10.6 μm absorption values of about 6×10^{-4} cm^{-1} for a 1 cm thick disc. However, samples would occasionally measure as high as 1×10^{-3} cm^{-1}, the reason for which was not immediately evident.

Using the baseline procedure developed previously (grind on silicon carbide and alumina papers, polish with black rouge and propanediol on Swiss pitch, and buff lightly on flannel with Linde A and propanol), each of the three basic operations (grind, polish, buff) was varied independently to check its effect on absorption (Table 7). An increase of 5X in grinding time increased absorption 3X. An increase of 5X in polishing time gave no change in absorption. Buffing on flannel for 10 sec/side with alcohol increased absorption 4X.

Table 7. Polycrystalline KCl Polishing Experiments to Show Contribution to Absorption at 10.6 μm

Sample	Polishing History	Absorption, cm^{-1}
167 disc 1	Baseline polish	6.0×10^{-4}
167-6 disc 2	Polish with 5X grind time	1.8×10^{-3}
164-5A disc 3	Polish with 5X polish time	7.5×10^{-4}
169-3 disc 10	Flannel buff, 10 sec/side, alcohol only	1.3×10^{-3}
All HCl samples have an absorption of $\sim 3 \times 10^{-4}$ cm^{-1}.		

These experiments showed that increased absorption was due to grinding (deep damage) and/or buffing on flannel (shallow damage). Therefore, we instituted a 2 min etch in HCl following grinding and are in the process of changing our final polishing cleanup to exclude the flannel buff. We believe that the low absorption values from our baseline process is the result of the thorough coverage of the flannel buff with Linde A during buffing. This is not as reliable as we wish, so we are searching for an alternate means of final cleanup.

In our search, we have found that Absorbond paper, a polyethylene-based material from Texwipe, Inc., does not scratch or damage the delicate surface of etched KCl. Under phase-contrast microscopy, which reveals damage both on and under the surface, resultant surfaces are shown from alcohol buffing on flannel, Politex Supreme, and Absorbond (Figure 8). The absorption measurements provide corroboration that Absorbond produces less damage. Our baseline polish, with the HCl etch after grinding and a final cleanup with Absorbond (instead of flannel) plus Linde A, has yielded a flat and parallel window (1 fringe, 10 sec wedge) with a 10.6 μm absorption of 5.8×10^{-4} cm^{-1}.

For KCl, the remaining problem is that Absorbond-wiped KCl retains some surface polishing abrasive (black rouge), which may initiate laser damage during testing. We have noted that Politex Supreme does not seem to change final flatness, nor does it raise absorption appreciably (Figure 8). Therefore, we will attempt to use it for final cleanup, possibly with an ultrasonic treatment, as does Honeywell. This combination of our polishing procedure, with its excellent flatness out to the edges, and a proper final cleanup should result in windows of consistently low absorption.

In summary, mechanical polishing of polycrystalline CaF_2 is being done without the deep damage and pits from coarse grinding. This is being accomplished by providing soft laps for large abrasive particles to sink into. An etchant composed of 3 HCl:1 HNO_3 plus three parts H_2O is being tested for chemical-mechanical finishing of CaF_2 and SrF_2.

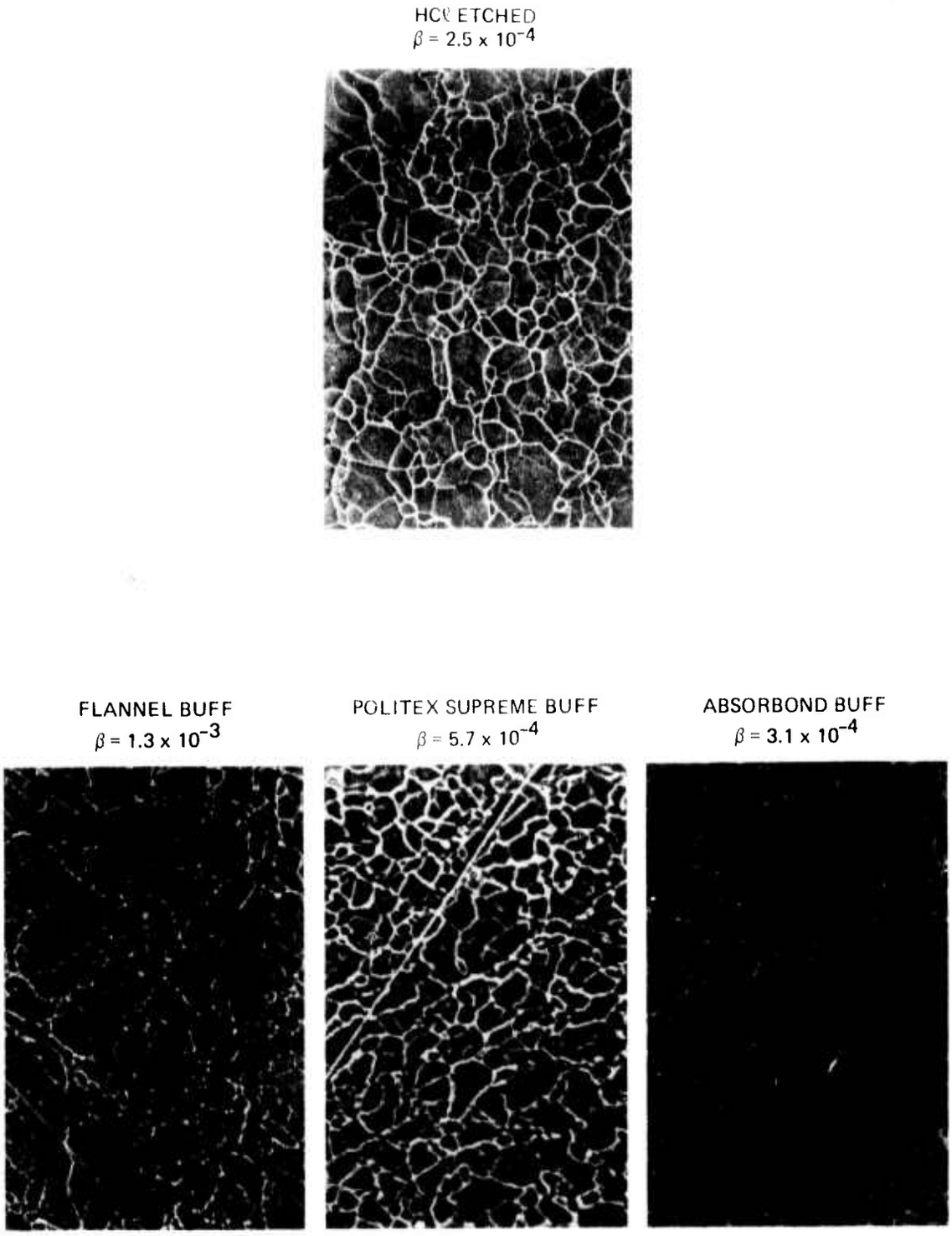

Figure 8. Effects of buffing etched, polycrystalline KCl. Phase contrast photographs at 322X.

Nonreproducibility of absorption values for our KCl polishing was traced to grinding and flannel-buffing procedures. An etch is now used to remove grinding damage, and Absorbond paper and Politex Supreme are being tested to supplant the flannel buff originally used for final cleanup.

C. WINDOW COATINGS

In previous studies of three layer 10.6 μm AR coatings for KCl, we observed that films of $As_2S_3/ThF_4/As_2S_3$ and $As_2S_3/KCl/As_2S_3$ (produced in a conventional vacuum system) had absorption losses of about 0.1% per surface. In contrast, $ZnSe/ThF_4/ZnSe$ produced under UHV conditions had an absorption loss of 0.05% per surface. As different designs and materials were used, it was possible to infer, but not to conclude, that the difference was due to vacuum conditions. An important feature of the Interim Report is the direct comparison of identical coating designs with identical substrate/film materials to determine the effect of the vacuum environment on coating performance.

An equally significant factor in the optical performance of the coatings is the presence of impurities in the raw materials used to form the coatings. For example, a significant amount of SiF_4 vapor was evolved when ThF_4 was melted. This was unexpected because SiF_4 has a very high vapor pressure and a boiling point of -86 C. Its stability in ThF_4, which is most likely due to the substitution of Si^{+4} for Th^{+4} in the lattice, could present a problem if it were also incorporated in the films. The superior optical performance of the films containing ThF_4 may be due in part to the procedure of pumping the SiF_4 out before depositing the films. The program also used a mass spectrometer to analyze the residual gases present during film deposition; this data was correlated to the optical performance of the films. Although the present study is limited to residual gas mass analysis (RGA) in the UHV system, the ultimate goal is to obtain similar information about film deposition in the standard vacuum system.

Although previous studies under DARPA and AFML contracts have produced low-loss coatings of ZnSe/ThF_4/ZnSe and ZnSe/KCl/ZnSe, the coatings appear to be somewhat sensitive to thermally induced cracking. This has been attributed to stress resulting from the low coefficient of expansion of ZnSe, its value being about 1/5 that of KCl. As a consequence, this study emphasized the high index materials As_2S_3 and As_2Se_3, which have expansion coefficients of about 2/3 that of KCl.

Although our prior work with As_2S_3 produced good films, the present work included the evaluation of As_2Se_3 films. The decision to do this was based on two facts. First, the multiphonon absorption bands for As_2Se_3 are at longer wavelengths than those for As_2S_3 (Ref. 1). Second, As_2S_3 films exhibit deterioration at temperatures above 75°C, but As_2Se_3 films appear to be stable to a temperature of 125°C. The stability of As_2Se_3 films permits deposition on heated substrates, which prevents the adsorption of water vapor in the low-index film. Also, the existence of As_2S_2 and As_2S_5 can present a problem in film stoichiometry for the sulfides,[2] whereas only As_2Se_3 is reported for the selenide.[9]

The optical absorption of KCl is higher at 9.27 μm than at 10.6 μm. In this work, we have measured the absorption of the substrates and the coated samples (whenever possible) at both wavelengths. The measurement procedure consisted of keeping the sample in the calorimeter and shifting the grating to sequentially obtain the two laser lines. The laser focus was at the same place, and the same general area was irradiated in both bases. Minor differences in irradiated area were due to differences in mode profiles for the 9.27 and 10.6 μm laser transitions.

Strong absorption bands (up to 5% decrease in transmission) were on occasion observed in the films at either 9 or 9.5 μm. Because of the importance of reducing absorption in films, this problem was given much attention. The evidence, although not yet conclusive, strongly supports the idea that these absorption bands are due to oxide impurities in the As_2S_3 and As_2Se_3 materials.

Although the principal effort during this period was to complete the studies of AR coatings for the 10 μm region, preliminary work was begun in the area of 2.7 and 3.8 μm coatings. This will become the dominant area in the second half of this program.

1. Experimental Apparatus

The UHV system used in this study is an all metal one that is sputter ion and titanium sublimation pumped. After bake out at 250°C, it has a base pressure of about 1×10^{-10} Torr when empty and about 1×10^{-9} when loaded with samples and film materials. The 2.5 cm diameter samples are mounted in a stainless-steel support which can be rotated and flipped so that four samples can be individually coated on both surfaces during a run. Two directly heated Knudsen-type evaporators are located about 16 cm below the samples. Transmission optical monitoring is used to control the film deposition. A detailed description has been included in the final report of last year's work.[2]

The conventional vacuum system consists of a turbomolecular-pumped 60 cm diameter stainless-steel bell jar that contains an LN_2 cooled Meisner trap. The base pressure of the system is in the low 10^{-7} Torr range. One or more samples are mounted on a fixed stage located about 40 cm above two directly heated evaporation sources. Film thickness is controlled by reflection optical monitoring. A 250 W lamp is used to heat the substrate.

2. Sample Preparation

After surface preparation by grinding and polishing, the KCl substrates are etched in concentrated HCl for 15 to 30 sec. The acid is removed by a 15 sec wash in propanol, and the sample is dried in hot Freon vapor. The surface is inspected with phase contrast, bright and dark field, and Nemarski microscopy. Photomicrographs are taken of about one third of the samples. Substrate absorption is determined by laser calorimetry. About 80% of the samples are measured at both

9.27 and 10.6 μm. Oxygen glow discharge cleaning of the sample before film deposition is used in both the UHV and the conventional systems.

3. Accomplishments

Single- and three-layer films were deposited on KCl in UHV and in conventional vacuum systems. The single-layer films of As_2Se_3 and As_2S_3 were deposited to establish the deposition parameters, characterize the purity of the raw material, and provide samples for a determination of optical properties: index of refraction, percent absorption, absorption coefficient, and damage threshold. Three-layer AR coatings of $As_2Se_3/KCl/As_2Se_3$ and $As_2S_3/KCl/As_2S_3$ were fabricated and tested. Preliminary work was begun on a 10.6 μm AR coating of $As_2Se_3/NaF/As_2Se_3$ and on single-layer films of materials which will be used in 2.7 and 3.8 μm AR coatings.

A summary of three-layer AR coatings of $As_2Se_3/KCl/As_2Se_3$ deposited under conventional vacuum and UHV conditions is presented in Table 8. Although there are some small differences in film thicknesses, the As_2Se_3 used, and the substrate temperature, these are not large enough to explain the distinct differences observed between the two groups of samples. On the average, the UHV samples have absorption losses that are about 20% of the losses of the samples from the conventional system. The contrast is most evident in a comparison of samples 78-13 and 78-5, which were designed to have a reflection minimum at 10.6 μm. These samples have the identical coating design as the UHV samples, the film thicknesses of which were set to obtain a reflection minimum at 9.27 μm. The predicted absorptions are based on an absorption coefficient of 1 cm^{-1} for As_2Se_3 and of 1.2 cm^{-1} for KCl. These values were obtained by evaluating single-layer films deposited under UHV conditions. Although the predicted values represent a lower limit for the UHV samples, the standard vacuum samples exhibit absorptions of 5 to 20 times the predicted values.

Table 8. As_2Se_3/KCl/As_2Se_3 AR Coatings on KCl

Sample No.	Film Thickness			Source of As_2Se_3	Substrate Temperature, C	Sample Absorption, %				Coating Absorption per Surface, %			
						9.28 μm		10.6 μm		9.28 μm		10.6 μm	
	As_2Se_3, μm	KCl, μm	As_2Se_3, μm			Uncoated	Coated	Uncoated	Coated	Actual	Predicted	Actual	Predicted
Deposited under Conventional Vacuum Conditions													
151-1	0.378	1.377	0.240	HRL-1	50	0.061	0.632	0.017	0.342	0.29	0.03	0.16	0.02
78-13	0.635	0.848	0.402	HRL-1	50	0.060	0.802	0.022	0.886	0.37	0.03	0.43	0.02
78-5	0.635	0.848	0.402	HRL-1	75	0.094	0.501	0.035	0.315	0.20	0.03	0.14	0.02
70-3	0.764	0.641	0.463	Vacuum outgassed HRL-1	75	0.057	0.358	0.021	0.437	0.15	0.03	0.21	0.02
164-2-11	0.729	0.432	0.421	ACC	25	(a)	0.605	0.094	0.508	<0.30	0.03	0.21	0.02
Deposited under UHV Conditions													
164-5A-10-48-3	0.556	0.742	0.352	ACC	25	0.137	0.211	(a)	0.059	0.037	0.024	<0.030	0.024
164-5A-11-48-4	0.556	0.742	0.352	ACC	25	0.111	0.148	(a)	0.045	0.019	0.029	<0.022	0.024
129-1-49-1	0.556	0.742	0.352	ACC	25	0.098	0.094	0.026	0.079	<0.047	0.029	0.026	0.024
129-2-49-2	0.556	0.742	0.352	ACC	25	0.071	0.148	0.021	0.156	0.039	0.029	0.068	0.024

(a) Not measured.

5795

Since two different sources* of As_2Se_3 had been used, we fabricated sample 164-2-11 under standard vacuum conditions using the ACC material. The absorption losses were essentially the same as that of the samples made with HRL material. The most significant aspect is that the two groups of coatings are distinctly different in absorption losses. This case is the clearest demonstration of the effect of vacuum environment on the ultimate properties of the film. It also points out the need for detailed analysis of the vacuum environment in the conventional systems to isolate the cause of the difference. At this time, the most probable cause is the formation of oxide impurities in the As_2Se_3 films.

Varying substrate temperature from room temperature to 75°C produced a small change in the absorption of films prepared under conventional vacuum conditions. Comparison of the average absorption of 151-1 and 78-13 with those of 78-5 and 70-3 shows approximately a 50% decrease in absorption for the higher substrate deposition temperature. In view of the stability of the As_2Se_3, further studies should be made to temperatures of about 125°C to determine if the higher substrate temperature under conventional vacuum conditions can reproduce the lower absorption of the UHV coatings. Run 146-2-11, which was made with a room-temperature substrate, exhibits approximately the same value. This seems to indicate that there is no temperature dependence below 50°C or that it is masked by the change in As_2Se_3 material.

All of the films in Table 8 have a reasonably broad transmission band at 10.6 μm. An example of the observed and theoretical transmission spectra are presented in Figures 9 and 10.

Vacuum clean up of the ACC's As_2Se_3 is believed responsible for the marked trend toward improved optical characteristics that accompanied the sequential preparation of single-layer UHV samples 45-BF-8-48-1 and 164-2-1-48-2 (see Table 9) and of triple-layer

---

*The sources of As_2Se_3 were Atomergic Chemical Corporation and HRL.

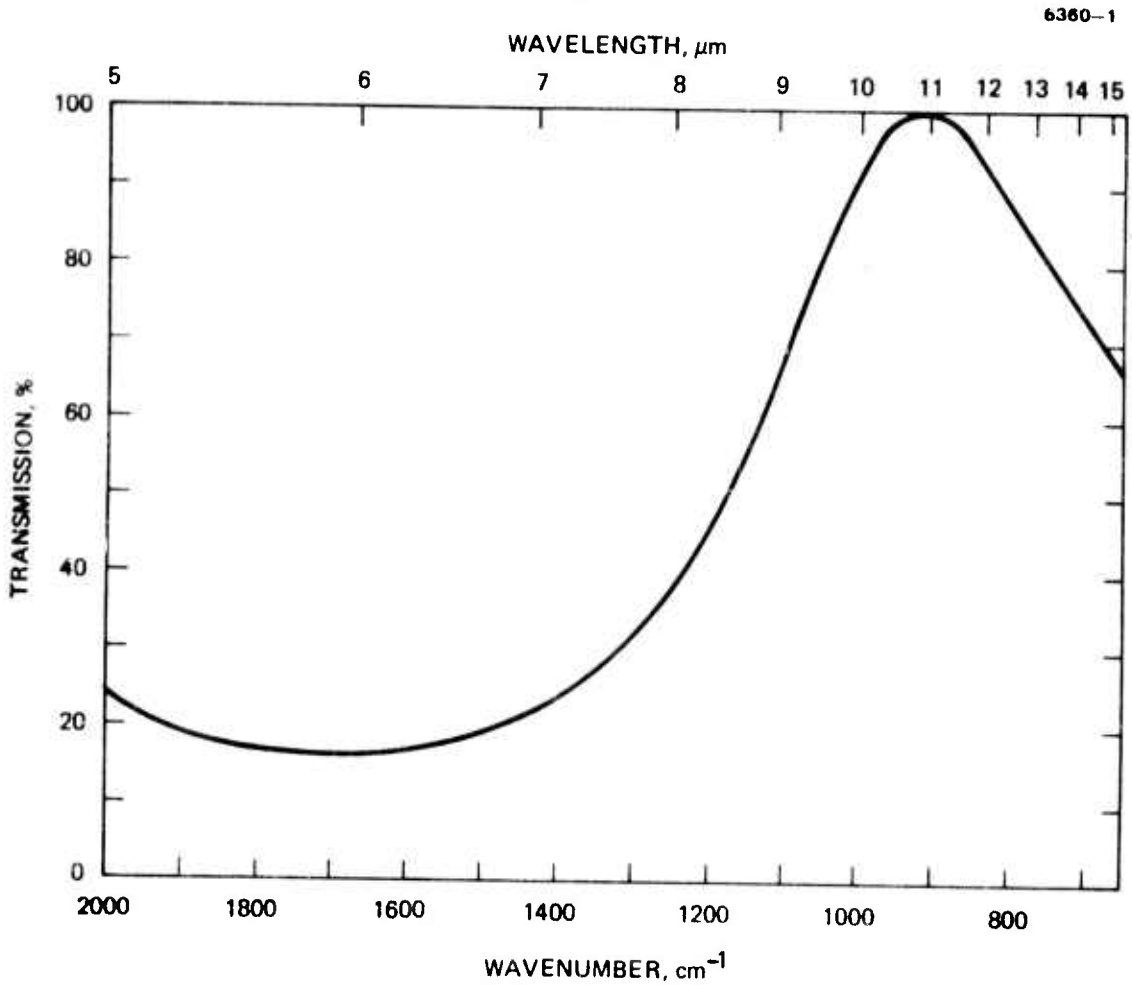

Figure 9. Transmission spectrum of sample 78-5.

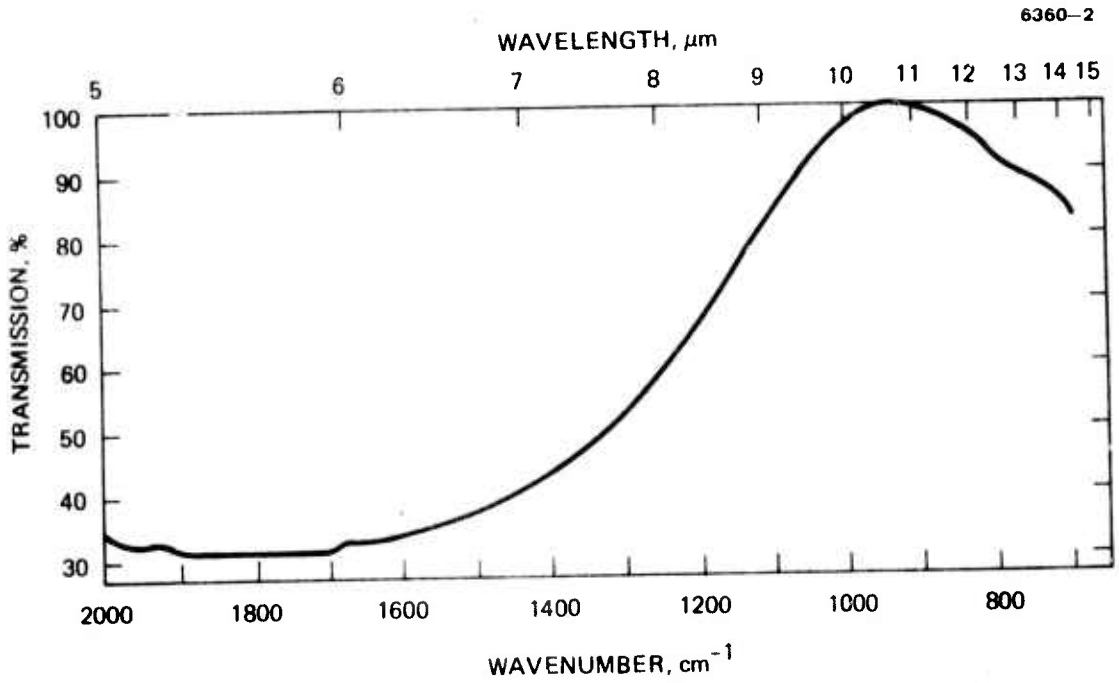

Figure 10. Theoretical transmission spectrum of sample 78-5.

Table 9. Single-Layer As_2Se_3 Films on KCl

Sample No.	Source of As_2Se_3	As_2Se_3 Thickness, μm	Sample Absorption, %				Coating Absorption, %		Absorption Coefficient, cm^{-1}	
			9.28		10.6		9.28	10.6	9.28	10.6
			Uncoated	Coated	Uncoated	Coated	Uncoated	Coated	Uncoated	Coated
Deposited under Standard Vacuum Conditions										
70-6	HRL-1	3.31	(a)	0.46	0.209	0.256	<0.46	0.23	<11	8.3
70-4	HRL-1	1.74	(a)	0.64	(a)	0.70	<0.64	<0.70	<16	<25
65-11	HRL-1	1.64	0.040	0.26	0.018	0.160	0.22	0.14	5.7	5.4
63-6	HRL-1	0.96	(a)	0.47	(a)	0.25	<0.47	<0.25	<78	<4[illegible]
Deposited under UHV Conditions										
45-BF8-48-1	ACC	1.69	0.14	0.62	(a)	0.16	0.48	<0.16	12	<5.6
164-2-1-48-2	ACC	1.67	0.065	0.175	(a)	0.14	0.11	<0.14	2.7	<4.2
67-A1-49-3	ACC	1.01	0.023	0.109	0.018	0.060	0.036	0.042	14	6.7
AFML Samples Deposited under UHV Conditions										
150-4-15-7-3	HRL-1	3.38	0.095	0.226	0.097	0.113	0.129	0.016	3.25	0.53
150-5-13-8-4	HRL-1	3.45	0.075	0.164	0.073	0.052	0.090	<0.052	2.30	<1.60
174-5-29-9-4	HRL-1	3.37	0.045	0.099	0.028	0.056	0.045	0.028	1.13	0.99
174-8-31-9-3	HRL-1	3.44	0.107	0.219	0.023	0.060	0.056	0.019	2.72	1.08

(a) Not measured.

5795

samples 164-5A-10-48-3 and 164-5A-11-48-4. This is particularly noticeable in that the first sample, 45-BF-8-48-1, had a 4% absorption dip at 9 μm (see Figure 11) and high absorption, but the second sample 164-2-1-48-2, had no absorption band (see Figure 12) and a much lower absorption at 9.23 μm. The absorption of As_2Se_3 is believed to have decreased, since the next two samples (164-5A-10-48-3 and 164-5A-11-48-4) had an observed absorption that is in agreement with the value predicted on the basis of an As_2Se_3 absorption coefficient of 1 cm^{-1}.

The vacuum effect is also very pronounced in the single-layer As_2Se_3 films. In Table 9, four UHV-deposited samples produced under an AFML program are included for comparison. Since substrate absorption was not measured in several cases, a complete comparison of coating absorption is not possible. But the UHV samples have an absorption that is about 20% that of the conventional vacuum samples. This is also seen in comparing the total absorption values for UHV and conventional vacuum samples.

The effect of impurities in the film materials is seen in a comparison between ACC and HRL-1 UHV-deposited films of As_2Se_3. The difference in absorption is distinct and was also observed in spectrophotometer measurements of thin plates of the As_2Se_3 glasses.

In the case of $As_2S_3/KCl/As_2S_3$ AR coatings, the vacuum environment has a small effect at 10.6 μm and a pronounced effect at 9.28 μm. These results are summarized in Table 10. At 10.6 μm, the five standard vacuum samples have an average coating absorption of 0.063% (range 0.045 to 0.078%). The eight UHV samples have an average absorption of 0.047% (range 0.012 to 0.104%) with six of the samples in the range 0.012 to 0.045%.

There is a significant difference at 9.28 μm. The standard vacuum coatings have absorption losses of about 0.2 to 0.4%, while six of the eight UHV samples have absorptions that are less than 0.1%. Just as in the As_2Se_3 case, the difference is associated with a 9 μm

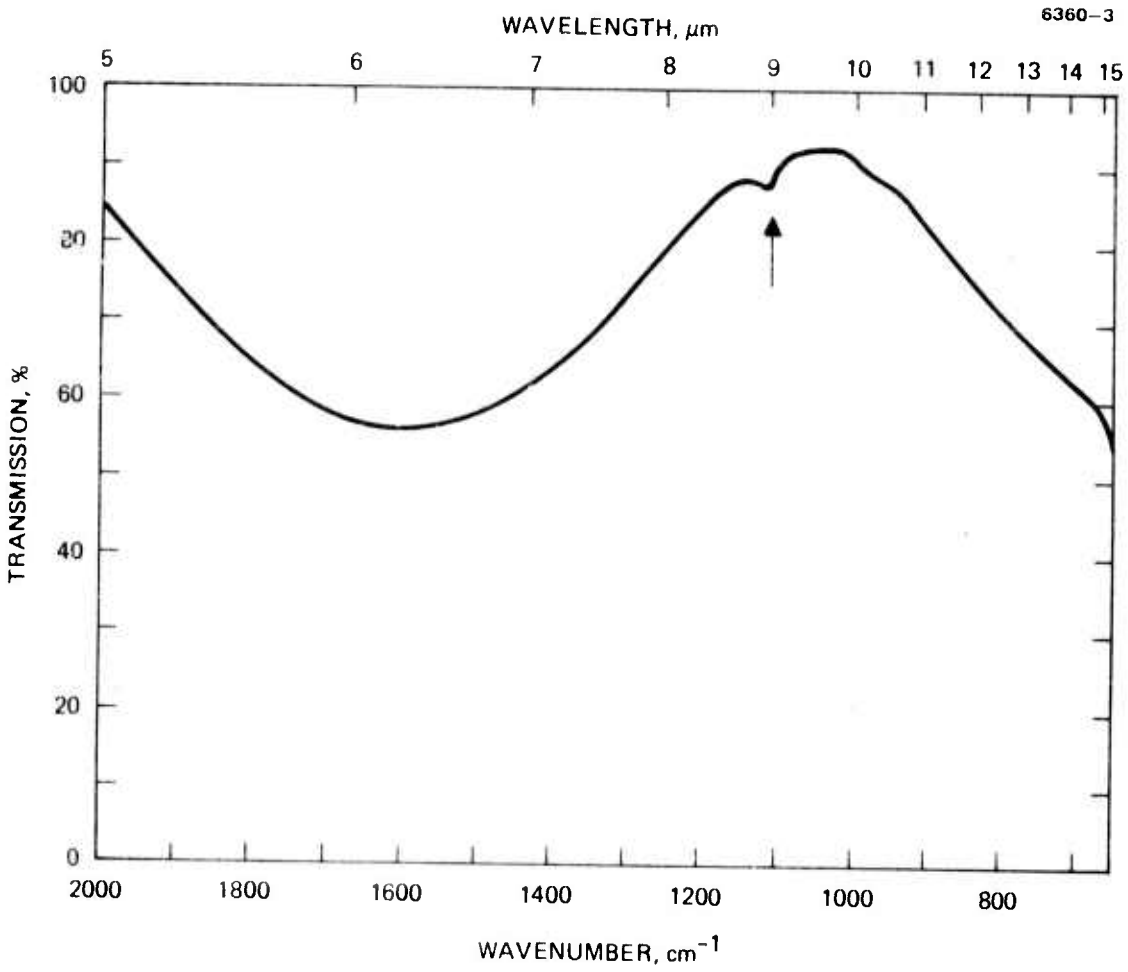

Figure 11. 45-BF-8-48-1 transmission spectrum showing 9 μm absorption dip.

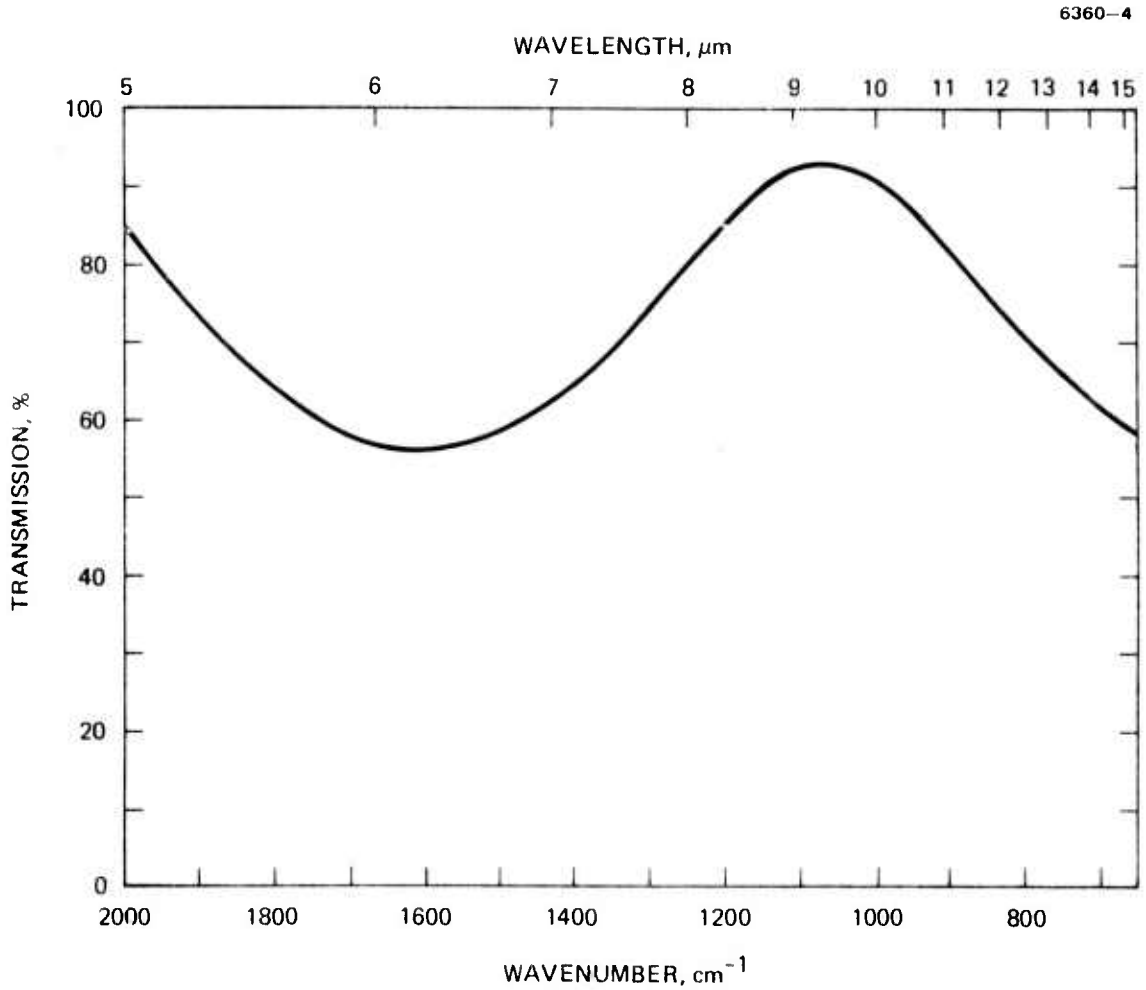

Figure 12. 164-2-1-48-2 trans spectra no dip.

Table 10. As_2S_3/KCl/As_2S_3 AR Coating on KCl

Sample No.	Film Thickness			Sample Absorption, %				Coating Absorption per Surface, %				Deposition Conditions
	As_2S_3,[c] μm	KCl, μm	As_2S_3,[c] μm	9.28 μm		10.6 μm		9.28 μm		10.6 μm		
				Uncoated	Coated	Uncoated	Coated	Actual	Predicted	Actual	Predicted	
63-11	0.697	1.075	0.403	0.043	0.507	0.019	0.163	0.23	0.04	0.072	0.029	Conventional vacuum
147-3-51-1	1.123	0.601	0.523	0.030	0.892	0.038	0.142	0.43	0.04	0.052	0.031	
147-1-51-2	1.123	0.601	0.523	0.027	0.900	0.037	0.152	0.44	0.04	0.078	0.031	
147-5-51-3	1.123	0.601	0.523	(a)	0.674	0.068	0.158	<0.34	0.04	0.045	0.031	
147-4-51-4	1.123	0.601	0.523	(a)	0.833	0.046	0.184	<0.42	0.04	0.069	0.031	
147-6-50-1	1.334	0.482	0.481	(a)	1.043	0.067	0.276	<0.52	0.04	0.104	0.033	UHV
147-8-50-2	1.203	0.510	0.534	0.260	0.159	0.086	0.154	<0.08	0.04	0.034	0.032	
147-7-50-3	1.092	0.592/0.789[b]	0.509	0.045	0.662	0.028	0.088	0.31	0.04	0.030	0.033	
147-13-50-4	1.092	0.592	0.509	0.026	0.178	0.015	0.088	0.076	0.04	0.036	0.031	
152-11-52-1	1.157	0.578	0.523	(a)	0.153	0.055	0.144	<0.08	0.04	0.045	0.031	
147-12-52-2	1.157	0.578	0.523	(a)	0.204	0.059	0.058	<0.10	0.04	<0.029	0.031	
147-10-52-3	1.157	0.578	0.523	(a)	0.138	0.042	0.066	<0.07	0.04	0.012	0.031	
152-9-52-4	1.157	0.578	0.523	(a)	0.247	0.041	0.206	<0.14	0.04	0.083	0.031	

[a] Not measured over run.
[b] One of KCl layers was accidentally over run.
[c] HRL As_2S_3 used in all cases.

5795

absorption band. A typical example of a standard vacuum sample is shown in Figure 13, and a UHV sample is shown in Figure 14. The theoretical transmission spectra is shown in Figure 15. Although both the As_2Se_3 and As_2S_3 exhibit sensitivity to residual gases, it is possible that the As_2S_3 is less reactive.

Sample 63-11 was tested by Dr. John Detrio at UDRI for 10.6 μm cw laser damage. The sample was undamaged and did not exhibit permanent strain when exposed to a focussed 750 W laser beam for 9 sec. This is estimated to correspond to a power density of about 110 kW/cm^2.

In the study of single-layer films of As_2S_3, we observed material impurity effects that were much larger than the vacuum environmental effects described previously. This data is presented in Table 11. A single sample (2-577) was deposited under conventional vacuum conditions. Three samples of the same HRL material were deposited under UHV conditions as part of an AFML program. There is insufficient data to determine if there is any difference between these coatings.

During the UHV deposition of the ACC material, we observed the evolution of a very large amount of water vapor, a significant amount of petroleum ether, and a trace amount of acetic acid. These compounds could have been the result of the following reaction process for the production of arsenic trisulfide. Arsenic oxide is reacted with H_2S in acetic anhydride to form a precipitate of As_2Se_3:

$$As_2O_3 + 3\ H_2S \rightarrow As_2S_3 \downarrow + 3\ H_2O \quad .$$

The water is consumed by reaction with the acetic anhydride to form acetic acid:

$$H_2O + (CH_3\ CO_2)_2O \rightarrow 2\ CH_3CO_2H \quad .$$

Petroleum ether is often used as a solvent to wash the reaction products.

The As_2S_3 was reacted in CS_2 at about 350°C for two hours to remove these impurities. The reaction was successful in removing nearly all of the impurities. Unfortunately, the coatings formed from this material (144-D10-47-1 and 152-5-47-2) had three times higher

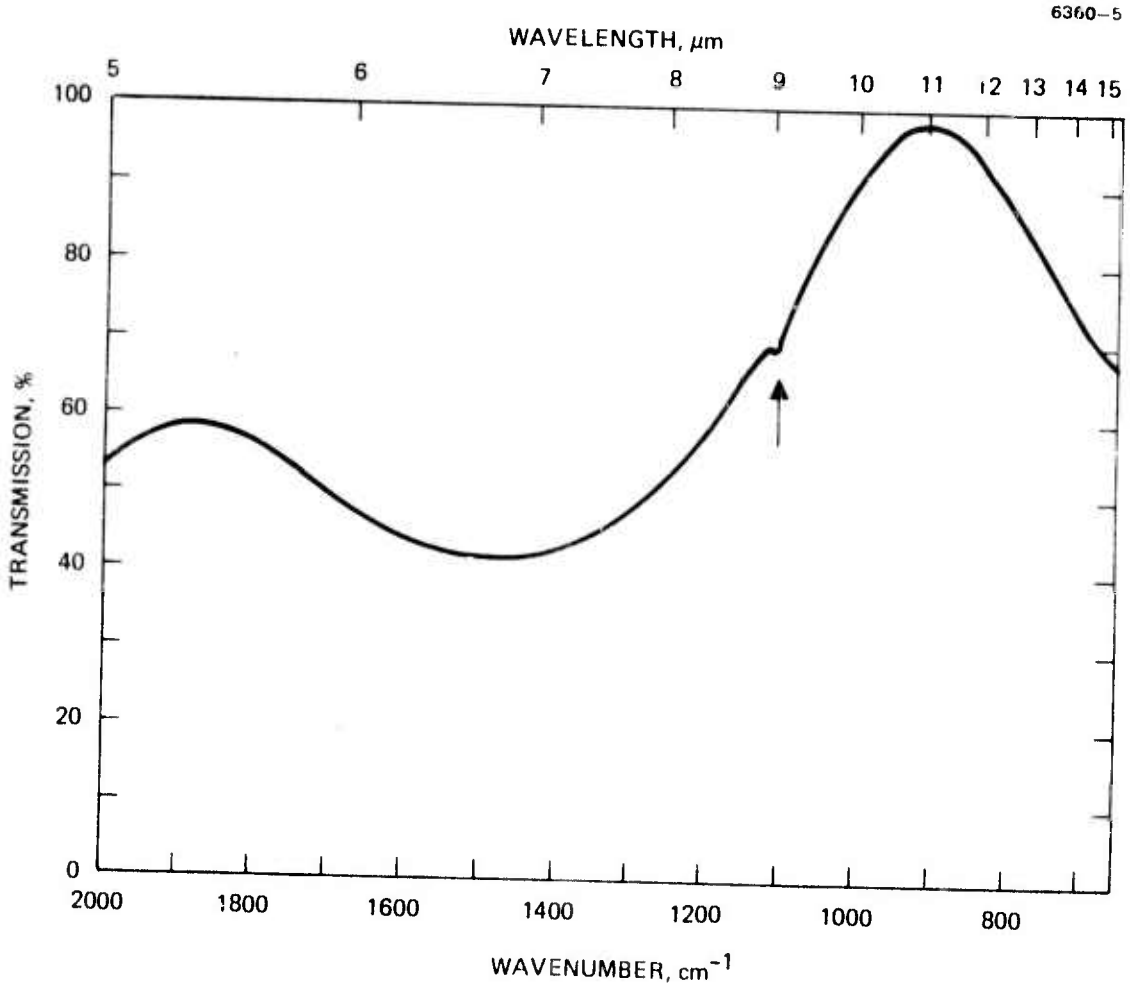

Figure 13. 147-5-51-3 AR coating transmission spectrum. Note dip at 9 μm.

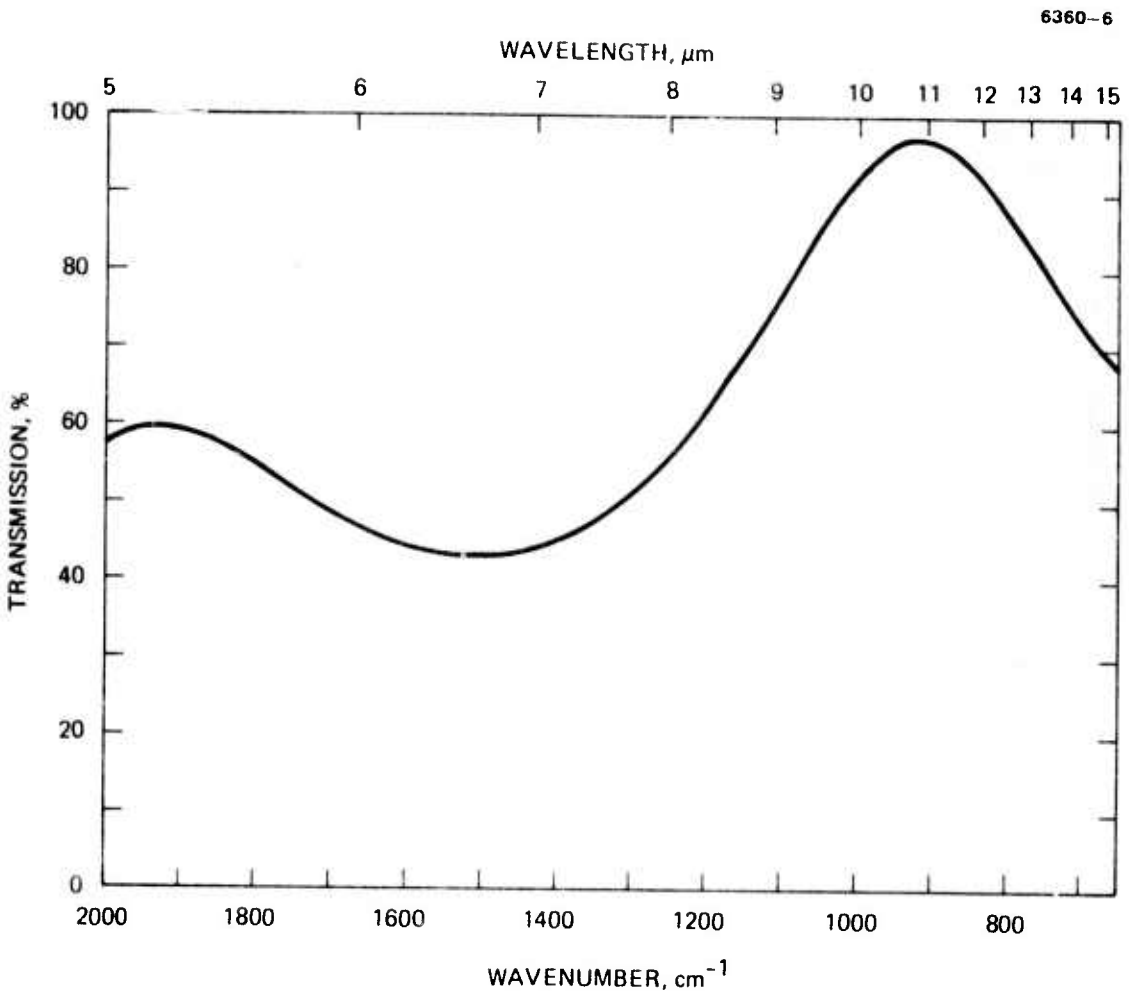

Figure 14. 147-13-50-4 coating transmission spectrum.

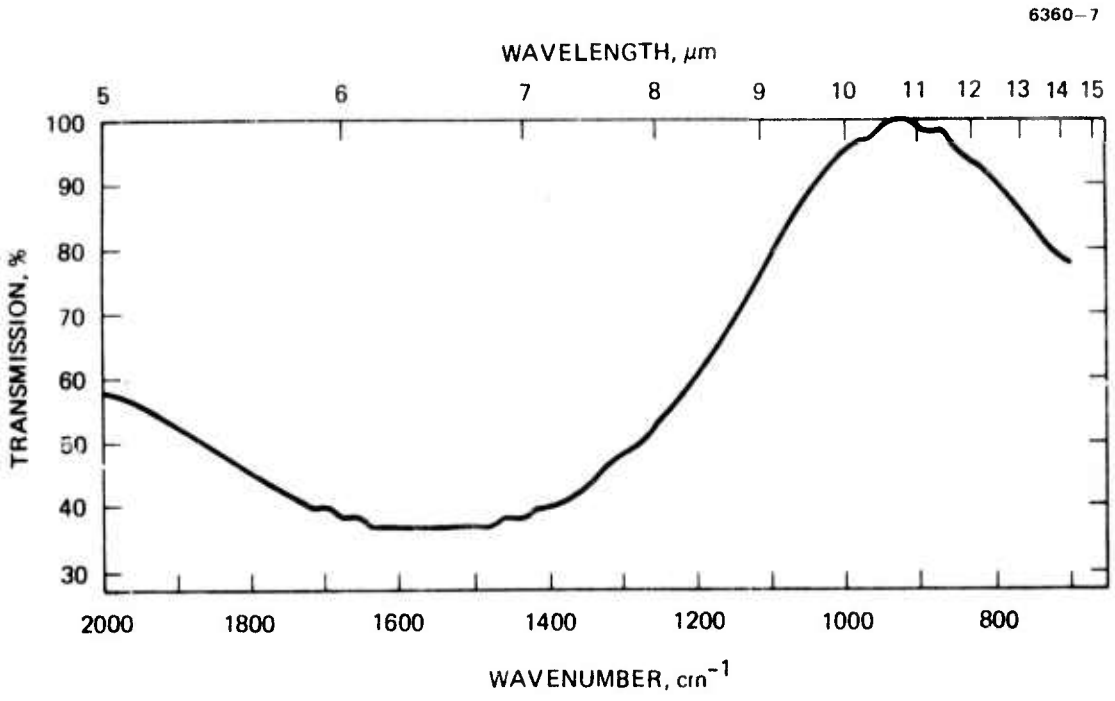

Figure 15. 147-13-50-4 theoretical transmission spectrum.

Table 11. Single Layer As_2S_3 Films on KCl

Sample No.	Source of As_2S_3	As_2S_3 Thickness, μm	Sample Absorption, %				Coating Absorption, %		Absorption Coefficient, cm^{-1}		Remarks
			9.28 μm		10.6 μm						
			Uncoated	Coated	Uncoated	Coated	9.28 μm	10.6 μm	9.28 μm	10.6 μm	
Deposited under Standard Vacuum Conditions											
2577	HRL	3.70	0.031	0.284	0.021	0.221	0.25	0.20	5.9	5.9	
Deposited under UHV Conditions											
152-1-46-1	ACC	2.15	0.12	0.36	(a)	(a)	0.28	--	12	-	Water evolved (see text)
152-3-46-2	ACC	2.14	0.08	0.33	(a)	(a)	0.25	--	11	--	Water evolved (see text)
144-D10-47-1	ACC reacted in CS_2	1.98	0.12	1.00	(a)	(a)	0.88	--	41	--	6% dip in transmission at 9 μm
152-5-47-2	ACC reacted in CS_2	1.98	0.09	0.97	(a)	(a)	0.88	--	41	--	6% dip in transmission at 9 μm
AFML Samples — UHV Deposited											
8-4-5-2	HRL	2.08	0.185	0.325	(a)	(a)	0.14	--	6.2	--	
8-1-5-3	HRL	2.08	0.081	0.270	(a)	(a)	0.19	--	8.4	--	
9-16-5-1	HRL	5.82	0.240	0.361	(a)	0.037	0.12	<0.09	2.0	<2.2	

[a] Not measured.

5795

absorption losses because of the presence of a significant 9 μm absorption band. This is shown in Figures 16 and 17. This was unexpected, since the reprocessed As_2S_3 did not show any significant outgassing during the deposition of the films. Electron microprobe analysis of the film did not reveal any contaminants. Because the microprobe is insensitive to oxygen, and because it is not a quantitative instrument, it is not possible to determine if As_2O_3 or As_2S_5 were the cause of the increased absorption.

Because the 9 μm absorption band was also seen in As_2Se_3 films, it appears that it is associated with arsenic, which is common to both films. Vasko[10] reports that As_2O_3 exists in three forms; cubic, monoclinic, and glassy. The cubic converts to the glassy at about 250 to 300°C. The glassy is similar to the monoclinic, which has a strong absorption at 1100 cm^{-1} or 9 μm. The cubic form exhibits an absorption band at 9.5 μm. The magnitude of these bands is dependent on the thermal history of the As_2O_3.

The presence of As_2O_3 would present a serious problem because it has about the same volatility as do As_2S_3 and As_2Se_3. Three additional batches of As_2Se_3 were prepared by different techniques to determine if oxides could be excluded. The HRL As_2Se_3 used in these film studies (HRL-1 shown in Figure 18) has about a 4% dip at about 8.9 μm. A second batch (HRL-2) of As_2Se_3 was prepared from 99.999% pure arsenic that had a black surface, which indicates that it is oxidized. This material has about 6 strong absorption bands that have been associated with oxide impurities.[11] The transmission scan of this material is shown in Figure 18. Two more samples of As_2Se_3 (HRL-3 and HRL-4) were prepared from arsenic metal that had a metallic (shiny) surface. These were free of any significant absorption bands in the 10 μm region and have smaller absorption bands at longer wavelengths (see Figure 18).

We attempted to use KBr powder pellet and Nujol mull techniques to trace these absorption problems in As_2S_3 and As_2Se_3, but were unsuccessful. The problem may be associated with grinding the materials in air. The transmission spectra presented in Figure 18 were obtained from segments of the As_2Se_3 glasses.

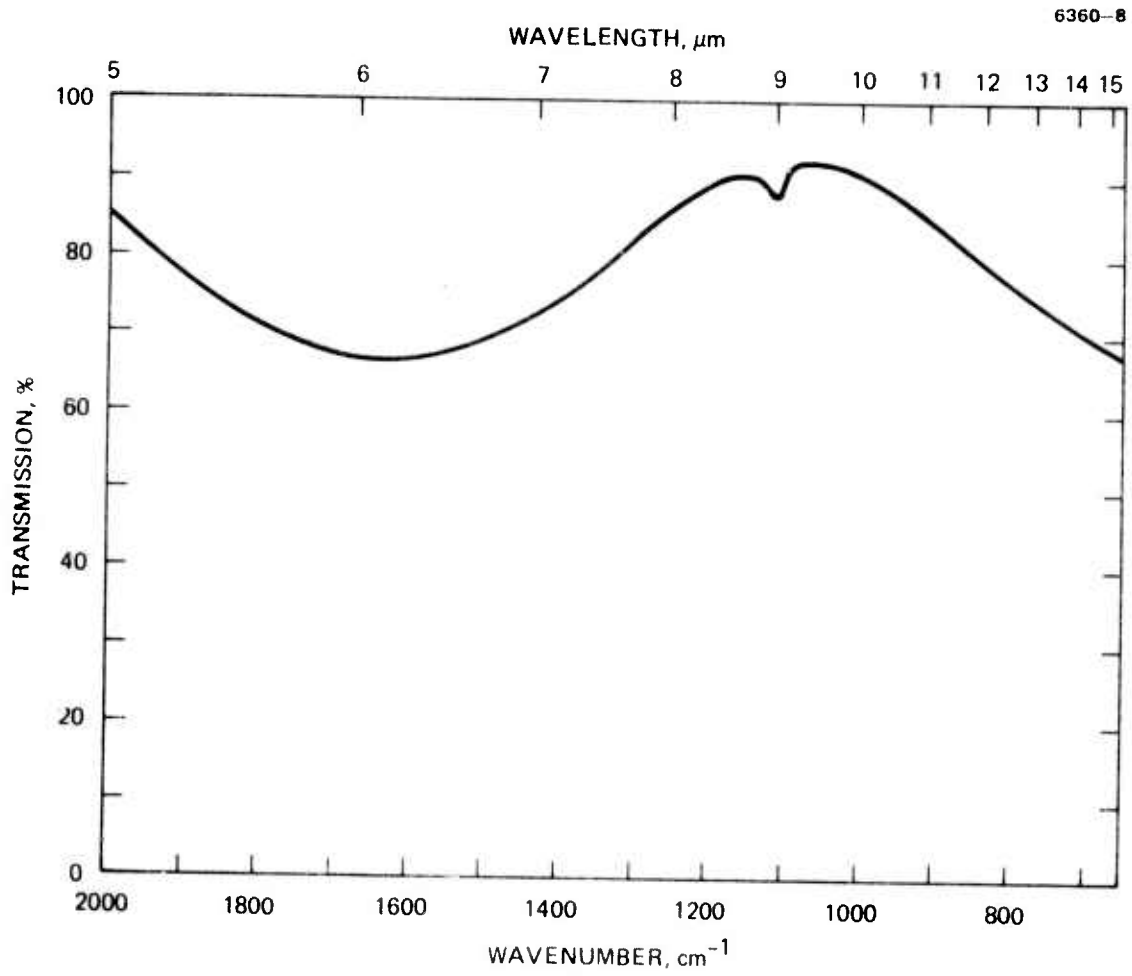

Figure 16. 144-D10-47-1 coating transmission spectrum.

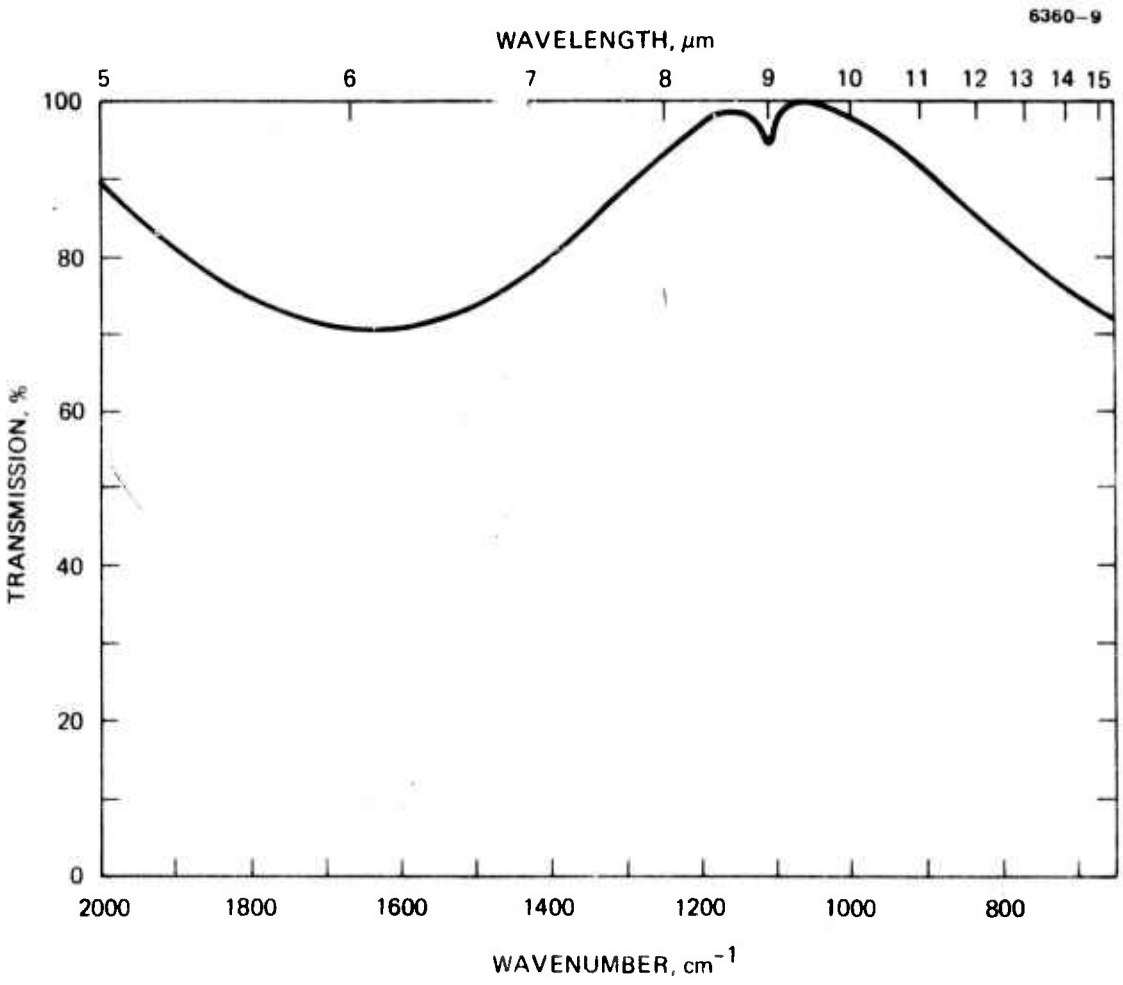

Figure 17. 152-5-47-2 coating transmission spectrum.

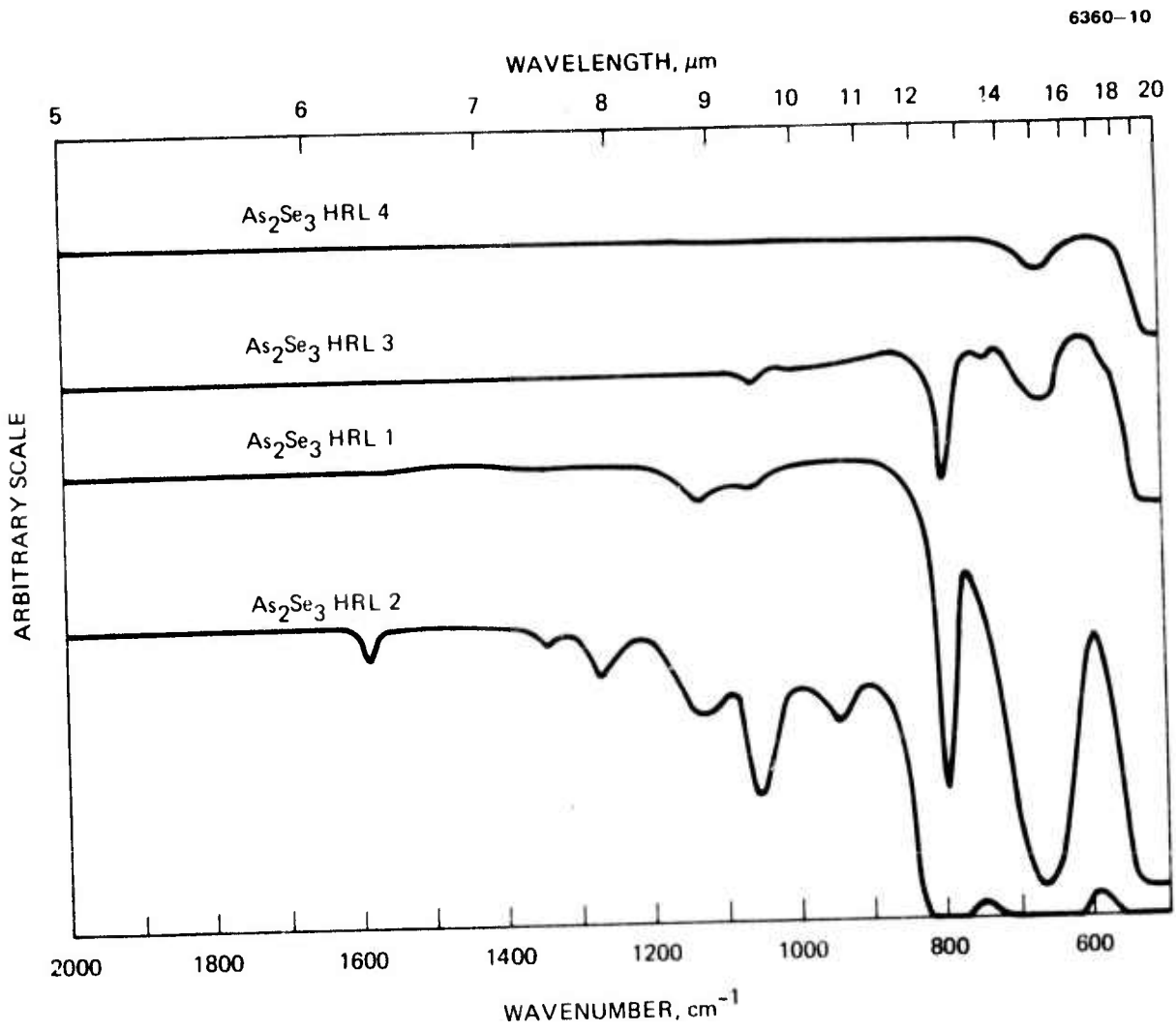

Figure 18. Composite HRL As_2Se_3 glasses: HRL-1, HRL-2, HRL-3, and HRL-4.

One sample of an $As_2Se_3/NaF/As_2Se_3$ AR coating on KCl was deposited under conventional vacuum conditions. Since the purpose of this first run was to establish optical monitoring to obtain a film with minimum reflection at 10.6 μm, the deposition was made on an unheated substrate. This resulted in water absorption in the NaF film. As a result, the AR coating had an absorption of 0.30% per surface.

A study of candidate materials for 3.8 μm coatings was initiated with the deposition of 0.5 λ single-layer films of YbF_3, PbF_2, ThF_4, NaF, LiF, and SrF_2 on CaF_2 substrates and on KCl substrates. These preliminary efforts were to establish deposition parameters. A detailed study of the optical properties of these films formed under conventional and UHV conditions will be made in the second half of the program.

During the course of this program and a companion, AFML-sponsored program, we measured the absorption of single and polycrystalline KCl at both 10.6 and 9.27 μm. To minimize any differences that might arise from surface variation, the samples were mounted in the calorimeter and sequentially irradiated at the respective wavelengths. Although the focal point was constant, there were variations in beam size caused by mode differences. In all cases, the absorption (β) was greater at 9.27 μm. A total of 23 samples of single-crystal KCl were tested. The average ratio of $\beta(9.27)/\beta(10.6)$ was 2.71 ± 0.93. A total of 22 polycrystalline KCl samples exhibited a ratio of 2.28 ± 1.06. The large standard deviations imply that these values should be considered to be from the same population and thus can be averaged to a ratio of 2.5.

The refractive indices of As_2S_3 and As_2Se_3 were determined by two techniques. The results of the modulated light ellipsometry are discussed in Section 4. B of this report. The second method (which involved observation of the channel spectrum of the film and an analysis of the position of the maxima and minima) was performed as described below.

Single-layer coatings were deposited on one face of a KCl substrate. The thickness of the films ranged approximately from 1 to 3 μm. A Beckman IR-12 spectrometer was used to obtain the transmission spectra. Tne film thickness was measured with a Zeiss interference microscope. Film thicknesses were also measured with a mechanical stylus instrument. These values were not used because they were not sufficiently accurate or reproducible.

The absolute accuracy of the method is limited by how accurately the film thickness was determined and how accurate the spectrophotometer trace was. The film thicknesses were measured at the edge of the film, and the optical measurements were taken in the center of the film. Also, thickness measurements at different places on the sample appeared to have a random variation of about 2%. In the As_2Se_3 case, four samples were used. A total of 28 data points were obtained in the range from 2.5 to 12 μm. At 10.6 μm, the index is 2.80, and the estimated error is ±0.03. A single sample of As_2S_3 with 13 data points gave a 10.6 μm value of 2.36 ± 0.03. Two of the As_2Se_3 samples, analyzed by the modulated light ellipsometer, produced index values of 2.843 ± 0.071 and 2.814 ± 0.101. The As_2S_3 index was determined to be 2.432 ± 0.039.

A determination of the refractive index in the range of 0.6 to 2.5 μm was made using a Cary spectrophotometer to obtain the transmission spectra. The transmission maxima and minima appeared to be shifted about 0.04 μm when compared to the Beckman data. The difference was not due to instrument error, since both spectrophotometers were checked and found to be accurate. Also, the difference was not due to sample position. It was most probably due to the use of a more convergent light beam in the Cary. The shift produced a 0.04 shift in the apparent refractive index.

4. Summary

We found that the vacuum environment has a very pronounced effect on the 9.28 and 10.6 μm absorption of the $As_2Se_3/KCl/As_2Se_3$ films, and on the 9.28 μm absorption of the $As_2S_3/KCl/As_2S_3$ films. It has a small effect on the 10.6 μm absorption of the latter films. The most probable explanation is that the As_2Se_3 may be more sensitive to oxidation by the residual gases during the film deposition.

Impurities were found in both the As_2S_3 and the As_2Se_3 materials that had a very pronounced effect on the film properties. In some cases, the impurities were more volatile and thus could be fractioned out of the parent material by vacuum outgassing. In others, the vapor pressure of both were approximately equal, thus precluding vacuum clean up.

Careful control of the starting materials and of the reaction system were found to be necessary to produce oxide-free As_2Se_3. This is essential, since there are several strong oxide absorption bands in the 10 μm region.

Both single and polycrystalline KCl, which is presently used as substrate material, have an absorption at 9.27 μm that is about 2.5 times greater than that at 10.6 μm. This may imply that some impurity is present that must be removed to achieve low absorption at 9.27 μm.

D. OPTICAL EVALUATION

1. Calorimetric Absorption Measurements

The most important aspect of the fabrication of high-power laser windows is the minimization of the losses in the bulk substrate and film coating materials. The predominant losses have been absorption of the laser radiation, particularly surface and film absorption. Methods were therefore derived for measuring very low levels of absorption in infrared materials, with adiabatic absorption calorimetry now the "standard" against which other methods are calibrated and evaluated. The current limit to laser calorimetry appears to be $\beta \approx 10^{-6}$ cm^{-1} for a bulk absorption coefficient in a long bar, with some crystals exhibiting absorption at 5.4 μm equal to or less than the sensitivity limit of the instrumentation. The following example illustrates the normal process. The crystal grower receives information on his product versus different growth conditions and then improves the product to the point where its properties exceed the measurement limits of the instrumentation. The optical evaluation procedures are then improved to measure the new crystals. This continues until the ultimate limit of the crystal or the instrumentation is reached. The requirements are less critical for the measurement of absorption in coatings and surfaces since they usually have absorption coefficient values an order of magnitude or more greater than the bulk crystal substrate. The problem then becomes one of separating the surface (either coated or uncoated) from the total absorption of the crystal. Several variations of the long bar technique pioneered by M. Hass[12] have been used for this and will be discussed in detail in subsequent paragraphs.

The general technique of adiabatic laser calorimetry has been extensively discussed in the literature and will not be reviewed here. References include: Final Technical Report (January 1977) Laser Window Surface Finishing and Coating Science[2] and papers by Deutsch[13] and Hass.[14]

a. CO_2 Laser Calorimeter

The CO_2 laser calorimeter system is illustrated in Figure 19. The output of the CO_2 laser is folded 180° by two mirrors and focused to a beam size of less than 1 mm with an AR-coated ZnSe lens of 46 cm focal length. An He-Ne alignment laser is folded into the CO_2 beam path by a ZnSe beamsplitter AR-coated for 45°.

A new calorimeter head has been designed for use at CO_2 and HF/DF wavelengths; it is illustrated in Figure 20. The body of the calorimeter is made of aluminum with removable front and back flanges, also of aluminum. The sample is mounted in a ring suspended from a nylon rod, as shown in Figure 21. Sharp-point nylon pins, one of which is spring loaded, actually hold the sample in place. The sample is aligned by removing the front flange, adjusting the tilt, and rotating the sample mount. The tilt adjustment is a new addition and has proven very helpful in careful alignment of samples. The windows, AR-coated ZnSe, are mounted on bellows with tilt adjustments in two directions (Figure 20). This enables the operator to align the windows perpendicular to the laser beam and reduces still further the chance of stray reflectances hitting the thermocouple. The thermocouples are Isonel-insulated 0.005 in. copper/constantan wire tightly twisted together. The reference thermocouples are embedded in a cylindrical copper block mounted around the nylon rod to which the sample holder is attached. This location places the reference out of the probable paths for scattered or sample-reflected radiation. Various shields are available for mounting on the sample holder but have not been needed for the samples measured.

The system is pumped by a high-pressure nitrogen Venturi or a carbon-vane roughing pump and liquid-nitrogen-cooled zeolite sorption pumps with the appropriate valve system. We decided to use a completely oil-free system to eliminate any possible contamination of window and sample surfaces from oil backstreaming from a mechanical pump. This type of pumping system also allows the atmosphere in the calorimeter to be carefully controlled for environmental studies.

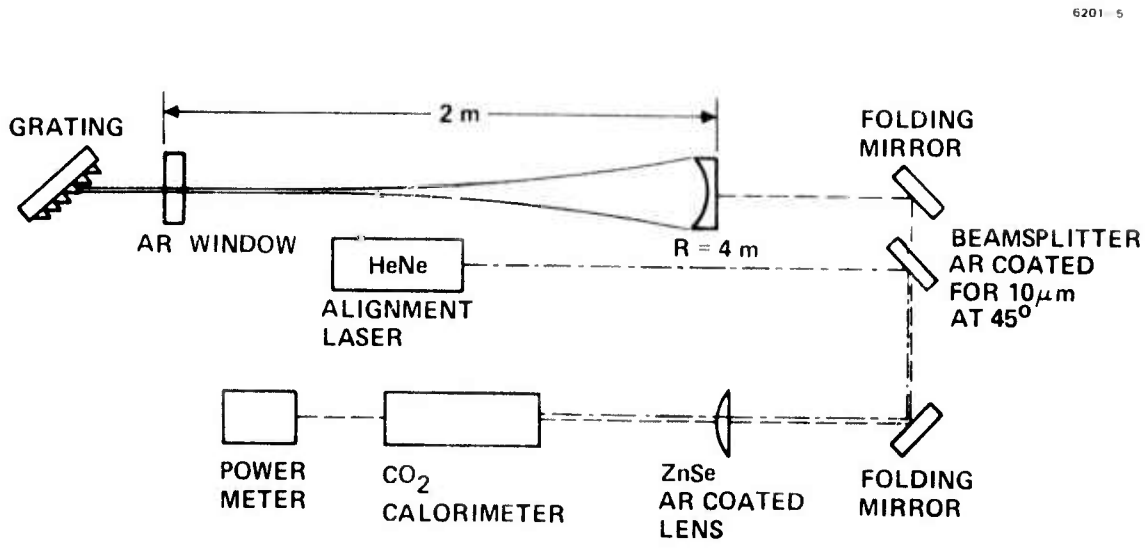

Figure 19. Optical train of the CO_2 laser calorimeter.

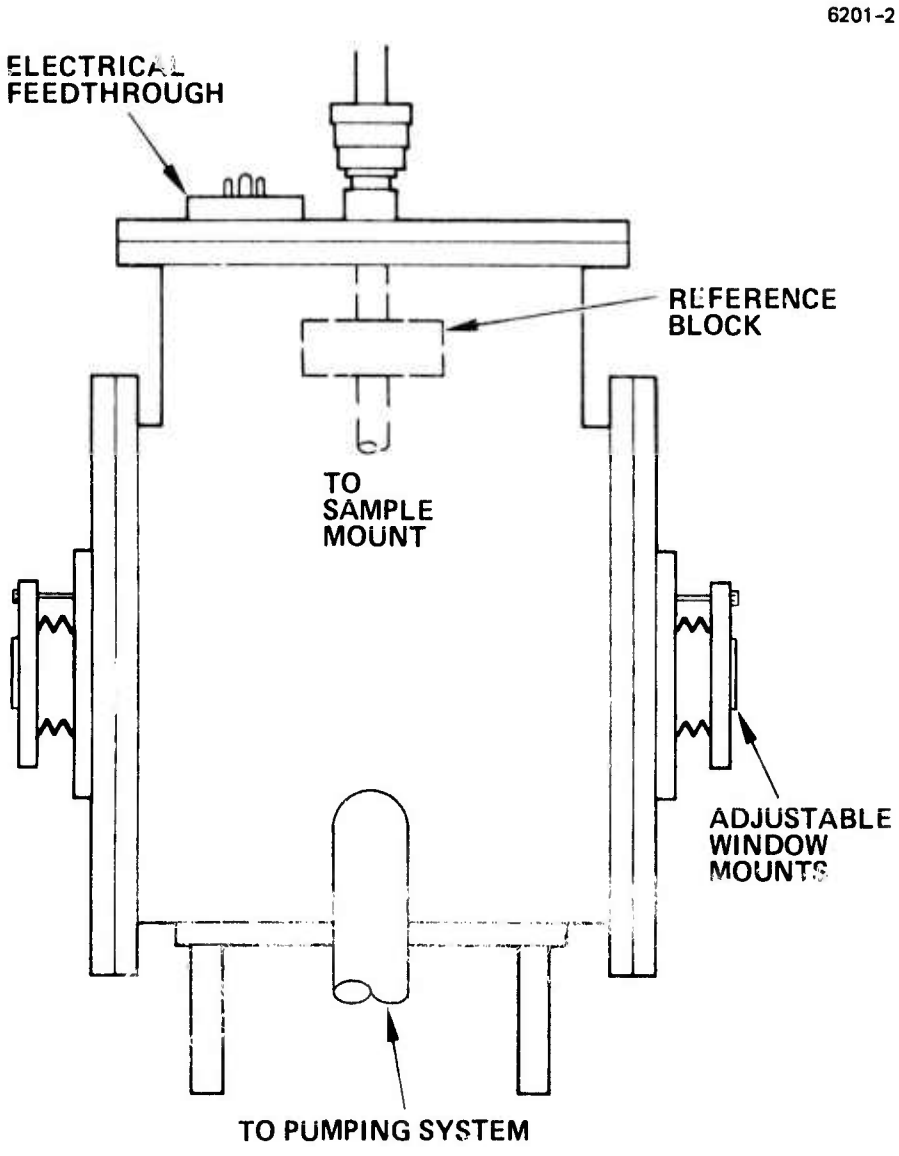

Figure 20. Vacuum calorimeter.

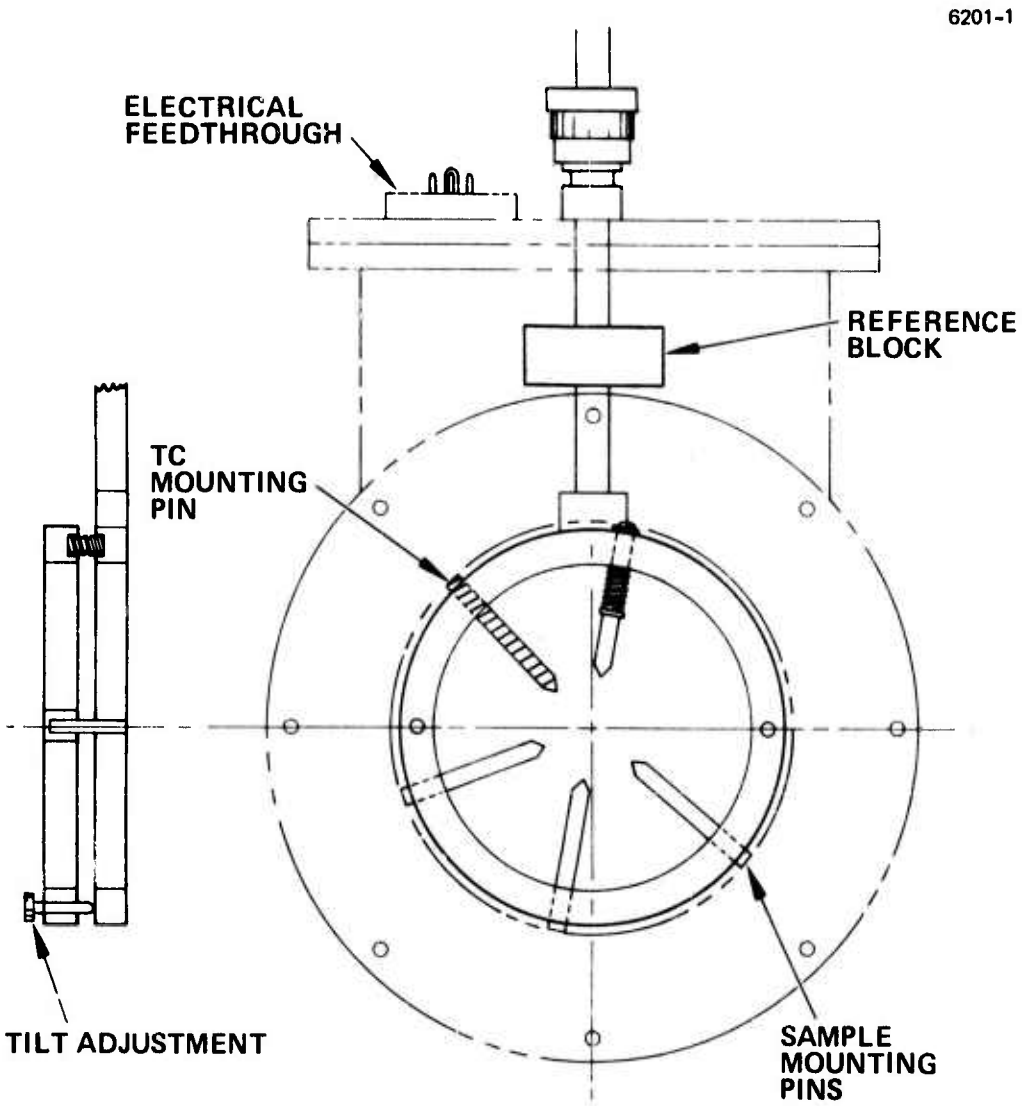

Figure 21. Calorimeter mount for window samples.

The tunable CO_2 laser used in the calorimeter is a 2 m optical cavity, hemiconfocal system with a 4 m radius, AR-coated ZnSe 85% output coupler. The grating occupies the other end of the optical cavity with a broad-band AR-coated window isolating the active medium. The laser is tunable from 9.2 μm to 10.8 μm over the mid-range of the R and P branches of the 001 → 020 and 001 → 100 vibrational modes of the CO_2 molecule. Power in individual lines varies from approximately 5 W to more than 10 W with power stability good to excellent in the high-gain lines and fair in the lower gain transitions. The laser is operated with a premixed gas (CO_2, 4 to 5%; N_2, 12.5 to 14.5%; with He comprising the balance)in a flowing mode in a water-cooled discharge tube. The grating is cooled by a stream of gaseous nitrogen directed at the rear surface of the metal substrate. An intracavity aperture can be used to limit the transverse modes, but optimal power stability seems to be obtained on multimode operation.

The results of measurements at 9.27 μm and 10.6 μm are presented in Table 12. The absorption coefficients for NdF_3 and ThF_4 are listed for information only since this data was reported on Contract F33615-76-C-5449.

The results for NdF_3 and ThF_4 are interesting because the values are considerably higher than those measured in transmission (2.9 cm^{-1} calorimetrically versus 6.3 cm^{-1} in transmission for NdF_3 and 1.2 cm^{-1} calorimetrically versus 3.1 in transmission for ThF_4). This discrepancy is common for absorption coefficients of this magnitude, but the cause is unknown.

For NaF, the values measured calorimetrically and in transmission on the Beckman IR-12 agree to within 5%, but the absolute values are an order of magnitude lower than for NdF_3 and ThF_4. For comparison, the AFCRL Compendium on High Power Laser Window Materials (1972) gives $\beta = 0.77$ cm^{-1} at 10.5 μm for NaF. The values listed in Table 12 for the RAP cast NaF are considerably better.

The NaCl samples were measured at 10.6 μm, 9.27 μm, and 5.3 μm with measurements planned at 2.8 and 3.8 μm. The results agree with the fact that NaCl is still in the multiphonon absorption

Table 12. CO_2 Absorption Measurements

Sample No.	9.2 μm β, cm^{-1}	10.6 μm β, cm^{-1}	Length, cm	Comments
NdF_3 H2888-06-1B		2.9	0.4445	RAP Bridgman
ThF_4 H2888-16A		1.2	0.5030	RAP Czochralski
NaF H2872-49a	0.11	0.62	0.6350	RAP cast
LiF	β(5.1) = 0.14 cm^{-1}		1.750	RAP cast material, absorption taken from Beckman scan
CsI		0.0004	0.6655	Harshaw Sample
NaCl				RAP Bridgman
B173-3	0.00026	0.0010	4.064	
B175-4	0.00029	0.00099	4.079	
B175-6	0.00041	0.00099	4.039	
B175-7	0.00088	0.0014	3.404	
KCl	β(10.6 μm) bulk (cm^{-1})	β(10.6 μm) surface + bulk (cm^{-1})		RAP Bridgman
B160	7.6×10^{-5}	1.2×10^{-4}	16.80	N_2/CCl_4
B161	6.3×10^{-5}	7.6×10^{-5}	17.50	$H_2/CO_2/CCl_4$
B162	1.0×10^{-4}	1.0×10^{-4}	17.82	He/CCl_4
KRS-5		0.0087	0.4724	

region at 10.6 μm, but not at 9.27 μm. The absorption coefficients at 9.27 μm are lower than those at the same wavelength for standard window samples of KCl where the 9.27 μm absorption is frequently greater than that at 10.6 μm, indicating the presence of an impurity absorption in either the bulk or surfaces. Some significant surface absorption is suggested by the larger absorption values measured for sample NaCl B175-7, the length of which is about 80% that of the other samples. The absorption coefficients measured at 5.3 μm for samples NaCl B175-4 and B175-7 were $\beta = 5.2 \times 10^{-5}$ cm^{-1} and 3.5×10^{-5} cm^{-1}, respectively.

The long bar technique[1] was used to separate the bulk and surface absorption at 10.6 μm of a series of KCl bars grown in different atmospheres (see Table 12). Although the measurements were taken in an air calorimeter, the reproducibility of the results was quite good. The implication of these measurements is that the cost of RAP processing could be lowered considerably since N_2 or perhaps even dry air could be used instead of He for the CCl_4 carrier medium. This series of measurements will be repeated in the new calorimeter at several CO_2 wavelengths.

b. CO Laser Calorimeter

Laser calorimetry was used to measure the optical absorption of several candidate window materials for application at CO laser wavelengths. These materials include KCl, CaF_2, SrF_2, and ZnSe. The long, thin-bar technique was used to separate bulk and surface absorption contributions by means of their time dependencies. One sample of KCl, known to be low absorbing at 10.6 μm, exhibited no measurable absorption within the sensitivity of the calorimeter ($\beta_t < 2 \times 10^{-6}$ cm^{-1}). The absorption coefficients measured for two samples of CaF_2 at 5.41 μm were higher than those measured by other investigators at 5.25 μm, but, when fitted to an exponential dependence on wavelength, compared favorably with currently measured values. To compare results from different laboratories, precise definition of the spectral power distribution is essential. The surface absorption

was, in all cases, small relative to similar measurements at 10.6 μm; in several cases it was not separable from bulk absorption by the technique used.

Details of the instrumentation and results obtained at 5.41 μm on the long bar samples are given in the paper presented at the Optical Society of America Topical Conference on Optical Phenomena in Infrared Materials (1 to 3 December 1976 in Annapolis, Maryland). The complete text of the paper is given in Appendix A.

Because of the apparent discrepancies in the measured values of the absorption coefficient of CaF_2 at 5.41 μm and 5.3 μm, the laser was modified to lower the intensity weighted mean wavelength by lowering the temperature of the laser medium. This was accomplished by switching to a dry-ice/ethanol cooling system (reservoir temperature = -40°C) from the ethylene glycol system used previously (reservoir temperature = 0°C). The lower temperature resulted in an average wavelength of 5.3 μm (in agreement with most other laboratories using CO laser calorimetry).

Results on NaCl and SrF_2 samples at 5.3 μm (unless otherwise noted) are given in Table 13. The NaCl samples are the same ones on which data was reported at 9.27 and 10.6 μm. The values at 5.3 μm are quite low, and the measurements should be repeated on more samples, including a long bar sample, to establish statistical limits and to separate surface and bulk absorptions.

The SrF_2 samples were supplied by UDRI from Raytheon Corp. and measured at UDRI. Initial measurements at HRL on the samples as received yielded reproducible results (note that the absorption of SrF_2 does not change with wavelength from 5.41 to 5.3 μm as compared with CaF_2, cf. Appendix A), but the values were more than double the results obtained by UDRI. Careful cleaning of the samples lowered the absorption coefficient to values that correspond to those measured at UDRI, illustrating that for this order of magnitude of absorption coefficient, at least, the values obtained by two different laboratories agree to well within the acknowledged experimental error of 10%.

Table 13. CO Absorption Measurements

Sample No.	5.3 μm β, cm^{-1}	length, cm	Comments
NaCl			
B175-4	5.2×10^{-5}	4.079	
B175-5	3.5×10^{-5}	3.404	
SrF_2			
1840			
11/3/76	5.9×10^{-4}		λ_{center} = 5.41 μm as received
12/1/76	5.7×10^{-4}		λ_{center} = 5.3 μm as received
1/18/77	2.5×10^{-4}		λ_{center} = 5.3 μm carefully cleaned
2/17/77	3.3×10^{-4}		Cleaned but not measured immediately
UDRI	2.0×10^{-4}		
1842			
11.5/76	4.5×10^{-4}		λ_{center} = 5.41 μm as received
12/3/76	4.2×10^{-4}		λ_{center} = 5.3 μm as received
1/18/77	2.6×10^{-4}		λ_{center} = 5.3 μm carefully cleaned
2/17/77	2.3×10^{-4}		λ_{center} = 5.3 μm carefully cleaned
UDRI	2.4×10^{-4}		

HRL participated in the CO Round Robin sponsored by UDRI and coordinated by John Detrio. The results of the four participating laboratories were presented and analyzed at the LWTVP meeting in Annapolis, Maryland, 20 April 1977. The results are summarized in Table 14. According to John Detrio, there was a small discrepancy in the masses measured at HRL and the other laboratories (Table 15), and this data is being checked. The balance used to measure the samples is periodically calibrated against a National Bureau of Standards set of calibrated weights and should be accurate. The difference is much less than other error sources in any case and can be neglected for the purpose of data analysis. With the exception of the Northrop data, a general increase in measured absorption coefficient with time is noted for the CaF_2 samples in Group II. Absorption versus time is plotted in Figure 22 for one sample from each subgroup. UDRI plans to remeasure the samples in the near future and the results will be reported when received. Even neglecting the apparent increase with time, the data agrees fairly well with an average standard deviation of 13%.

c. HF/DF Calorimetry

As high-power chemical lasers became increasingly important, the emphasis in our optical absorption studies shifted from CO_2 and CO wavelengths to the 2 to 4 μm region of the DF/HF chemical laser. Transparent coatings and materials have been investigated at both 3.8 (DF) and 2.7 (HF) μm using a small cw chemical laser and calorimetric techniques to measure the absorption coefficient β. Since fluoride materials still remain the prime candidates for low-loss applications, our studies at the chemical laser wavelengths have been directed primarily toward CaF_2 and SrF_2. Single-layer thin films of fluoride, oxide, and semiconducting materials have been deposited on these materials to survey candidates for use in low-loss, multilayer dielectric stacks. Of all the materials surveyed to date, the fluoride and semiconducting coatings have had the smallest absorption, while the absorption of the oxides has been approximately ten times higher.

Table 14. Interlaboratory Comparison Study — CO Laser Calorimetry
Group II

Absorption Coefficient $\beta(cm^{-1}) \div 10^{-4}$

Laboratory	Date	Group A — II				Group B — II				Clean
		Average	1337	1429	1507	Average	1375	1387	1508	
Hughes	3-3-77					11.1	12.0	13.0	8.5	HU
		10.47	15.0	7.6	8.8	11.0	12.0	13.0	8.1	CTRL
Northrop	11-9-76					7.15	8.24	7.78	5.43	NO
		6.54	9.43	5.09	5.09					CTRL
Raytheon	9-1-76					8.37	8.80	9.50	6.8	RA
		8.33	12.6	5.9	6.4	7.93	8.90	8.90	6.0	CTRL
UDRI 1	10-18-76					7.99	9.59 9.22	7.73 7.35	7.00 7.02	UD
		7.44	9.74 10.0	5.47 5.94	7.30 6.16	7.25	9.02 6.72	7.83 7.42	5.59 6.89	CTRL
						9.00	10.5 11.3 8.88	8.77 7.53	8.07 7.92	UD
UDRI 2	2-2-77									
		10.24	11.4 14.9 13.3	7.32 7.41	9.44 7.94	10.56	11.4 10.8	11.8 12.1	8.72 8.51	CTRL

Table 15. Interlaboratory Comparison Study

Laboratory	$C_p \frac{2n}{n^2+1}$, $\frac{J}{g\,^oC}$	Mass Length, g/cm											
		1427	1506	1509	1373	1429	1507	1382	1428	1445	1375	1387	1508
Hughes	0.8075				36.18	36.13	36.39				36.18	36.06	36.09
Northrop	0.8586	35.97	36.16	36.06	36.13	36.04	36.15	36.08	35.98	36.07	36.12	36.05	35.98
Raytheon	0.8075				36.16	36.05	36.22				36.21	36.10	36.01
UDRI	0.8362	35.91	36.28	36.10	36.08	36.05	36.18	36.09	36.11	36.17	36.17	36.11	36.04
Mean	0.8275	35.94	36.22	36.08	36.14	36.07	36.24	36.09	36.05	36.12	36.17	36.09	36.03

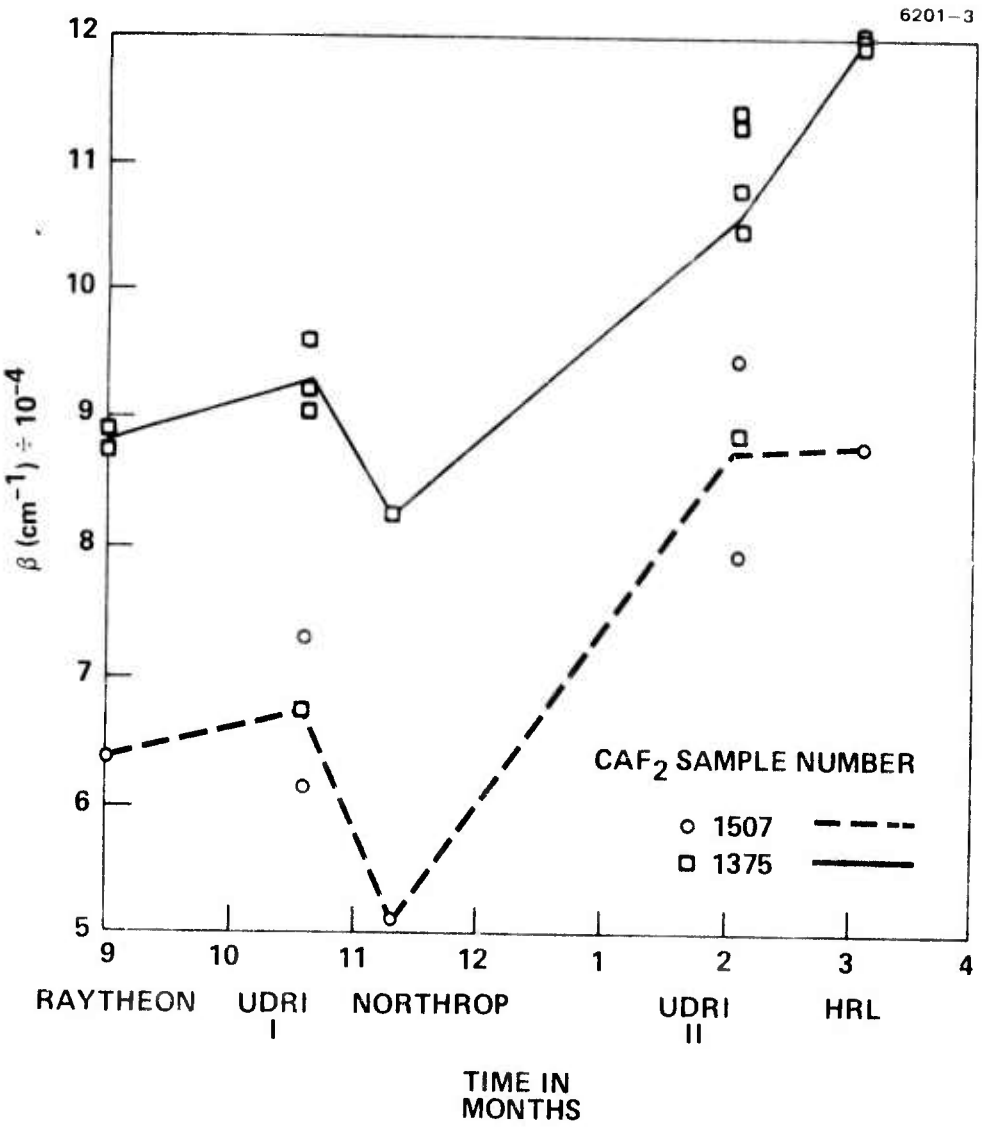

Figure 22. CaF_2 absorption coefficient time line.

The fluoride substrates themselves had absorption coefficients somewhat dependent on surface finishing and cleaning methods but, in general, the HF β was found to be 3 to 4 times greater than the DF β.

A major objective of this work, in addition to surveying candidate materials for use as low-loss windows and coatings on DF/HF lasers, is to study the nature of the higher absorption observed at 2.7 μm (HF). The optical absorption coefficient was measured using a cw DF/HF chemical laser and a conventional air or vacuum calorimeter. The physical arrangement and optical alignment of these basic components of our calorimetric set-up are shown in Figure 23. The system shown is by now fairly conventional, and only the few features peculiar to DF/HF laser calorimetry need mentioning. The rf noise from the discharge tubes is minimized by using a screen cage surrounding the tubes and by keeping the calorimeter away from the tubes, as shown in Figure 23. Even so, there is still some slight noise of approximately 0.03 μV when the laser is operating. This does not, however, cause error in our calorimetry even when the 1 μV scale of the nanovolt null detector is being used. The lens and calorimeter windows are AR-coated CaF_2 for both 2.7 and 3.8 μm.

The cw DF/HF chemical laser shown in Figure 24 was purchased from M. B. Ferguson and Company (in association with the University of Alabama in Huntsville). When using the external optics as pictured, the laser delivers approximately 4 to 7 W of DF power and about 9 W of HF power. In normal usage (500 mA discharge tube current; 600 cfm pumping speed; and partial pressures of 2 Torr He, 1.5 Torr H_2 or D_2, 0.5 Torr SF_6, and 0.1 Torr O_2), a single output coupler is used for both DF and HF radiation. Because the DF output mirror will provide about 3 W of HF power, it will not be necessary to change the optics for DF and HF measurements. The stability of the laser is $\pm 2\%$ DF and $\pm 5\%$ HF.

Cleaning the sample before taking measurements is especially important at the chemical laser frequencies. Surface absorption at 2.8 μm can occur because of the presence of OH^- ions, and absorption at 3.5 μm (near DF laser wavelengths) can occur when C-H bonds are present. To minimize the latter source of surface absorption, the

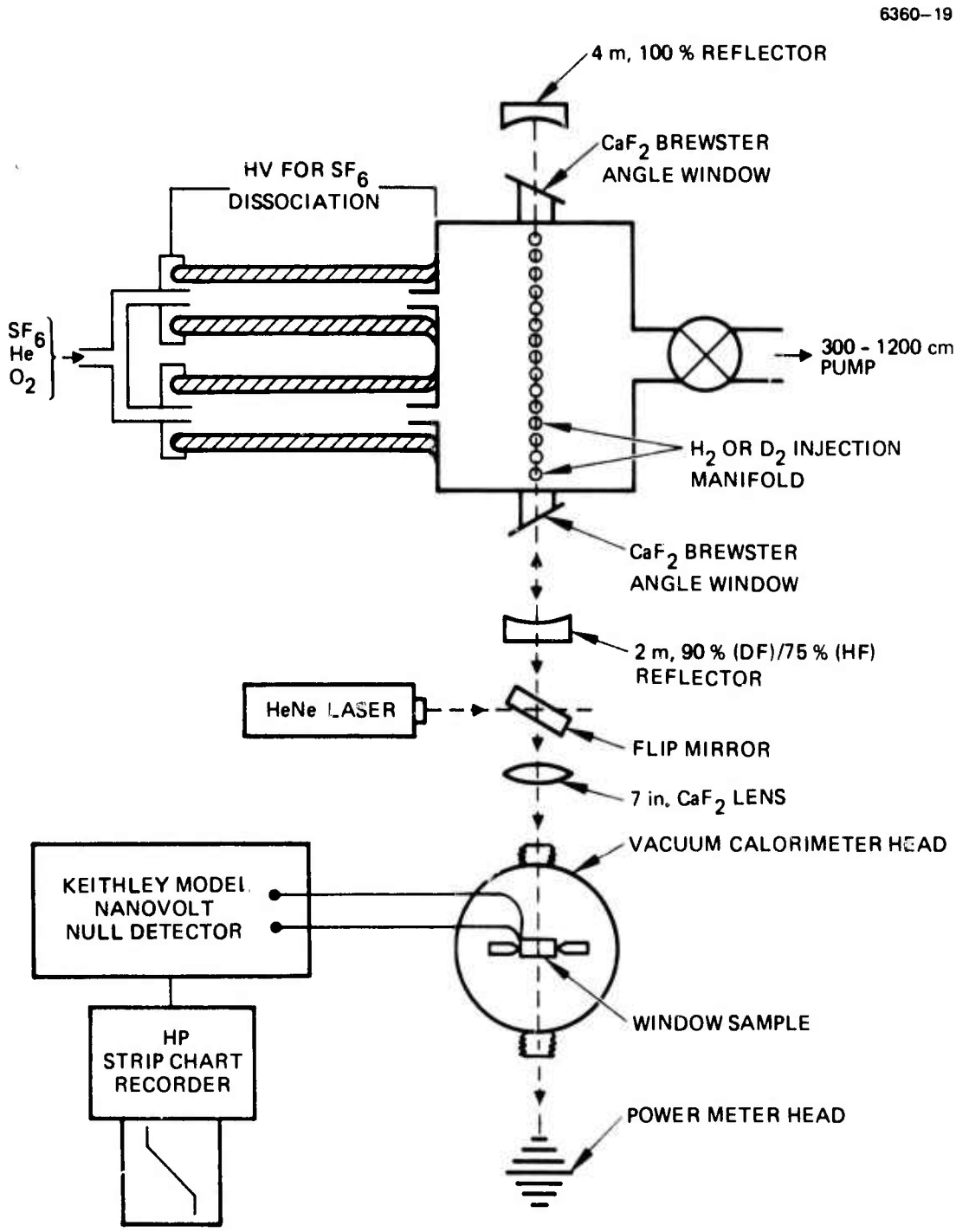

Figure 23. Physical arrangement and optical alignment of calorimeter components.

M12014

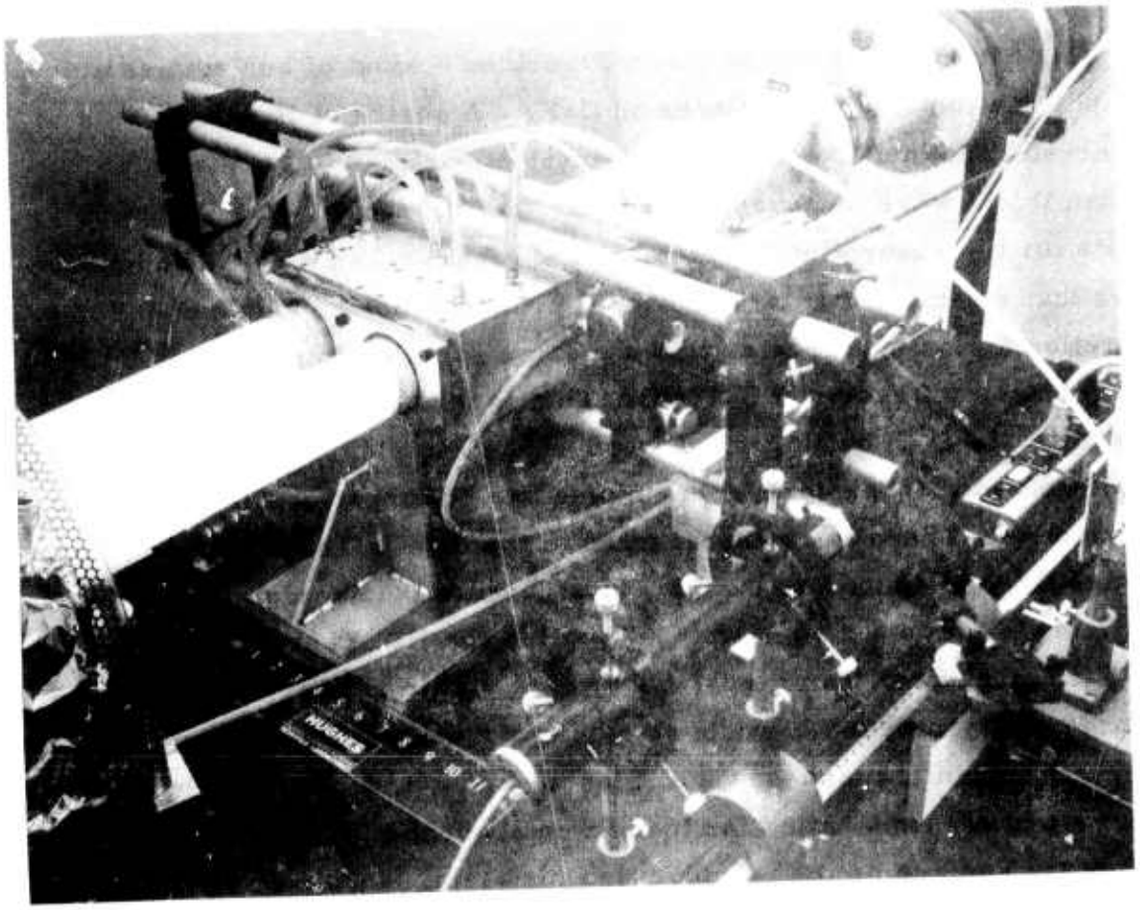

Figure 24. cw DF/HF chemical laser.

sample is final cleaned in a freon degreaser using trichlorotrifluoroethane (Blaco-Tron TF). Before this cleaning, the fluoride samples are sometimes washed with soap (Decontam) and water. Proper cleaning frequently reduces the total absorption coefficient by a factor of between 1.5 and 2 of the uncleaned, as-received sample.

(1) Results: Alkaline Earth Fluorides — Most of our studies at DF and HF wavelengths have been on CaF_2. A series of Harshaw (polycrystalline) and Optovac (single crystal) samples (6 cm diameter by 1 cm thick) were measured at both DF and HF frequencies. The results for the absorption coefficients are given in Table 16. The table shows that a sample that was protected with a carbolene film had an absorption factor of 2 greater than the same sample after cleaning in the degreaser (cf sample FC-18-H). This is probably the result of the removal of the C-H bonds, which were on the sample on removal of the carbolene film. Therefore, the samples are no longer protected in this manner. There is a general trend to the data in Table 16: the average DF β is about 5 to 6 x 10^{-4} cm^{-1}, while the average HF β is approximately 2 to 3 x 10^{-3} cm^{-1}. That is, the HF absorption is nearly 3 to 4 times greater than the DF absorption. This result, which is of fundamental significance, would also be important from a systems point of view if a need for high-power HF laser windows were to develop. The most likely explanation for the higher absorption is absorption by OH^- on the surface or in the bulk of the material. Different polishing and cleaning methods, such as those not using H_2O, will be tried to reduce HF β's, although the bulk material may ultimately limit performance at these wavelengths.

In general, at both DF and HF wavelengths, the absorption in the CaF_2 material studied by us and by others is extrinsically limited. Since the intrinsic, or multiphonon, absorption coefficient calculated at 3.8 μm for CaF_2 is 6.5 x 10^{-8} cm^{-1}, extrinsic processes need be considered at these frequencies. Future plans include controlled surface absorption experiments to attempt to determine the nature and source of the higher absorption at 3.8 and 2.7 μm.

Table 16. Absorption Coefficients at DF and HF Wavelengths for Polycrystalline Harshaw (H) and Single Crystal Optovac (O) Calcium Fluoride

Sample No.	Length, cm	β(DF), cm^{-1}	β(HF), cm^{-1}	Comments
FC-17-H	0.947	$6.33 \pm 1.5 \times 10^{-4}$	1.74×10^{-3}	
FC-18-H	0.985	$1.26 \pm 0.04 \times 10^{-3}$	--	Carbolene film removed
FC-18-H	0.985	$6.34 \pm 0.19 \times 10^{-4}$	--	Cleaned in film degreaser
FC-16-H	1.033	$5.0 \pm 0.5 \times 10^{-4}$	--	
FC-19-H	1.00	$8.94 \pm 0.09 \times 10^{-4}$	--	
FC-13-O	1.082	5.0×10^{-4}	1.8×10^{-3}	
FC-22-H	1.004	$1.06 \pm 0.02 \times 10^{-3}$	$1.94 \pm 0.16 \times 10^{-3}$	Cleaned in freon degreaser
FC-12-O	1.029	$8.21 \pm 0.4 \times 10^{-4}$	$2.39 \pm 0.51 \times 10^{-3}$	Cleaned in freon degreaser
FC-14-O	1.085	$6.89 \pm 0.63 \times 10^{-4}$	$1.69 \pm 0.1 \times 10^{-3}$	Cleaned in freon degreaser
FC-15-O	1.092	$9.30 \pm 1.3 \times 10^{-4}$	$2.16 \pm 0.41 \times 10^{-3}$	Cleaned in freon degreaser
FC-4-O	1.07	$2.89 \pm 0.03 \times 10^{-4}$	$2.91 \pm 1.0 \times 10^{-3}$	Cleaned in freon degreaser
FC-40-H	0.995	$3.92 \pm 0.08 \times 10^{-4}$	$3.20 \pm 0.27 \times 10^{-3}$	Mechanical polish by HRL
FC-39-H	0.998	$3.60 \pm 0.17 \times 10^{-3}$	$6.48 \pm 0.48 \times 10^{-3}$	Mechanical polish by Harshaw
FC-25-H	0.961	$2.64 \pm 0.26 \times 10^{-4}$	$2.24 \pm 0.6 \times 10^{-3}$	Cleaned in freon degreaser
FC-3-O	1.034	$5.83 \pm 0.1 \times 10^{-4}$	$2.50 \pm 0.05 \times 10^{-3}$	Cleaned in freon degreaser
FC-8-O	1.044	$6.22 \pm 0.8 \times 10^{-4}$	$1.80 \pm 0.3 \times 10^{-3}$	Cleaned in freon degreaser
FC-6-O	1.025	$5.98 \pm 0.18 \times 10^{-4}$	$2.24 \pm 0.5 \times 10^{-3}$	Cleaned in freon degreaser
FC-11-O	1.065	$6.14 \pm 0.3 \times 10^{-4}$	$2.11 \pm 0.2 \times 10^{-3}$	Cleaned in freon degreaser
FC-1-O	0.900	$4.76 \pm 0.06 \times 10^{-4}$	$2.62 \pm 0.02 \times 10^{-3}$	Cleaned in freon degreaser
FC-26-H	0.920	$5.78 \pm 0.04 \times 10^{-4}$	$2.94 \pm 0.03 \times 10^{-3}$	Cleaned in freon degreaser
FC-40-H	0.995	$8.48 \pm 0.07 \times 10^{-4}$	$2.31 \pm 0.4 \times 10^{-3}$	HRL etch-polish
FC-39-H	0.998	$3.57 \pm 0.009 \times 10^{-3}$	$4.57 \pm 0.1 \times 10^{-3}$	HRL etch-polish
FC-2-O	1.028	$6.34 \pm 0.07 \times 10^{-4}$	$2.08 \pm 0.036 \times 10^{-3}$	Cleaned in freon degreaser
FC-27-H	0.950	$7.23 \pm 0.025 \times 10^{-4}$	$8.54 \pm 0.023 \times 10^{-4}$	Cleaned in freon degreaser

(2) Results: Single-Layer Coatings on CaF_2 – Many of the substrates characterized above were coated with low-loss materials, which will subsequently be used in AR and enhanced dielectric reflector coatings. Table 17 lists the films ($\lambda/2$ at 3.8 μm) studied at 3.8 and 2.7 μm. Whenever possible, the uncoated β's are also listed. As expected, the fluoride films exhibit low total absorption, and the oxides have substantially higher β's. Again, since the HF β's are proportionally higher than the DF β's, OH^- is suspected to be in the coating. The higher values for the oxide materials are most likely due to the affinity of oxides to OH^- absorption. More work must be done to improve these coating materials since oxides have particularly attractive mechanical and environmental properties. Since the latter property is very important for resistance to the caustic HF or DF chemical laser environments, these materials would be most useful as an outer layer (against hostile atmosphere) in a dielectric stack.

(3) Results: Alkali Halides – Polycrystalline Rb-doped KCl was measured coated (AR) and uncoated at 3.8 and 2.7 μm. The results, given in Table 18, show the wide variation in β's encountered as the surface of the sample was polished and cleaned. As might be expected, the absorption is lowest after an acid etch, and highest after coating. Again, the HF β's are higher than the DF β's.

(4) Results: New Materials – Single crystal ThF_4 and NdF_3 were also studied at 3.8 and 2.7 μm. These materials were prepared in a program to purify and grow high-quality starting material for thin-film deposition. The absorption for ThF_4 (see Table 19) is reasonably low at 3.8 μm, but the β for NdF_3 is quite high.

(5) Results: Measuring the Infrared Absorption in Thin-Film Coatings – Traditionally, the optical absorption in thin dielectric films has been obtained by comparing the absorption in coated and uncoated substrates. A new technique has been developed in which the absorption of the film is obtained directly without resorting to comparison or difference methods. This method relies on the separation of surface and

Table 17. Thin Film Coatings on CaF_2; β Coated and Uncoated

Sample No.	Coating	Length, cm	β(DF), cm^{-1}	β(HF), cm^{-1}
FC-8-0	YbF	1.062	$1.67 \pm 0.2 \times 10^{-3}$	---
	UNC		$6.22 \pm 0.8 \times 10^{-4}$	$1.80 \pm 0.3 \times 10^{-3}$
FC-16-H	PbF_2	1.033	$2.33 \pm 0.1 \times 10^{-3}$	4.90×10^{-3}
	UNC		$5.0 \pm 0.5 \times 10^{-4}$	---
FC-23-H	LiF	0.931	$1.64 \pm 0.02 \times 10^{-3}$	$7.94 \pm 1.2 \times 10^{-3}$
	UNC		---	---
FC-25-H	NaF	0.963	$3.18 \pm 0.05 \times 10^{-3}$	$1.44 \pm 0.1 \times 10^{-2}$
	UNC		$2.64 \pm 0.26 \times 10^{-4}$	$2.24 \pm 0.6 \times 10^{-3}$
FC-27-H	As_2S_3	0.965	$2.23 \pm 0.3 \times 10^{-3}$	$4.03 \pm 0.16 \times 10^{-3}$
	UNC		$7.23 \pm 0.025 \times 10^{-4}$	$8.54 \pm 0.023 \times 10^{-4}$
FC-28-H	As_2Se_3	0.982	$2.03 \pm 0.06 \times 10^{-3}$	$5.56 \pm 0.2 \times 10^{-3}$
	UNC		---	---
FC-29-H	SrF_2	0.930	$7.78 \pm 0.49 \times 10^{-3}$	$5.79 \pm 0.11 \times 10^{-2}$
	UNC		---	---
FC-18-H	ThF_4	0.985	$1.23 \pm 0.12 \times 10^{-3}$	$5.34 \pm 0.15 \times 10^{-3}$
	UNC		$6.34 \pm 0.19 \times 10^{-4}$	---
FC-22-H	Si	1.004	$1.98 \pm 0.06 \times 10^{-2}$	$4.41 \pm 0.24 \times 10^{-2}$
	UNC		$1.06 \pm 0.02 \times 10^{-3}$	$1.94 \pm 0.16 \times 10^{-3}$
FC-13-0	Al_2O_3	1.08	$2.22 \pm 0.02 \times 10^{-2}$	$6.27 \pm 0.12 \times 10^{-2}$
	UNC		5.0×10^{-4}	1.8×10^{-3}
FC-12-0	MgO	1.029	$1.72 \pm 0.06 \times 10^{-2}$	$5.94 \pm 0.1 \times 10^{-2}$
	UNC		$8.21 \pm 0.4 \times 10^{-4}$	$2.39 \pm 0.51 \times 10^{-3}$

Table 18. Absorption Coefficient in Polycrystalline, Rb-Doped KCl

Sample No.	Surface Condition	Length, cm	β(DF), cm^{-1}	β(HF), cm^{-1}
59-D2	As-received	1.0262	$6.94 \pm 0.1 \times 10^{-4}$	$3.12 \pm 0.1 \times 10^{-3}$
	Mechanically polished flat		$2.25 \pm 0.02 \times 10^{-3}$	$5.76 \pm 0.4 \times 10^{-3}$
	HCl etch ~10 sec		$5.77 \pm 0.1 \times 10^{-4}$	$2.68 \pm 0.05 \times 10^{-3}$
	AR coated		$4.89 \pm 0.15 \times 10^{-3}$	$1.29 \pm 0.02 \times 10^{-2}$
57-C5	As-received	1.0274	$7.29 \pm 0.36 \times 10^{-4}$	$3.06 \pm 0.5 \times 10^{-3}$
	Mechanically polished flat		$4.32 \pm 0.2 \times 10^{-3}$	$9.85 \pm 0.3 \times 10^{-3}$
	HCl etch ~20 sec		$2.94 \pm 0.2 \times 10^{-4}$	$2.97 \pm 0.12 \times 10^{-3}$
	Buff and re-etch		$4.29 \pm 0.12 \times 10^{-4}$	$3.15 \pm 0.21 \times 10^{-3}$
	AR coated		$1.21 \pm 0.12 \times 10^{-2}$	---
54	As-received	1.026	$9.17 \pm 0.54 \times 10^{-4}$	---
	HCl etch ~10 sec		$8.65 \pm 1.6 \times 10^{-4}$	---
	HCl etch ~20 sec		---	$2.88 \pm 0.8 \times 10^{-3}$
	Re-run		$5.79 \pm 1.5 \times 10^{-4}$	$3.0 \pm 0.03 \times 10^{-3}$
	AR coated		$3.09 \pm 0.21 \times 10^{-3}$	---

Table 19. Absorption Coefficient for New Coating Materials

Material	Length, cm	β(DF), cm^{-1}	β(HF), cm^{-1}
ThF_4	0.238	$4.1 \pm 0.16 \times 10^{-3}$	$1.7 \pm 0.11 \times 10^{-2}$
NdF_3	0.445	1.10	2.25

bulk heat that results from laser calorimetric measurements on long, bar-shaped samples. Single-layer films of As_2S_3, CaF_2, ThF_4, and PbF_2 were deposited on a KCl bar and the absorption coefficient of each film was extracted from the slopes of the temperature-time curves.

A paper describing this work was presented at the OSA-sponsored conference on Optical Phenomena in Infrared Materials, 1-3 December 1976, Annapolis, Maryland. The manuscript has been accepted for November 1977 publication in the special issue of Applied Optics devoted to this conference. Appendix A contains a preprint of this manuscript.

2. Ellipsometry

We have improved the stability of the modulated light 10.6 μm ellipsometer developed on the previous program. The improved ellipsometer was used to determine the refractive index and the thickness of several UHV-grown film samples and the refractive index of a previously unmeasured substrate material. These results were obtained using recently implemented computer simulation and data processing programs that aid the operator in the selection of the best possible measurement conditions (i.e., the initial laser polarization and incidence angle for which the accumulated error in the end result from measurement inaccuracy and system noise is minimized).

Much of the effort on the ellipsometer has been directed toward obtaining improved modulator stability. A dual opto-electronic stabilization system developed for this purpose is partly operational. The apparatus was used to measure the indices of a single-crystal ThF_4 substrate and of As_2Se_3 and As_2S_3 films on KCl substrates. The confidence limits on the measured refractive index are within tolerance, and the measured film thickness is obtained with an accuracy as good as or better than that obtained by Tolansky interferometry.

a. Accomplishments

(1) Ellipsometer Development (Stability Improvement) — The 10.6 μm modulated light ellipsometer became operational during the last program (see RADC-77-40-Jan 1977). With this instrument, we measured the refractive index of several substrate and film materials of interest to high-powered laser window technology. These materials included ZnSe, KCl, and CdTe substrates; ZnSe films on KCl substrates; and ThF_4 films on ZnSe substrates. The measured data was in good agreement with accepted index values (i.e., published data and our own independent empirical determinations).

However, the spread in our raw data yielded an accuracy of only about 2 to 4%, and we felt that the inherent accuracy of the method should be an order of magnitude better. Re-examination of our data showed that part of our measurement error was due to a temporal variation of the modulation index (dynamic strain level of the modulator). This variation was subsequently traced to a change in modulator temperature due to internal elastic power dissipation and changes in environmental temperature. A contributing source of this variation was traced to the 0.9 μm wavelength modulator monitor/drive control feedback system, which passed through the same set of AR coatings as the 10.6 μm laser. Since these coatings had been designed to pass the 10.6 μm laser beam with low loss, their performance at 0.9 μm was suspect. Tests showed that their transmission was low at 0.9 μm. The possibility of transmission variation due to Fabry Perot effects also existed, and a dual coating was designed for the modulator. A segment of the coating near the monitor system was tuned for maximum transmission at 0.9 μm; the remainder, covering most of the modulator window area, was tuned to 10.6 μm. The resultant device produced much stronger modulator monitor signals than previously observed. With the monitor signals now strong enough to be displayed directly on the oscilloscope, we observed an unacceptably large thermal phase shift between the modulator reference and the modulator monitor signals. This phase shift occurs between the voltage which drives the

modulator and the strain wave in the modulator medium. It is a consequence of the thermal change in resonant frequency of the modulator bar relative to that of the quartz crystal piezoelectric driver bars. This factor also contributes to the temperature dependence of modulator efficiency.

One possible solution to the problem was to use a phase shift versus frequency filter to compensate for this effect. This was ruled out because the harmonics of the drive frequency also modulate the transmitted beam. Another possibility was to use a dual monitor system for the modulator: one monitor signal to provide a reference for all signal-processing operations, and a second used in the modulation index servo loop. The latter approach was implemented; it required several modifications to the modulator system. These modifications are discussed below.

Light-emitting diode (LED), silicon photodiode detector pairs were installed in the modulator housing opposit the 0.9 μm AR-coated region of the modular bar (see Figure 25). A crossed polarizer and analyzer were placed on either side of the modulator to produce extinction of the 0.9 μm light in the absence of any modulator drive signal. With the modulator drive signal "on," optical energy passing through these monitor systems is modulated at twice the modulator drive frequency. A mica quarter-wave plate oriented at 45^{o} placed before one of the analyzers causes that monitor channel to produce a signal at the modulator drive frequency. This signal serves as a reference signal. At high modulator drive, the monitor signal at 2 ω goes to zero and the reference signal (ω) remains high. However, we found that one characteristic of phase modulation at high modulator drive was the generation of harmonics in both the monitor and reference channels. A suitable set of low-pass filters was then designed and installed in the photodetector amplifier circuitry to eliminate the undesired harmonics. After these modifications were made, the modulator drive servo system was tested, and the troublesome phase shifts were found to have been almost entirely eliminated. A schematic of the dual detection electronics is shown in Figure 26. Residual phase errors are

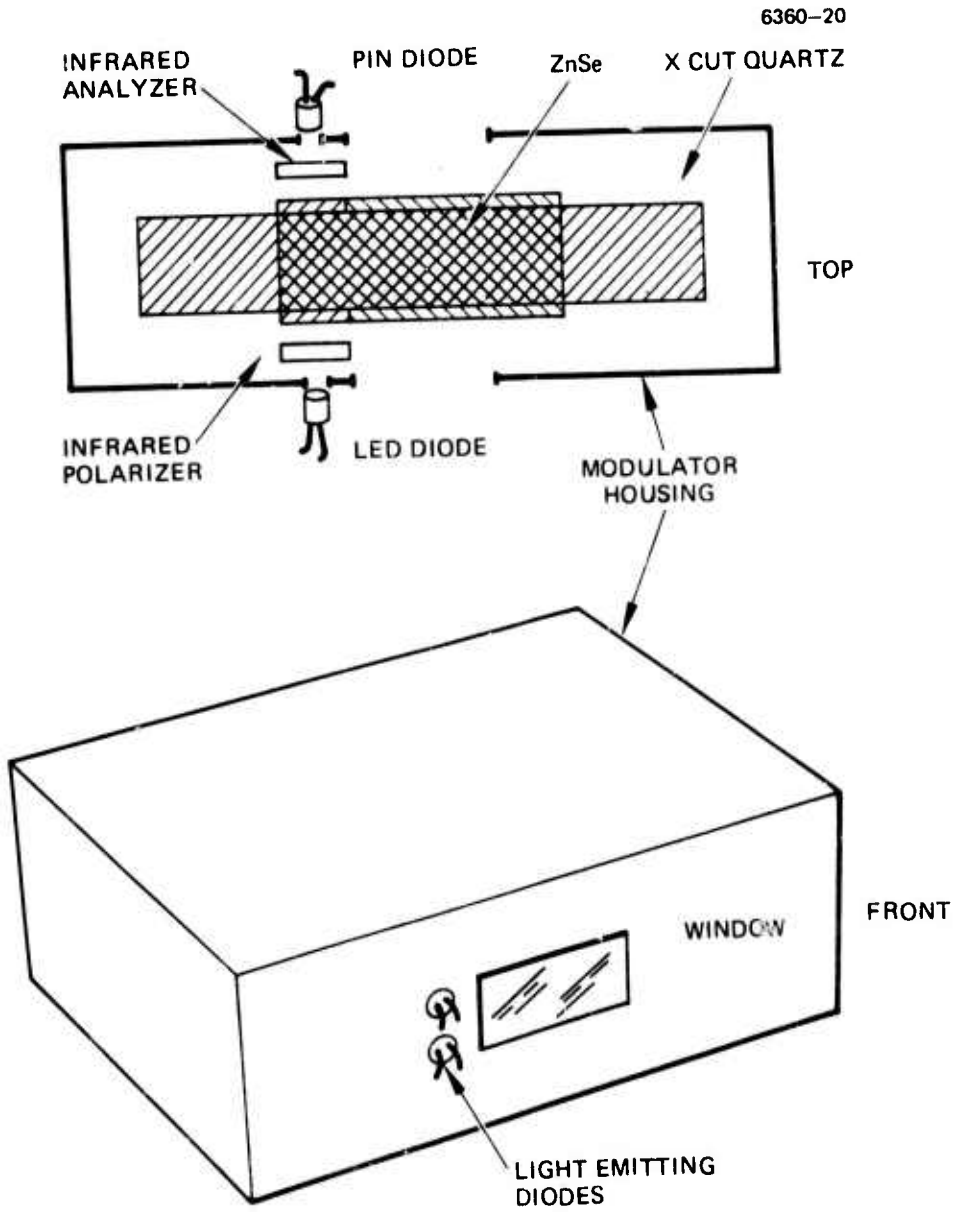

Figure 25. Stabilized modulator using two photodiodes.

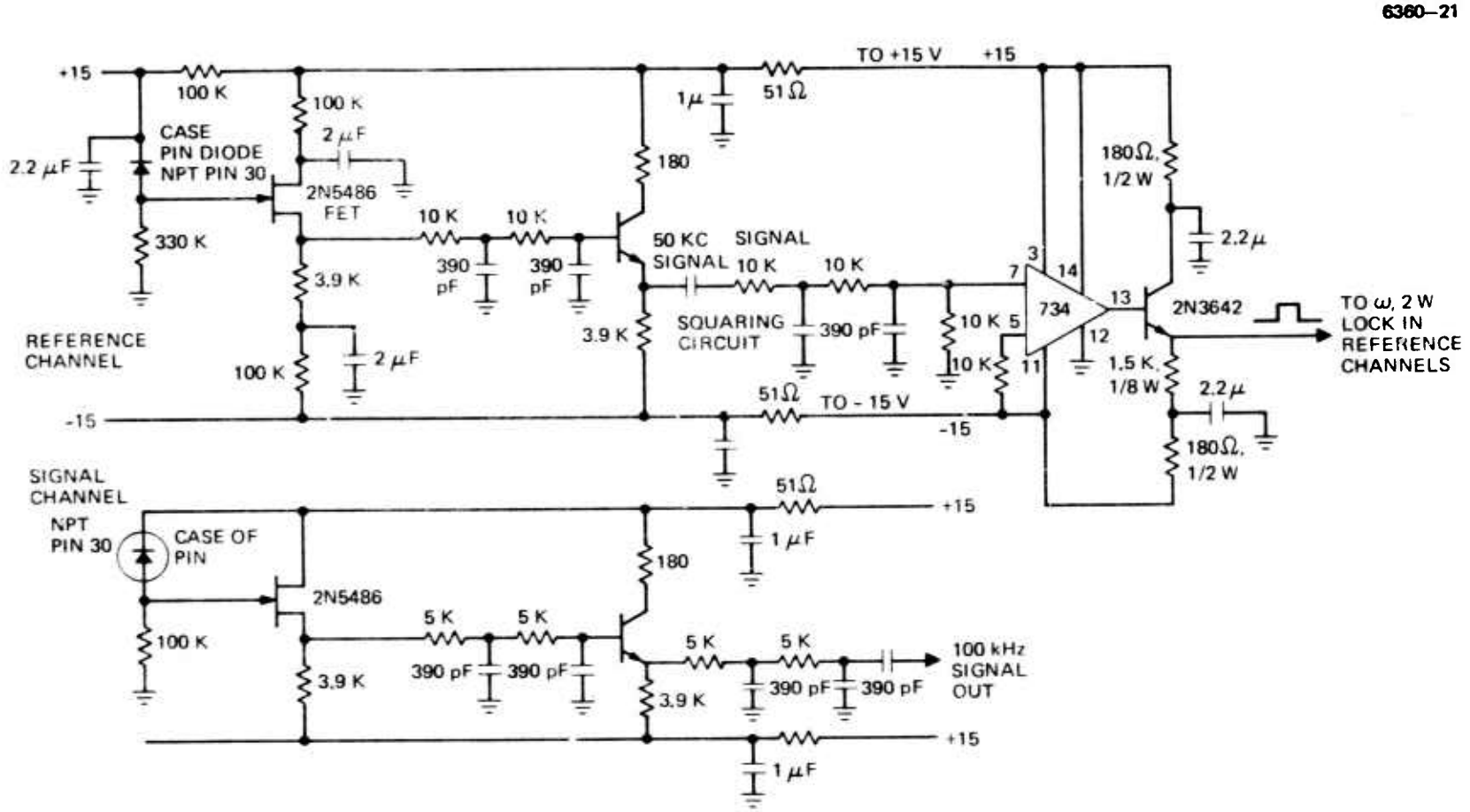

Figure 26. Dual detector signal conditioning circuitry for modulator drive servo control system.

attributed to instabilities in the lock-in amplifiers used in the system. In the future these may be eliminated by using dual channel lock-in amplifiers, which yield the correct value of the signal amplitude regardless of signal phase.

b. Data Processing

An extensive series of programs has been written connecting the equations of the modulated light ellipsometer to the McCracken ellipsometer program. These programs are designated by the code numbers D45, D45 NT, E45, S45, D90, D90 NT, E90, and S90. The letters D, E, and S correspond to data, error, and simulation, 45 and 90 correspond to the initial polarization of the laser, and NT corresponds to simultaneous calculation of index and thickness. Those programs not designated with the suffix NT require the film thickness as part of the input data, and they calculate the complex refractive index. The 45^{o} case is generally used for measuring dielectrics, and the 90^{o} case for measuring metals. An extensive error analysis[2] indicated the necessity of this programming. We discovered that optimum system accuracy was obtained over an angular measurement range that depended on the indices of the specific substrate and/or film being measured, and that the algebraic signs of the signal ratios R_1, ($V\omega/Vdc$), and R_2, ($V2\omega/Vcc$), varied with these index values and the angles of measurement. In the experimental apparatus, these signals were generated by phase-sensitive detectors (lock-in amplifiers), the phases of which could be arbitrarily set to yield positive or negative values of the algebraic signs of R_1 and R_2. Therefore, a road map of measurement error and of the algebraic sign of the signal ratios was needed; it was provided by the new programming.

The results of these error programs[15] applied to one film system are presented in Figures 27, 28, and 29. In essence, combining the results presented in Figures 27 and 28 shows that signal ratio errors of 1% and sample alignment errors of 0.1^{o} would affect the results by less than 1% if the measurements were made within $\pm 5^{o}$ of 60^{o}. Figure 29 presents the effects of R_1 and R_2 errors on the measurement

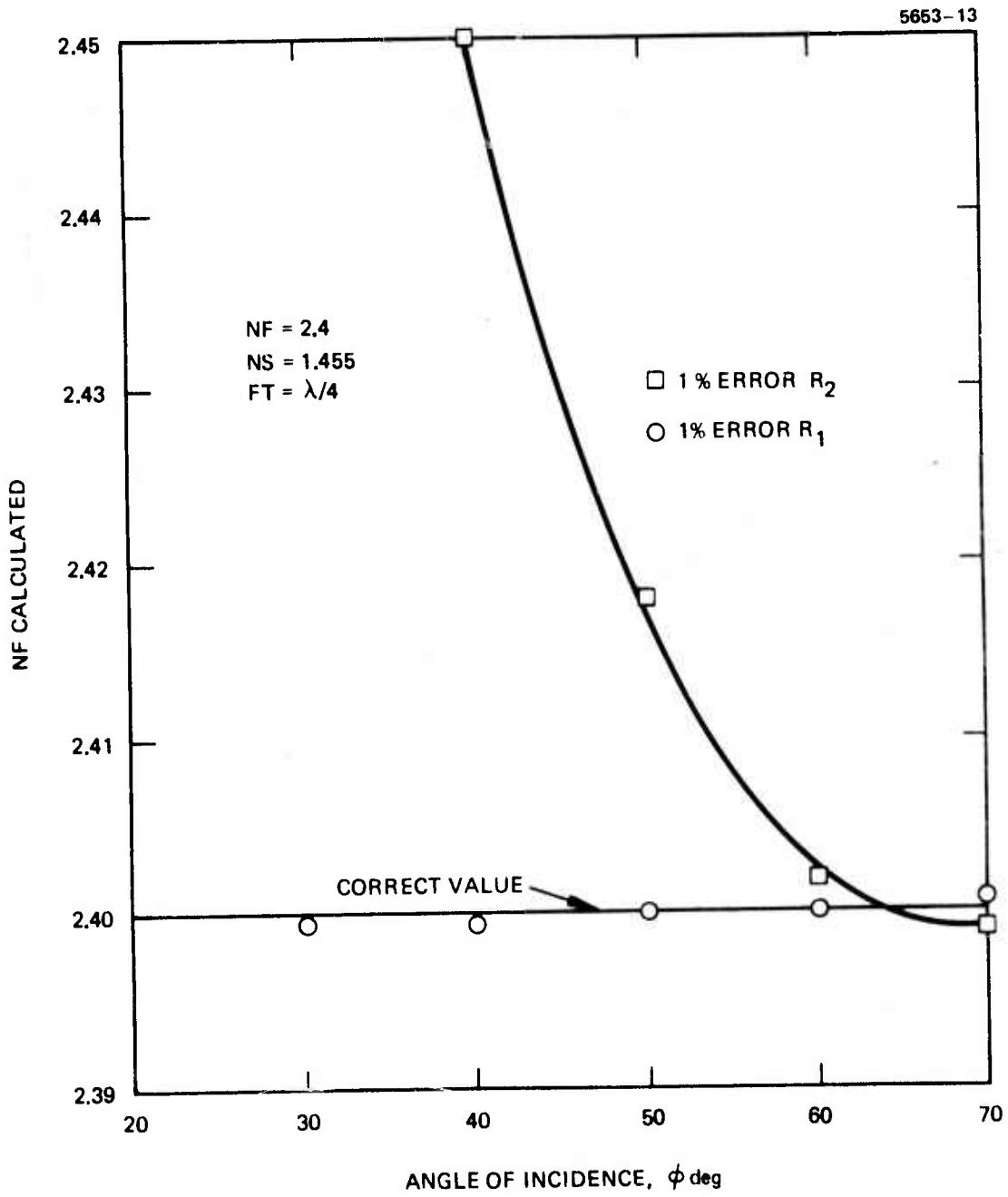

Figure 27. Typical variation of N with ϕ for 1% error in R_1 or R_2 with film index = 2.4, substrate index = 1.455, and film thickness = $\lambda/4$.

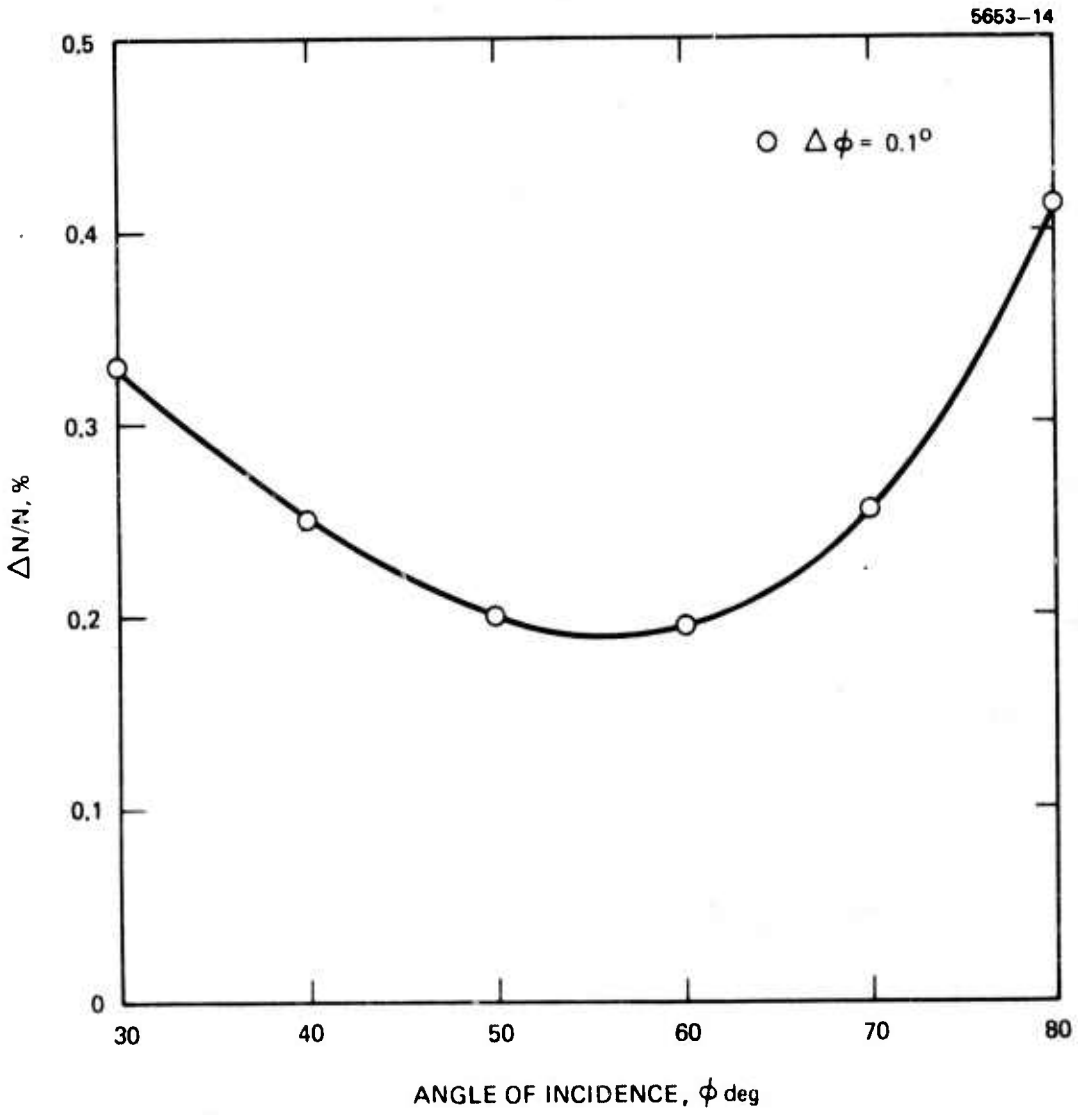

Figure 28. Fractional variation of refractive index with angle ϕ for sample alignment error.

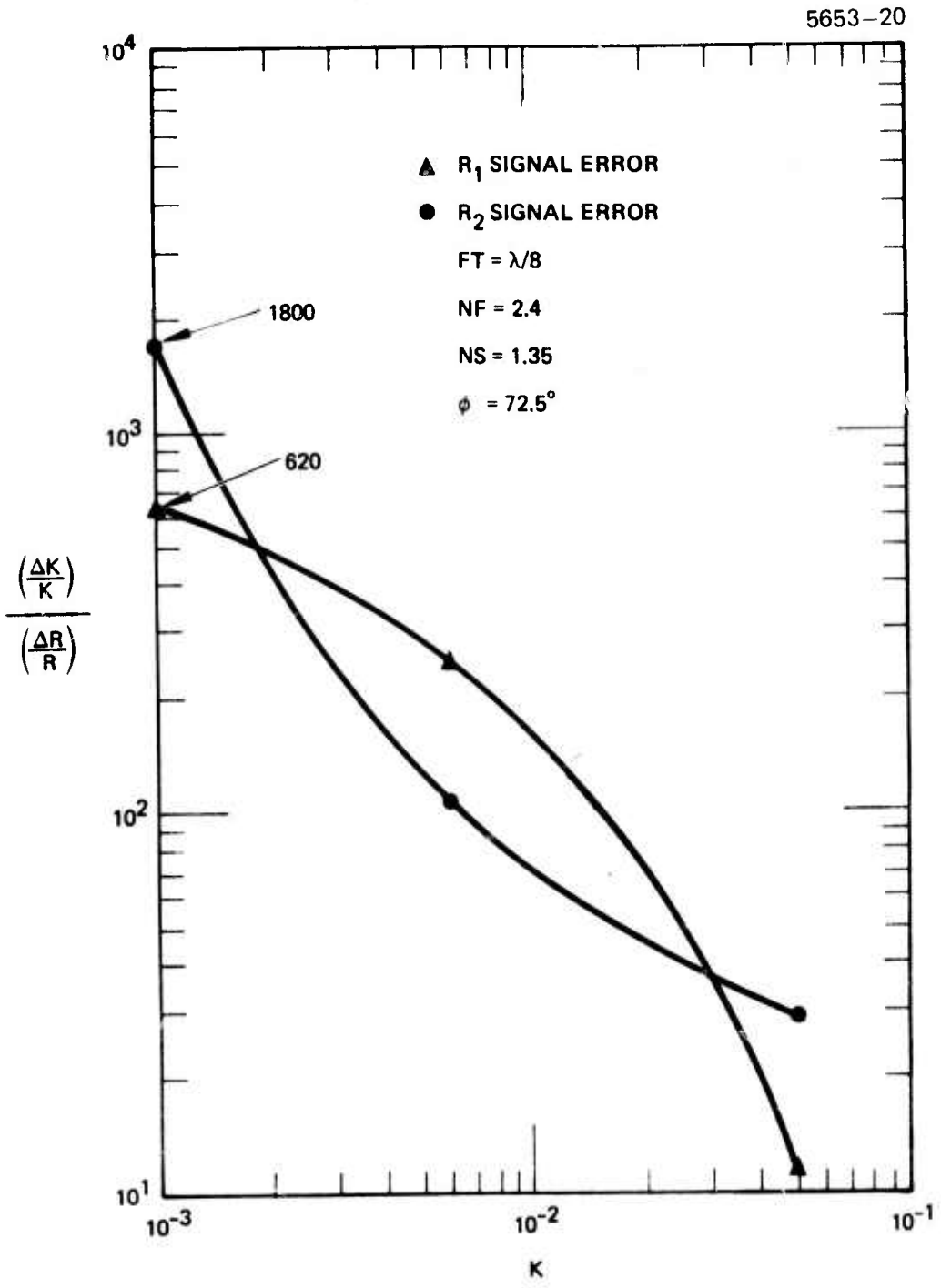

Figure 29. Dependence of the imaginary refractive index, K, on signal ratio error as a function of K.

Table 20. Measured Film Index Data

5653-17R1

MATERIAL	FILM THICKNESS	ANGLE OF INCIDENCE	REAL INDEX (N)		ACCEPTED REAL INDEX VALUE	IMAGINARY PART (K)		ATTENUATION CONSTANT (α)
ZnSe	0.653 μm	65°	2.532			-0.090		
ON	($\simeq\lambda$/8)	67.5°	2.497	2.49 ± 0.03	2.40	-0.079	-0.067 ± 0.025	1900 ± 710
KC1		70°	2.481			-0.070		
		72.5°	2.456			-0.032		
			(DEVIATION 2.5%)					
ZnSe	0.994 μm	67.5°	2.588			-0.100		
ON	($\simeq\lambda$/4)	72.5°	2.263	2.45 ± 0.014	2.40	-0.105	-0.067 ± 0.042	1900 ± 1200
KC1		75°	2.496			-0.022		
		77.5°	2.471			-0.041		
			(DEVIATION 1.5%)					
ThF_4	0.970 μm	60°	1.314			-0.095		
ON	($\simeq\lambda$/8)	62.5°	1.317			-0.055		
ZnSe		65°	1.328	1.33 ± 0.02	1.35	-0.052	-0.059 ± 0.025	944 ± 400
		67.5°	1.353			-0.067		
		70°	1.341			-0.027		
			(DEVIATION 1%)					
ThF4	3.529 μm	57.5°	1.411			-0.088		
ON	($\simeq\lambda$/2)	60°	1.425			-0.063		
ZnSe		62.5°	1.420	1.37 ± 0.06	1.35	-0.053	-0.162 ± 0.104	2593 ± 1660
		65°	1.294			-0.240		
		67.5°	1.320			-0.260		
		70°	1.311			-0.269		
			(DEVIATION 0.5%)					

of K, the imaginary part of the refractive index. The significance of the K error is discussed below.

The results of the thin-film index measurements reported in the previous contract are repeated in Table 21 where the entries were obtained using our recently implemented computer programs for processing raw ellipsometer data. The values reported for K were anomalously larger than expected. Although several explanations were considered for this anomaly, we now believe that we know the source of the error.

In our earlier work, we measured the film thickness of the samples in a Tolansky interferometer to an accuracy of $\pm 2\%$ and then input this film thickness into the D45 program to calculate N and K, the real and imaginary components of the refractive index. Based on the results of our error analysis, this program was expected to lead to the highest measurement accuracy for N and K. Some of our samples yielded ellipsometrically determined K values much larger than those determined from calorimetric measurements. To better understand this result, we computed the error sensitivity $(\Delta K/K)/(\Delta R/R)$ as a function of K. The results, plotted in Figure 29, indicate that the error in determining K at low values of K is approximately 1000 times the error in the R_1 or R_2 measurement. This finding partially explains the discrepancy in K if one assumes that the sample is lossy. However, for lossless samples, ΔK should still be zero. Recently we found it necessary to ellipsometrically measure both the film thickness and the index of refraction of some samples because we were not permitted to metallize the samples for Tolansky film thickness measurements. We turned to another version of the McCracken Program (D45 N, T), which is in the process of being adapted to the ellipsometer system. This program calculates both N and T, given Δ and ψ. It is useful only for films that are lossless or transparent at the wavelength of interest. We used Δ and ψ values taken from the D45 program and obtained N and T values that were in good agreement with rough data obtained by other means. What is most significant is that this program also will calculate a value of K if a search range on K is specified. In most

Table 21. Ellipsometric Measurements of the Refractive Index of Various Laser Window Materials and Films

Substrate	Film	Measured Index Value	Accepted Index
KCl	ZnSe	2.473 ± 0.094	2.402
ZnSe	ThF_4	1.350 ± 0.046	1.350
ZnSe	--	2.451 ± 0.014	2.402
CdTe	--	2.693 ± 0.028	2.692
KCl	--	1.473 ± 0.013	1.455
KCl[a]	As_2Se_3	2.831 ± 0.050	~2.8
KCl[a]	As_2S_3	2.432 ~ 0.050	2.377
ThF_4[a]	--	1.302 ~ 0.013	1.350

[a]New data.

cases, two solutions for T, N, and K were obtained, one of which always had a very low value for K. Further investigation of the dynamics of this program (D45 NT), and of the D45 program showed that the computer adjusts either the values of N and K with T fixed or N, T, and K with K small to fit the ellipsometer generated values of Δ, ψ, and ϕ (the angle of incidence). If the input value of T is in error, the D45 program will use an erroneous value of K to fit the input data. In the other case, where both N and T are calculated, the computer can optimize the fit to input Δ, ψ, and ϕ data with the lowest possible value of K within a specified search range. Our conclusion from the foregoing is that, because we cannot easily measure the film thickness of our samples by some other technique to greater accuracy than that produced by the low loss McCracken Program (D45 NT), we should avoid the D45 program when measuring low-loss materials. However, for materials with a high loss (i.e., large value of K), the low-loss McCracken program will not work, and D45 must be used. If sufficient time is available, we will examine the effects of signal ratio errors and incidence angle errors on the accuracy of simultaneously measuring N and T for low-loss films in the D45 NT Program.

c. Measurement Results

Measurements were made on a ThF_4 single crystal and on As_2Se_3 and As_2S_3 films on KCl substrates at 10.6 μm. These results are listed in Table 21 and are in good agreement with accepted index values for these materials. The ThF_4 index measurement must be considered as preliminary because it represents measurement of a single sample, and surface finish effects can alter the results.

Measurements were made of the thickness of As_2Se_3 and As_2S_3 films deposited on KCl. The results, listed in Table 22, are in good agreement with Tolansky film thickness estimates. Accurate Tolansky measurements could not be made because the films could not be metallized without destroying them. The ellipsometer program that produced these results extracts N and T simultaneously from the data and assumes K is zero or small. If K values are also important, it is

Table 22. Ellipsometric Film Thickness Measurement (Concommitant with Index Measurement) Compared with Tolansky Thickness Measurement

Substrate	Film	Ellipsometer Measured Thickness, μm	Tolansky Thickness Estimate,[a] μm
KCl	As_2Se_3	3.245 ± 0.059	3.313 ± 0.166
KCl	As_2Se_3	1.017 ± 0.057	0.968 ± 0.048
KCl	As_2S_3	3.747 ± 0.037	3.970 ± 0.199

[a]Unmetallized dielectric film measurement.

necessary to obtain thickness values to better than 1% by some other technique (e.g., Tolansky interferometry) and to process the data in the D45 program, which yields N and K when given T and the Δ, data.

Some of the data obtained from an ellipsometric simulation study of As_2Se_3 on KCl are presented here. The variables Δ versus ψ and R_1 versus R_2 were plotted, with film thickness and angle of incidence as parameters. The film refractive index values chosen for this study were 2.8 and 2.83; the results are shown in Figures 30, 31, and 32. Figure 30 shows that, for a specific value of film thickness, there is a range of angles of incidence for which the Δ's and ψ's for the two films are almost identical even though their refractive indices differ by 1%. We also observe that this angular range, over which poor accuracy results, changes with film thickness. This set of results has been replotted in Figure 31 with the film thickness as the independent variable. This form of data presentation would be useful if the data were taken at a fixed angle of incidence and the film thickness were varying. In this case, it appears that the best resolution occurs for measurements made at large angles of incidence ($\sim 75^{\circ}$) and for film thicknesses greater than $2\lambda/20$.

These Δ, ψ results were obtained from a calculation of the Fresnel coefficients of films using the NBS McCracken program. Therefore, they are only representative of the material properties of the film substrate system, and they are not related to the type of ellipsometer used in the measurements. On the other hand, the type of ellipsometer used will influence the results obtained. In some types of ellipsometers, the angles Δ and ψ are measured directly by rotating optical components, and the error in determining the angle of these components becomes the error in Δ and ψ. In the modulated light ellipsometer, the parameters measured are signal ratios R_1 and R_2, which are the ratios of the signal voltages at frequencies ω_1 and ω_2 to the dc signal voltage generated by the optical detector. We have calculated the signal ratios R_1 versus R_2, with film thickness as a parameter, with our ellipsometer computer simulation program. The same set of materials (As_2Se_3 on KCl) was studied with the film index

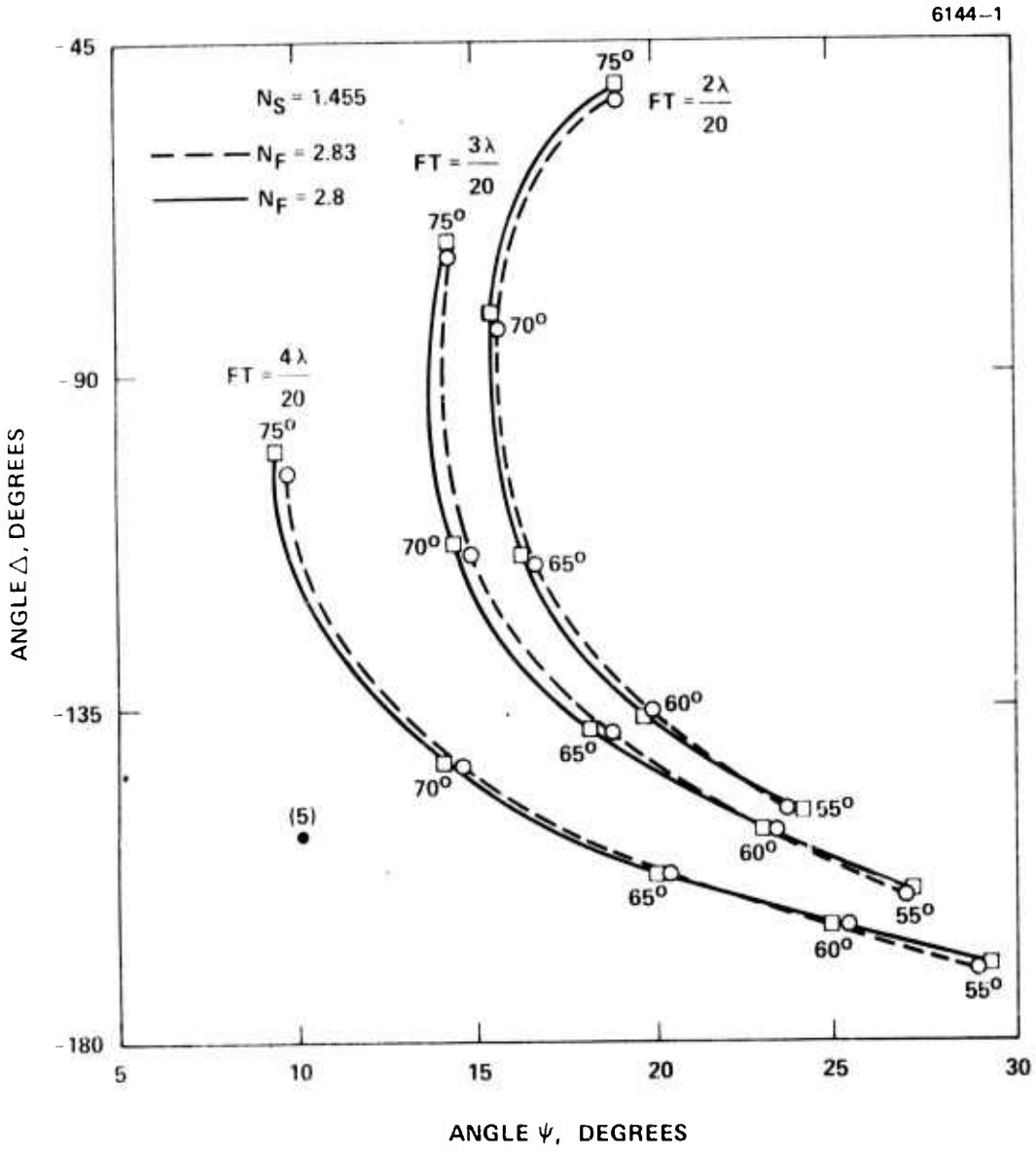

Figure 30. Variation of ellipsometric variables Δ and ψ, with film thickness (FT) and angle of incidence (ϕ) as parameters.

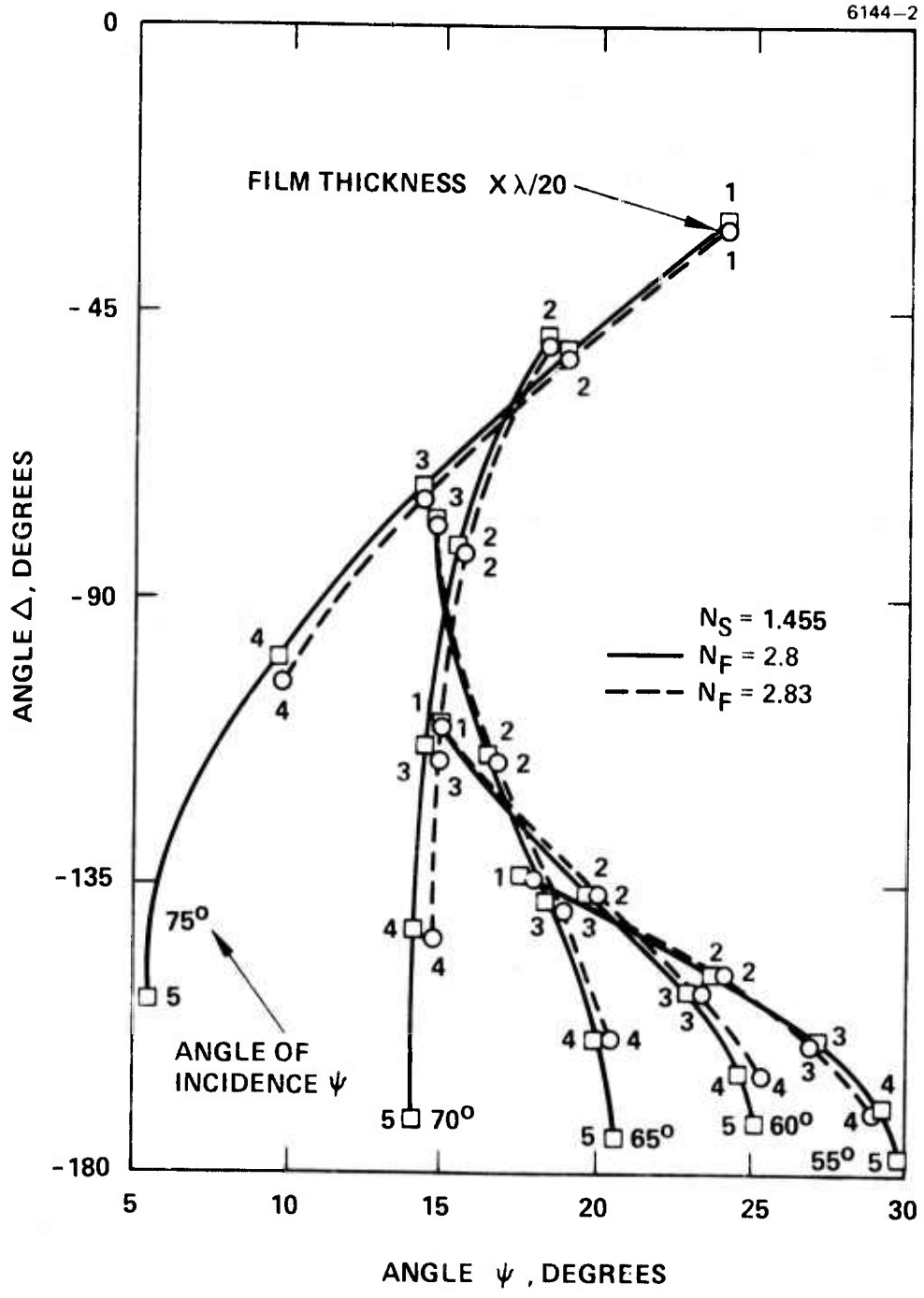

Figure 31. Variation of ellipsometric variables Δ and ψ, with film thickness (T) and angle of incidence (ϕ) as parameters.

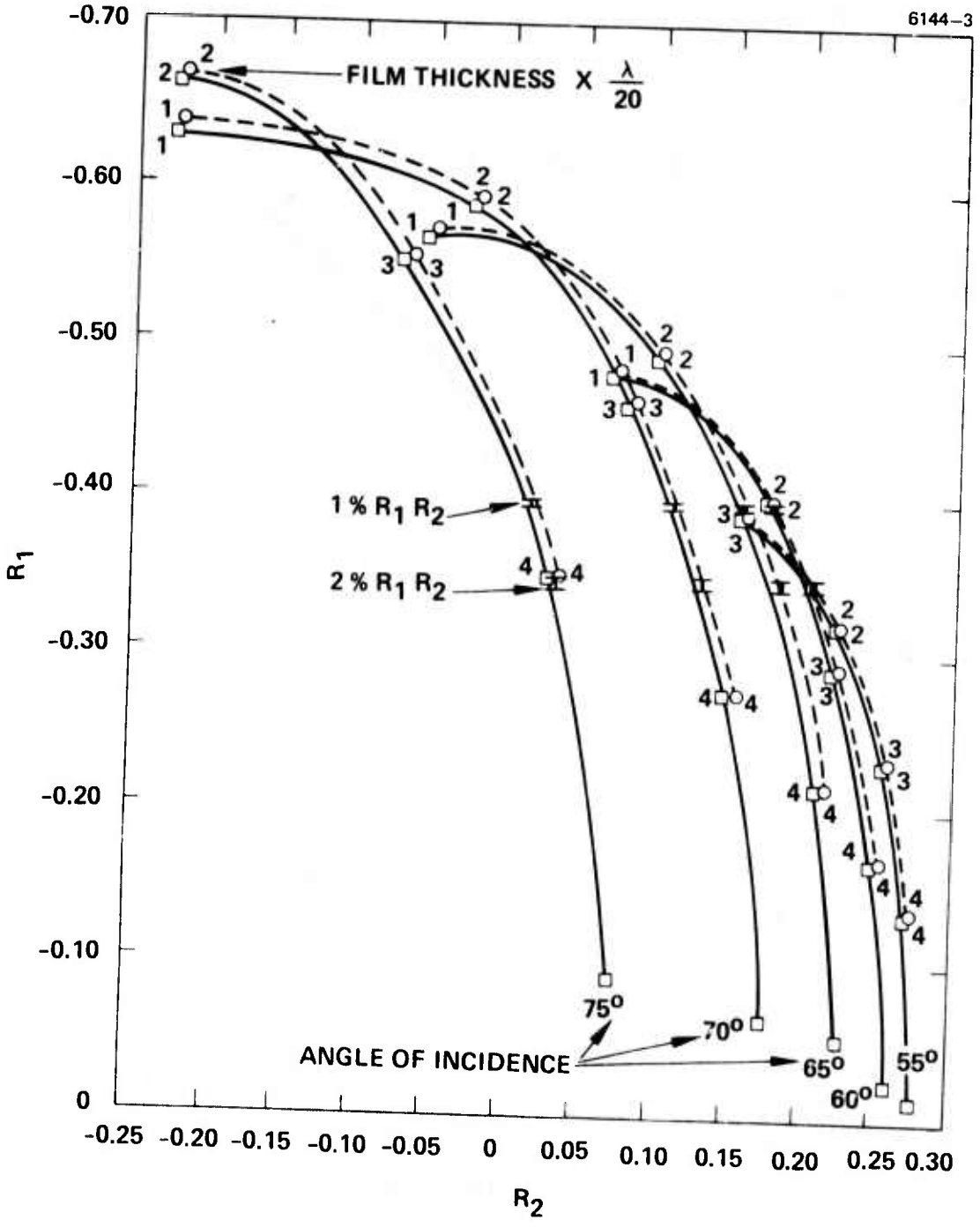

Figure 32. Dependence of R_1 and R_2 on the film thickness As_2Se_3 on KCl.

having values of 2.8 and 2.83. These results are presented in Figure 33. The two curves of varying film thickness are closer together at smaller angles of incidence than at larger angles. Also, at smaller angles, the curves tend to merge for smaller film thicknesses. The conclusion is that larger angles of incidence and larger film thicknesses will produce better results. Error bars for ΔR_1, ΔR_2 = 1% and 2% are also shown on the figure. As R_2 approaches zero, ΔR_2 also becomes small, but the signal level becomes unusable. Thus, one is restricted to absolute values of R_2 greater than 0.01 because of signal-to-noise requirements. The 2% error rectangle for the 65^o angle of incidence curves clearly lies on the line n = 2.83. This means that with a signal ratio measurement error of 2%, the index of refraction can be determined to 1%. These results are based on a simulation program that assures no errors in component alignment or sample alignment and that ignores modulator stability fluctuations. These graphical results are presented here to provide the reader with some insight into the usefulness of the computer measurement simulation program.

SECTION 3

FUTURE PLANS

In this section we outline our future plans for the research effort in the next report period. These plans are presented in the same order as the technical presentations in the previous sections.

We will continue to study the surface finishing and coating of laser windows to improve the laser damage resistance of windows and window coatings of interest in this program.

Work at DF/HF wavelengths will be increased as investigations at CO_2 and CO wavelengths are completed. An effort will be made to determine the nature and cause of the higher absorption observed at HF wavelengths. This will be done, in part, by using long bars of window materials to enable the separation of surface and bulk absorption coefficients.

Plans for the next quarter include development of the Ge modulator, additional measurements of As_2Se_3 and As_2S_3 films, and initial measurement of strain in films by mechanically straining the coated substrates.

Window coatings for KCl will be extended to include As_2Se_3/NaF/As_2Se_3 and $As_2Se_3/YbF_3/As_2Se_3$; this should complete the KCl work. The major efforts will then be directed to coatings for DF/HF applications in the 2.8 μm to 3.8 μm wavelength regions on CaF_2 or SrF_2 window substrates.

SECTION 4

PAPERS AND PRESENTATIONS

Three papers were presented at the Conference on Optical Phenomena in Infrared Materials, 1-3 December 1976, at Annapolis, Maryland. The titles of the papers are as follows:

- 10.6 μm Ellipsometer Measurements of Refractive Indices of IR Materials.
- Bulk and Surface Calorimetric Measurements at CO Wavelengths (included as Appendix A).
- New Technique for Measuring the Infrared Absorption in Thin Film Coatings (included as Appencix B).

REFERENCES

1. R.C. Pastor, R.R. Turk, A.C. Pastor, A.J. Timper, and R.L. Joyce, "A New Mechanism to Inhibit Grain Growth in Forged KCl,"

2. "Laser Window Surface Finishing and Coating Science," Final Technical Report, Hughes Research Laboratories, Jan. 1977. RADC-77-40.

3. Armington, H. Posen, J. Bruce, and H. Lipson, "The Effect of Reactive Processing on Window Properties of NaCl," Proc. 4th Conf. Infrared Laser Window Materials, Tucson, Arizona (1974).

4. R.C. Pastor and K. Arita, Mat. Res. Bull. 10, 493 (1975).

5. R.C. Pastor and K. Arita, Mat. Res. Bull. 11, 1037 (1976).

6. R.C. Pastor and M. Robinson, Mat. Res. Bull. 11, 1327 (1976).

7. A. Klugman and R.F. Schneidmiller, "Investigation of Crystal Orientation Influence on Thin Film Coatings for CaF_2 Laser Windows," Final Report, Oct. 1975, for AFML, Wright-Patterson AFB, Ohio, Contract F33615-75-C-5190.

8. R.E. Howard, et al., "Multiphonon Absorption in Chalcogenide Glasses," in Optical Properties of Highly Transparent Solids, S. Mitra and B. Bendow, eds. Plenum Press.

9. Handbook of Chemistry and Physics, 54th Ed., CRC Press (1973).

10. A. Vasko, and D. Lexal, "Oxygen Impurities and Defects in Chalcogenide Glasses," I SRB, Journal of Non-Crystalline Solids 4, 311-21 (1970).

11. M. Maklad, et al., "Infrared Transmission in Chalcogenide Glasses," Third Conf. on High Power Infrared Laser Window Materials, Nov. 12-14, 1973, AFCRL-TR-74-0085.

12. M. Hass, J.W. Davisson, H.B. Rosenstock, and J. Babiskin, Appl. Opt. 14, 1128 (1975).

13. T.F. Deutsch, J. Electron. Materials 4, 663 (1975).

14. M. Hass, et al., J. Appl. Phys. 45, 3959 (1974).

15. M.E. Pedinoff, M. Braunstein, and O.M. Staffsud, "10.6 μm Ellipsometer MSMTS of Refractive Indices of IR Materials," to Pical Meeting on Optical Phenomena in IR Materials, Opt. Soc. Am., 1-3 Dec. 1976, Annapolis, Md.

APPENDIX A

BULK AND SURFACE CALORIMETRIC MEASUREMENTS AT CO WAVELENGTHS*

S. D. Allen and J. E. Rudisill

Hughes Research Laboratories

Malibu, California

*Work was sponsored by the Defense Advanced Research Projects Agency and monitored by RADC/ETSO Hanscom Air Force Base, Massachusetts 07131

Abstract

Laser calorimetry was used to measure the optical absorption of several candidate window materials for application at CO laser wavelengths. These materials include KCl, CaF_2, SrF_2, and ZnSe. The long, thin bar technique was used to separate bulk and surface absorption contributions by means of their time dependencies. One sample of KCl, known to be low absorbing at 10.6 μm, exhibited no measurable absorption within the sensitivity of the calorimeter ($\beta_t < 2 \times 10^{-6}$ cm^{-1}). The absorption coefficients measured for two samples of CaF_2 at 5.41 μm were higher than those measured by other investigators at 5.25 μm, but, when fitted to an exponential dependence on wavelength, compared favorably with currently measured values. To compare results from different laboratories, precise definition of the spectral power distribution is essential. The surface absorption was, in all cases, small relative to similar measurements at 10.6 μm; in several cases it was not separable from bulk absorption by the technique used.

I. Introduction

Measuring the optical losses in materials which are candidates for high-power laser windows remains a high priority. Of particular importance have been optical absorption losses, both in the bulk and at the surfaces. Differentiating between bulk and surface contributions is necessary in directing efforts toward improving either material growth or surface finishing techniques. Several methods have been used to separate these contributions. One method measures the total absorption of a sample as it is incrementally decreased in length.[1] The bulk absorption coefficient and surface absorption are represented, respectively, as the slope and intercept of the resulting curve. One problem with this method lies in the inability to reproduce the same surface loss as sample length is changed. Another method is to measure absorption as a function of time on a bar of sufficient length that the bulk and surface contributions are separated in time.[2] The work presented here uses the latter technique to measure bulk and surface absorption of various materials using a multiline CO laser.

There has been little agreement among different laboratories in measurements of the absorption coefficient of candidate window materials at CO laser wavelengths. Early data taken at Hughes Research Laboratories (HRL) illustrated the importance of using vacuum enclosures for sample measurements, but more recent discrepancies cannot easily be ascribed to differences in calorimeter configuration. It is more likely that actual wavelength-dependent phenomena are being observed as the output of the various lasers used for calorimetry in

this wavelength range varies from a low of 5.15 μm center wavelength at Northrup Research and Technology Center[4] to a high of 5.41 μm center wavelength at HRL. Data taken on alkali halides, alkaline earth fluorides, and ZnSe will be discussed along with detailed descriptions of the calorimeter and the laser used in taking this data.

II. Experimental Apparatus

The laser calorimeter system is illustrated in Fig. 1. The output of the CO laser is folded 180° and focused with an AR-coated CaF_2 lens with a nominal focal length of 45.7 cm. A He-Ne alignment laser runs counter to the CO beam and is used for both sample and laser alignment.

The calorimeter head (illustrated in Fig. 2a,b) is constructed of standard glass pipe parts. The windows are AR coated CaF_2 designed so that all alignment adjustments can be made outside the vacuum chamber. The flange on which the sample holder is mounted has its own optical bench rider and can be placed on the same optical bench as the vacuum head while sample alignment is accomplished. This arrangement has proven reasonably easy to use and has yielded reproducible alignment results. For the long bars, two mounting circles are used and the bar is suspended on nylon monofilament cradles and secured by a monofilament loop attached by a spring to the lower support bar. A vacuum feedthrough provides connections for four thermocouple pairs to the Keithly 150B microvoltmeters used to measure the thermocouple output. The thermocouples are Isonel-insulated

0.005 in. copper/constantan wire tightly twisted together. The reference thermocouples are embedded in a copper block which is electrically and thermally isolated from the rest of the system.

The sample thermocouples were attached using cyanocrylate cements to glue the thermocouples either directly onto the bar or onto a silver mirror deposited on the bar. These particular cements transmit in the infrared, have very fast curing times (several seconds), and are easily removed by dissolving in acetone. Samples were polished on all faces and silver mirrors approximately 1 cm in diameter were deposited on an edge surface of each of several cyrstals at the entrance, exit, and center positions to eliminate direct scattering to the thermocouples. As shown in Table 1, no consistent lowering of the directly scattered radiation was observed on bars with the mirror thermocouple attachment. This evidence is suggestive only, as the same sample was not run with and without mirrors and as the amount of direct scattering depends strongly on alignment.

The system is pumped by a high-pressure nitrogen Venturi roughing pump and liquid-nitrogen-cooled zeolite sorption pumps with the appropriate valve system. It was decided to use a completely oil-free system to eliminate any possible contamination of window and sample surfaces from oil backstreaming from a mechanical pump. Typical pressures achieved in the system are less than 10 m Torr.

The CO laser used in the calorimeter is a 2 m optical cavity, hemiconfocal system with a 4 m radius molybdenum substrate dielectric-enhanced reflector, and an output coupler (ZnSe substrate) with an AR

coating on one side and a 94% reflector on the other side. The laser is operated in a flowing mode with a premixed gas consisting of O_2 (0.121%), N_2 (18.31%), CO (3.09%), and He (comprising the balance). The laser tube is cooled to 0°C by a closed ethylene glycol/water refrigeration system. The CO laser oscillates between several transverse modes, yielding an effective overall spot size of approximately 5 mm. To avoid scattering caused by such a large spot size, the beam is focused as shown in Fig. 1 to a spot size of less than 1 mm.

Power output with the laser operating at 0°C is 8 to 10 W cw as measured by a Coherent Radiation, Inc., power meter. After an initial warm-up period, total power output is stable to ±1% over periods of several hours. Representative power distribution spectra (normalized to 10 W total output power) are given in Figs. 3 and 4. Although the individual line intensities vary considerably, the intensity weighted average mean wavelength is reproducible, 5.41 μm ±0.01 μm. The apparatus used to measure the spectral power distribution is illustrated in Fig. 5. It consists of an Optical Engineering CO_2 Spectrum Analyzer (operated in second order for CO wavelengths) with the thermally sensitive display screen replaced by an aluminum plate coated with absorbing paint with a slot placed so that it is not viewed by the diffracted beam. In this slot rides a Teflon holder with a slit-shaped $LiTaO_3$ pyroelectric detector aligned to intercept the diffracted beam. The detector is 1.3 mm wide and 5 mm long and the output is fed into a PAR 122 lock-in amplifier tuned to the frequency of the chopper. A reference signal is supplied to the lock-in amplifier by a GaAs LED/Si detector pair mounted on the chopper.

III. Results

The results of the CO laser absorption measurements are presented in Table 1. Initial tests on the calorimeter apparatus were carried out with KCl sample B62-B because of its previously measured low absorption at 10.6 μm ($\beta = 7.0 \times 10^{-5}$ cm^{-1} and $\beta_s = 4.0 \times 10^{-4}$ per surface with the absorption coefficients defined by $\beta_t \ell = \beta \ell + 2\beta_s$). As shown in Table I, when direct scattering levels were reduced to below detectable levels by careful alignment and shielding of the thermocouples, the measured absorption coefficient was zero with an approximate upper limit of 2×10^{-6} cm^{-1}, set by the noise level of the system. An experimental absorption curve under the best alignment and shielding conditions established with this sample (Fig. 6) exhibited no detectable direct scattering or change in slope when the sample was irradiated. The upper limit to the absorption of the sample was established by plotting the heating curve, drawn in Fig. 6, for an assumed absorption coefficient, $\beta_t = 4 \times 10^{-6}$ cm^{-1}. Another KCl boule (B55) did yield measurable absorption coefficients (cf. Table 1) in the 10^{-5} range. This sample had evaporated silver mirrors to which the thermocouples were attached; in the process of depositing the mirrors, some contamination of the masked surfaces occurred. This sample exhibited sufficient surface absorption to enable it to be separated from the bulk absorption. Surface absorption was still quite low, $\beta_s = 7.3 \times 10^{-5}$ per surface, approaching the limit of detectability for a sample with a bulk absorption of $\beta = 2.1 \times 10^{-5}$ cm^{-1} and $\ell = 16.25$ cm.

Two samples of KCl doped with 1.75% RbCl, one single crystal and one press forged, were measured. The forged sample (B156-5) was

taken from an initial forging attempt at HRL and exhibited some veiling when observed in a high-intensity collimated visible beam. This veiling was evident in that the observed bulk scatter was greater than surface scatter in this particular sample. In most samples, the reverse is true. For single-crystal RbCl (1.75%) doped with KCl (sample B166 in Table I), the surface absorption is barely separable from the bulk absorption, with the bulk absorption comparable to the early KCl sample, B55, and low relative to values measured at 10.6 μm.

The ZnSe sample (I-23, furnished by Raytheon Corporation) was of sufficient length (L = 21.25 cm) to separate bulk and surface absorption, providing there was significant surface absorption. The calculated time[5] ($\tau = \ell^2/6\kappa$, where κ is the thermal diffusivity) required for the temperature rise generated by the surface absorption to reach the center thermocouple was 1.54 min. If the surface absorption were equal to or greater than the bulk absorption, two heating curves should be easily discernable; however, only one slope was observed in the heating curve, indicating surface absorption, $\beta_s \leq 2 \times 10^{-3}$ per surface. The total absorption value measured, $\beta_t = 9.5 \times 10^{-4}$ cm^{-1}, compares favorably with a value of $\beta = 1.6 \times 10^{-3}$ cm^{-1} given by Deutsch.[1]

Two CaF_2 samples were measured, VHP-614 (Raytheon cast CaF_2) and H 2888-03-a (HRL RAP single crystal). The Raytheon cast sample was cut from a larger piece used by Raytheon to measure total absorption versus length. Their values[6] measured with a dry ice and ethanol cooled CO laser (center wavelength = 5.25 μm) were: $\beta = 4.3 \times 10^{-4}$ cm^{-1} and $\beta_s = 3.8 \times 10^{-5}$ per surface. It was impossible with this sample to

separate bulk and surface absorption via the time dependence of the heating curve. The total absorption was considerably higher than the value measured by Raytheon.

This large a discrepancey cannot be ascribed to differences in calorimeter configuration, particularly since low absorption values were obtained for several KCl samples using this same calorimeter. Since the center wavelengths of the CO lasers at Raytheon and HRL are known to differ, a comparison of the predicted absorption of CaF_2 at the two wavelengths was made. Table II lists the absorption versus wavelength of CaF_2 predicted by extrapolation of the multiphonon edge, as determined by Deutsch.[7] Ideally, the absorption should be calculated at each laser line, but, as previously noted, the intensities of the individual lines vary while the intensity weighted average wavelength remains the same to ± 0.01 μm. In order to predict the qualitative behavior of the absorption coefficient as a function of wavelength in this region, total intensity was assumed to lie at the center wavelength. Assuming the Raytheon value of the total absorption coefficient ($\beta_t = 5.4 \times 10^{-4}$ cm^{-1}) at 5.25 μm and extrapolating according to the above exponential dependence to 5.41 μm yields the HRL measured absorption coefficient to within the experimental error (calculated $\beta_t = 9.8 \times 10^{-4}$ cm^{-1} versus measured $\beta_t = 9.0 \times 10^{-4}$ cm^{-1}). This rough calculation assumes, of course, the same exponential dependence for surface absorption as for bulk absorption, but surface absorption contributes little to the total absorption in this sample.

The single-crystal HRL RAP-grown CaF_2 sample (H 2888-03-a) measured at 5.41 μm has a total absorption coefficient, $\beta_t = 5.9 \times 10^{-4}$ cm^{-1}. Reversing the extrapolation used above yields an estimated absorption at 5.25 μm, $\beta_t = 3.2 \times 10^{-4}$ cm^{-1}, which is comparable with the best results obtained to date.

This particular crystal, as noted in Table I, exhibited considerably more direct scattering than other single-crystal samples. This can probably be attributed to the presence of a large crack on one side of this boule.

The high absorption coefficient reported for the single-crystal SrF_2 sample should not be taken as indicative of currently available material. This sample was cut from an early boule which cracked upon cooldown during growth.

IV. Conclusions

Very low absorption of a selected boule of RAP-grown KCl (B62-B) was measured at 5.41 μm. The total absorption of the sample was below the measurement limit of the system, $\beta_t \leq 2 \times 10^{-6}$ cm^{-1}, and served to define the sensitivity of the calorimeter.

The absorption coefficients measured for two samples of CaF_2 at 5.41 μm were higher than those measured at 5.25 μm but, when fitted to an exponential wavelength dependence,[7] compared favorably with currently measured values. In the case of the sample (VHP-614) previously measured at Raytheon, the HRL absorption coefficient extrapolated to 5.25 μm was within 10% of the Raytheon measured 5.25 μm absorption coefficient.[6] To compare results from different laboratories, precise definition of the spectral power distribution is essential.

The absorption coefficient measured at 5.41 μm of ZnSe also compared favorably with the previously reported value: $\beta_t = 9.5 \times 10^{-4}$ cm^{-1} at HRL versus $\beta = 1.6 \times 10^{-3}$ cm^{-1} reported by Deutsch[1] in 1973.

With the exception of two KCl samples, the surface absorption was not distinguishable from the bulk at 5.41 μm by the long bar method, indicating a β_s equal to or less than the bulk absorption for these samples. For example, for a bar of length ℓ = 10 cm and $\beta = \beta_s$ in the equation $\beta_t = \beta + 2\beta_s/\ell$ the ratio of the initial and the final slopes would be:

$$\frac{\beta}{\beta_t} = .83$$

which is measurable but close to the limit of discrimination for the low absorption coefficients measured. The absorption losses due to the surfaces were in all cases small compared with similar measurements at 10.6 μm.

V. Acknowledgments

The authors wish to acknowledge the technical advice of O. Stafsudd of UCLA on the construction of the CO laser and the advice and support of M. Braunstein, Assistant Manager, Chemical Physics Department, Hughes Research Laboratories. We would also like to thank J. Pappis and P. Miles of Raytheon and R. Pastor of Hughes Research Laboratories for furnishing samples and data.

Table I. Absorption Results

Sample	Length (cm)	Absorption (cm^{-1})		Scattering[b]	Surface Treatment	Comments
		Bulk	Surface Plus Bulk			
KCl B 55	16.25	2.1×10^{-5}	3.0×10^{-5}	1.5×10^{-6}[a]	Etched	Some contamination of surface when Ag mirrors applied
KCl B 62-B	13.49					Impossible to distinguish surface and bulk
			$<2 \times 10^{-6}$	none	Etched	See Fig. 6 for actual curve, 1 μV scale, ambient temperature not stable.
KCl B 166 (1.75% RbCl)	12.90	1.6×10^{-5}	2.0×10^{-5}	9.0×10^{-7}	Polished	Difficult to distinguish surface and bulk
KCl B156-5 (1.75% RbCl) P.F.	8.50		5.5×10^{-5}	4.8×10^{-6}[a]	Polished	Bulk scattering (middle thermocouple) > Surface scattering (entrance thermocouple)
ZnSe 1-23 (Raytheon)	21.25		9.5×10^{-4}	7.2×10^{-6}	Etch-polish	Surface scattering (entrance thermocouple) = 3 x bulk scattering (middle thermocouple)
CaF_2 VHP-614 (Raytheon)	6.955		9.0×10^{-4}	2.3×10^{-6}	As received	Some scratches on surfaces from cutting; one rough edge
CaF_2 H 2888-03-a	4.991		5.9×10^{-4}	8.1×10^{-6}	Polished	Slight wedge and large crack on one side of boule
SrF_2 H 1773-44	6.357		1.7×10^{-3}	1.7×10^{-6}[a]	Polished	Early boule

[a] These samples were run with deposited Ag mirrors under the thermocouples.

[b] Relative to transmitted power at center thermocouple.

T2060

Table II. Predicted Wavelength Dependence of Absorption Coefficients of CaF_2

Wavelength (μm)	$\beta \times 10^4$ (cm^{-1}) (Deutsch)	$\beta \times 10^4$ (cm^{-1})	
5.2	1.26		
5.25	1.53	5.4[a,b]	3.2
5.3	1.86		
5.4	2.70		
5.41	2.80	9.8	5.9[a,c]
5.5	3.8		
5.6	5.5		

[a]Experimental value.

[b]Raytheon (1976).

[c]HRL (1976).

T2061

References

1. T. F. Deutsch, J. Electronic Materials 4, 663 (1975).

2. M. Hass, J. W. Davisson, H. B. Rosenstock, and J. Babiskin, Appl. Opt. 14, 1128 (1975).

4. P. Kraaty and P. J. Mendoza, Proc. of the Fourth Annual Conf. on IR Laser Window Materials, Tucson, Jan. 1975, p. 213.

5. H. S. Carslaw and J. C. Jaeger, Conduction of Heat in Solids, 2nd Edition (Oxford Univ. Press, London, 1959).

6. P. Miles, Raytheon Corporation, personal communication.

7. T. F. Deutsch, J. Phys. Chem. Solids 34, 2091 (1973).

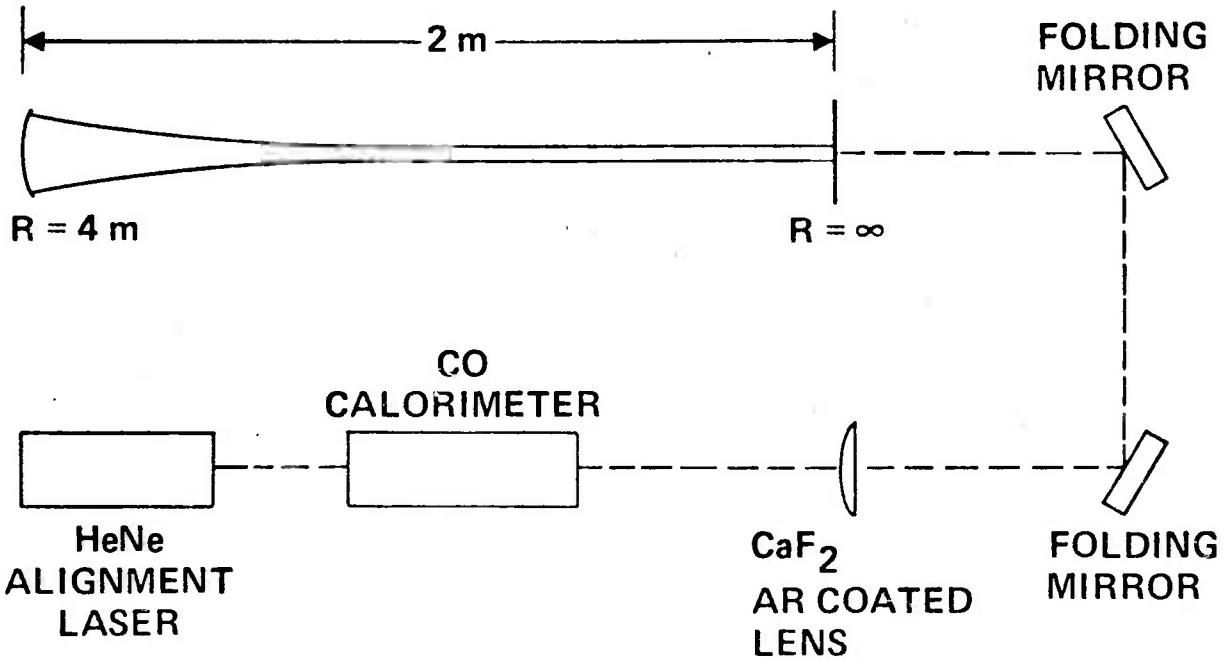

Fig. 1. Optical train of the CO laser calorimeter.

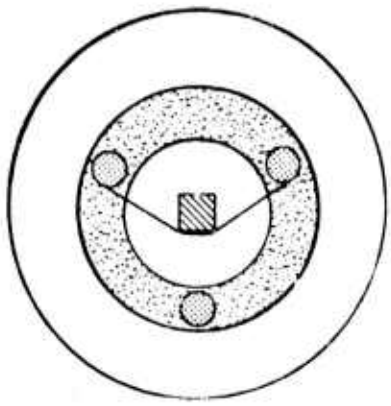

CROSS SECTION
THROUGH SAMPLE HOLDER
SHOWING BAR SUSPENSION

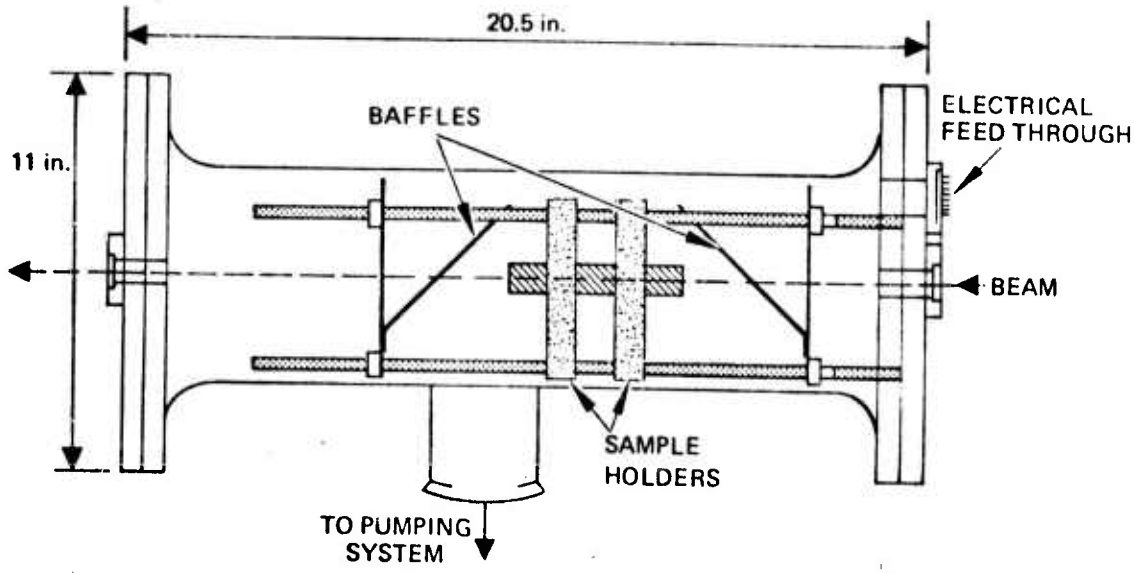

Figure 2a. CO laser calorimeter and sample mount.

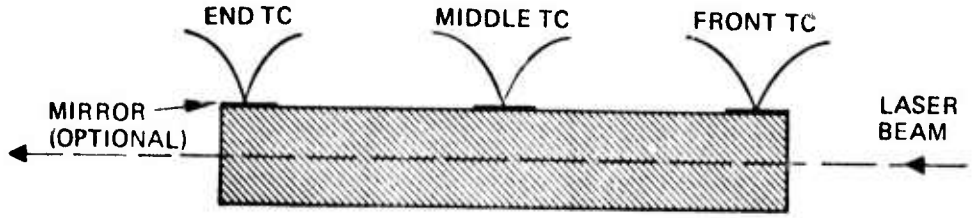

2b. TC placement on sample.

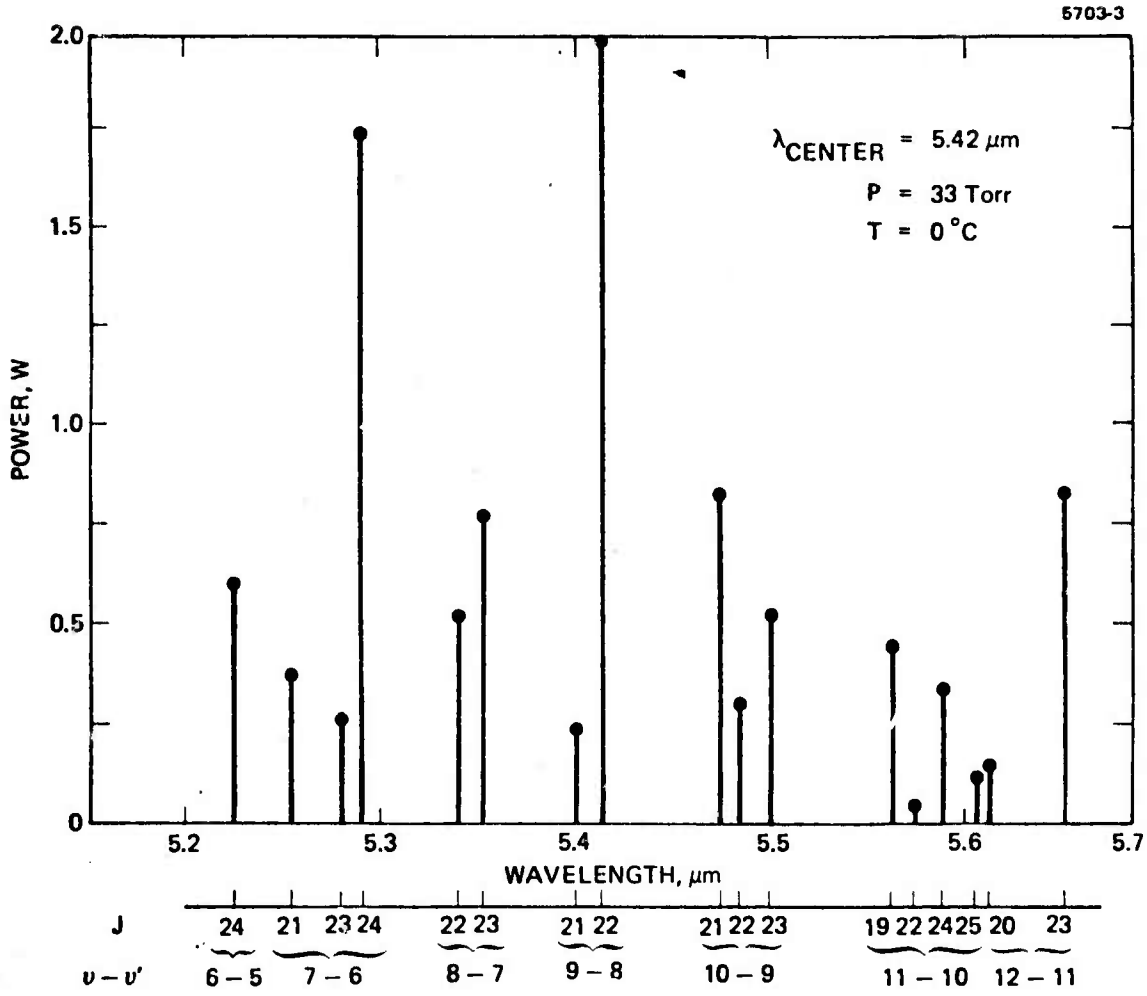

Fig. 3. Sample spectral power distribution of 0° C CO laser.

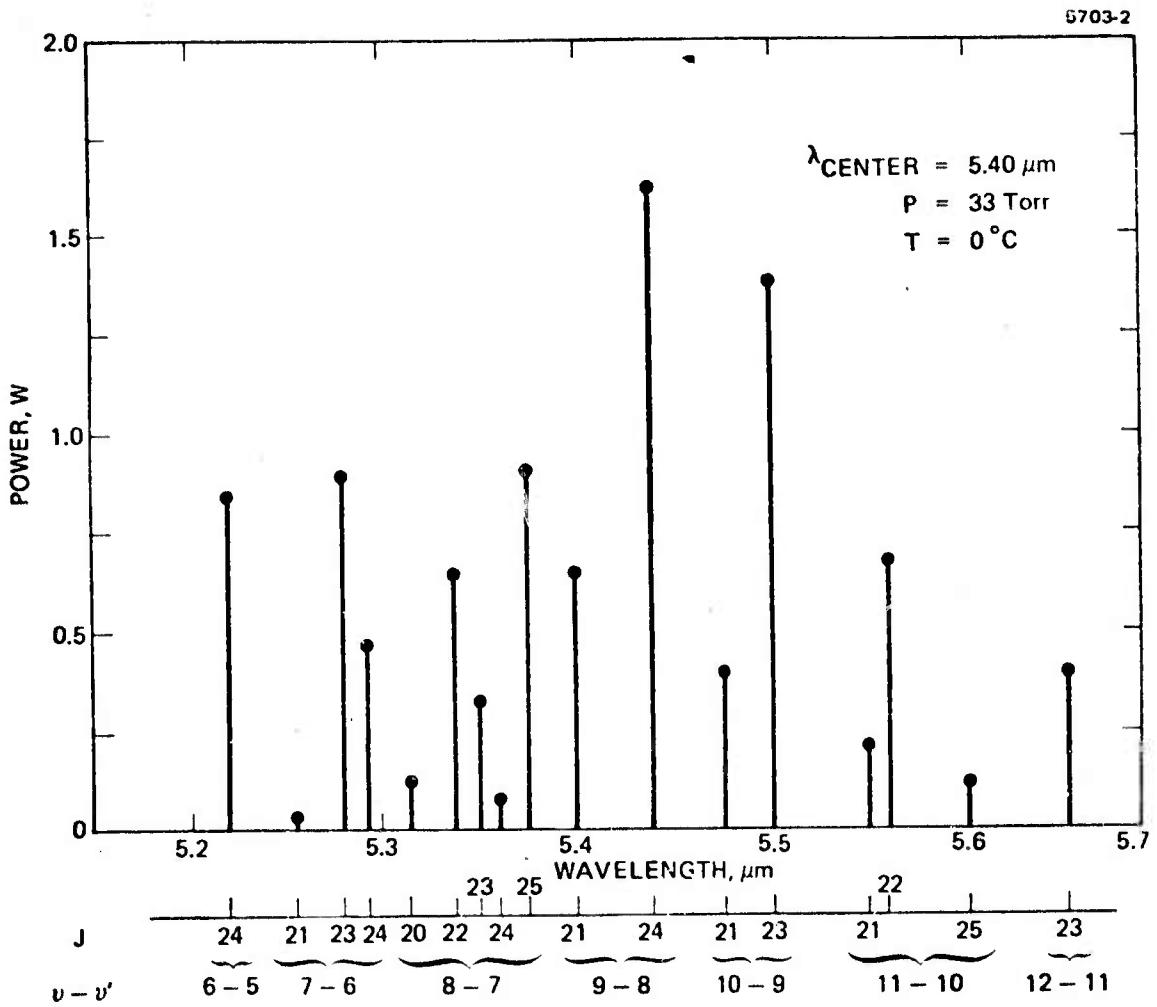

Fig. 4. Sample spectral power distribution of 0° C CO laser.

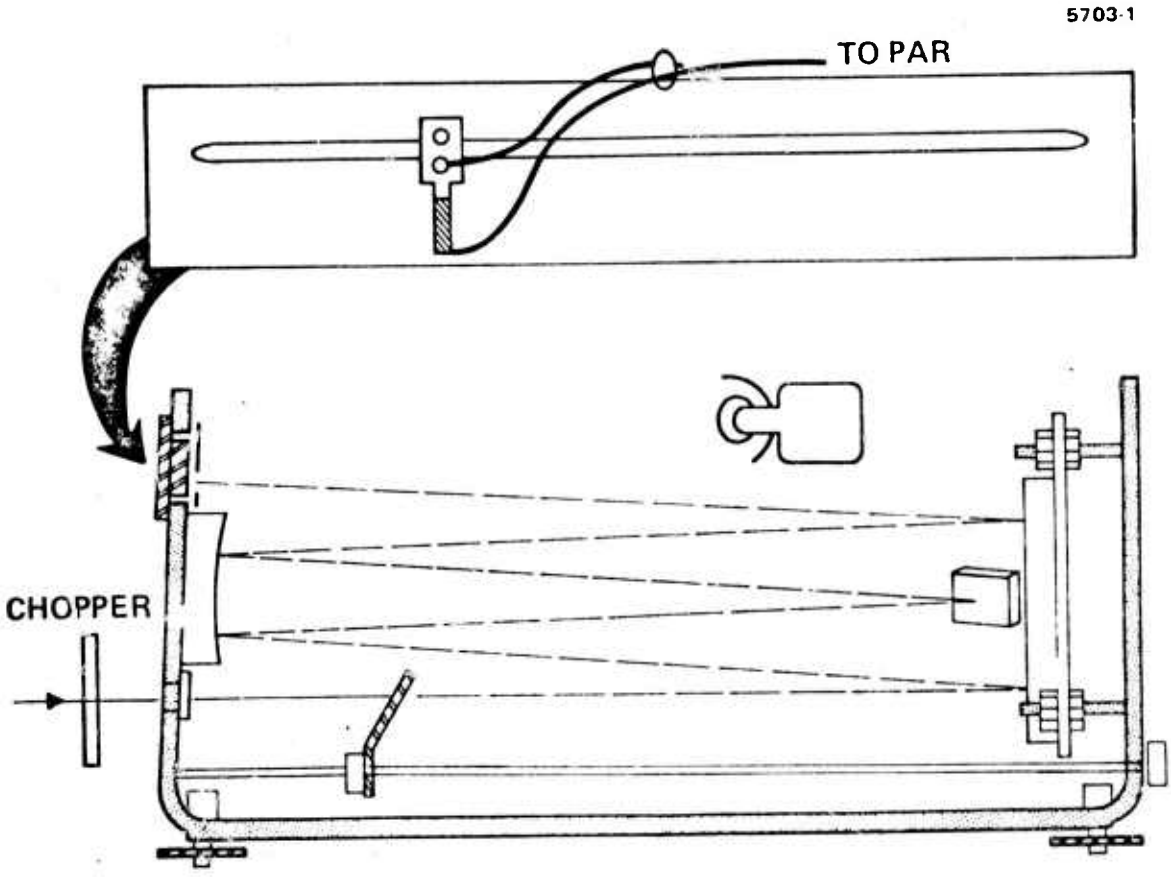

Fig. 5. Optical Engineering CO_2 Spectrum Analyzer with slit-shaped pyroelectric detector and chopper.

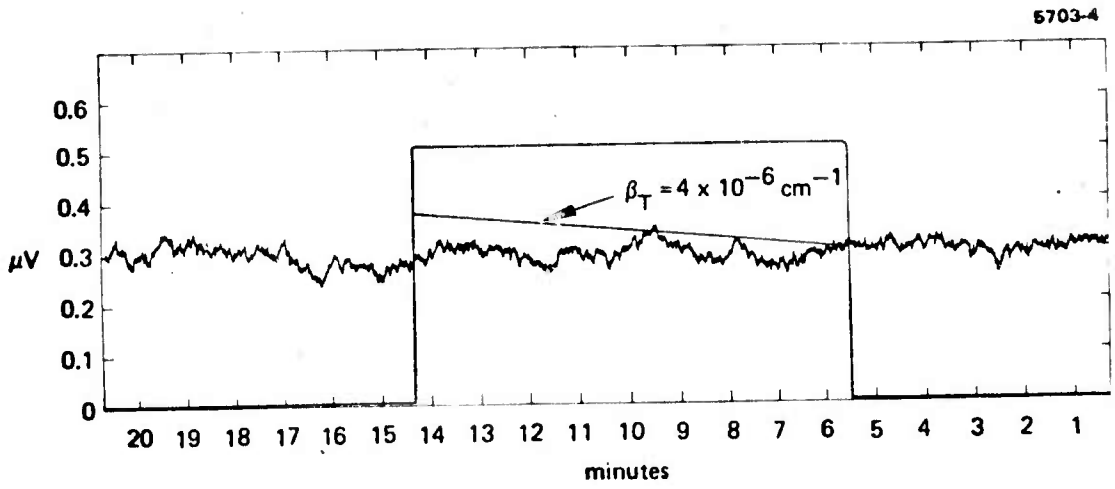

Figure 6. Sample CO calorimeter curve for KC1 B62–B.

LIST OF FIGURE CAPTIONS

Fig. 1. Optical train of the CO laser calorimeter.

Fig. 2. CO laser calorimeter.

Fig. 3. Sample spectral power distribution of 0° C CO laser.

Fig. 4. Sample spectral power distribution of 0° C CO laser.

Fig. 5. Optical Engineering CO_2 Spectrum Analyzer with slit-shaped pyroelectric detector and chopper.

Fig. 6. Sample CO calorimeter curve for KCl B62-B.

APPENDIX B

A NEW TECHNIQUE FOR MEASURING THE INFRARED ABSORPTION IN THIN FILM COATINGS

James A. Harrington, Morris Braunstein,
and J. Earl Rudisill

Hughes Research Laboratories
Malibu, California 90265

ABSTRACT

Traditionally, the optical absorption in thin dielectric films has been obtained by comparing the absorption in coated and uncoated substrates. A new technique has been developed in which the absorption of the film is obtained directly without resorting to comparison or difference methods. This method relies on the separation of surface and bulk heat that results from laser calorimetric measurements on long, bar-shaped samples. Single layer films of As_2S_3, CaF_2, ThF_4, and PbF_2 were deposited on a KCl bar and the absorption coefficient of each film was extracted from the slopes of the temperature-time curves.

I. INTRODUCTION

Low loss, thin dielectric films are often required as antireflection and enhanced reflection coatings at the common infrared laser wavelengths. In order to reduce the losses in films it is necessary to study the optical absorption in the films themselves. Traditionally, this absorption has most often been obtained by making laser calorimetric measurements of the absorption in the coated and uncoated substrate and then comparing these two values. For some of the low loss films currently produced, however, this comparison method can lead to spurious results owing to the difficulty in extracting meaningful film absorption when coated and uncoated substrate absorption coefficients are nearly identical. In order to circumvent these problems inherent in any difference or comparison method, a new technique, which relies on the separation of surface and bulk absorption in long, bar-shaped samples, has been exploited to directly obtain the absorption coefficient in the film.

M. Hass, et al.[1] and H. Rosenstock, et al.[2,3] have shown that it is possible to separate surface and bulk contributions to the total absorption by making laser calorimetric measurements on long, bar-shaped samples. This separation occurs because the transit time for surface heat to travel down a long rod is greater than the transit time for bulk heat. Measurements of temperature-time

curves obtained from thermocouples placed at strategic positions along the length of a bar can, therefore, yield values of the surface absorption alone.[2]

The absorption may be measured in a thin film by a simple extension of this long-bar technique to films deposited on long, low-loss bars. Fig. 1 is a schematic representation of what one would ideally expect from laser calorimetric studies on a long bar with a thin film on one end. The temperature-time curves that would be expected from thermocouples placed at the front (nearest the film), middle, and back of the sample are shown in the lower half of the figure.

The front thermocouple should sense a strong, essentially instantaneous temperature rise when the laser is turned on owing to the proximity of the thermocouple to the high (relative to the bulk) absorption of the film. This temperature rise will also include the effect of scattered light, as well as, after some delay, the absorption arising from the bulk material. These contributions, however, should be small and, for the bulk absorption, calculable from the other temperature-time curves. In principle, therefore, the film absorption β_F can be extracted from this curve.

The middle thermocouple will most often, after a small initial jump due to scattered light, exhibit two distinct slopes in the heating curve. The first slope is a measure of the bulk absorption coefficient β_B because this portion of the heating curve is essentially only sensitive to heat arriving at the thermocouple from the beam axis. After a characteristic time τ_1, which is given approximately by $\tau_1 \sim (L/2)^2/6\kappa$, where L is the length of the bar and κ the thermal diffusivity of the material,[2] heat from the film and from the uncoated surface arrive at the thermocouple. These contributions along with the bulk heat combine to give the second slope from which β_F and the uncoated surface absorption β_S can, in principle, be calculated. After the laser is turned off, a small, sharp dip should be observed due to the decrease in scattered light and then a slow increase and decrease in temperature as the bar thermalizes.

The back thermocouple will also exhibit a rapid temperature rise due to scattered light and surface heat from the uncoated surface. Following this, a bulk absorption region occurs which is analogous to

the first slope produced at the middle thermocouple. After a characteristic time $\tau_2 \sim (L^2)/6\kappa$, the heat from the film at the far end of the sample arrives at the thermocouple and combines with the bulk heat to produce the second slope. In principle, the uncoated surface heat also contributes to the first and second slopes but in practice, as discussed in the results in Sec. III, this heat is small and is balanced by heat losses.

In order for this technique to be successful it is obvious that one would like to have all β's be negligible compared to β_F. We have chosen a very low-loss KCl bar for our measurements of β_F in a variety of thin films. In these measurements the film is the dominant absorber and the trends indicated in Fig. 1 are born out in practice. (cf Sec. III).

II. EXPERIMENTAL METHODS

The absorption coefficients in film-bar combinations were measured using a conventional, vacuum calorimeter and a CO laser delivering approximately 5 watts of cw power. The bars were suspended by fine threads kept away from the thermocouples in an

arrangement similar to that used by Pinnow and Rich.[4] The thermocouples used were 5 mil, copper-constantan with enamel insulation. In order to reduce the amount of light scattered directly into the thermocouple, silver films were evaporated on the bar and then the thermocouples were placed on top of the silver spots. This method greatly reduced the scattered light which tended at times to be rather intense due to scattering by the thin film on one end. During some of the latter measurements, the bars were silvered along one whole side or the entire bar, except for the ends, was silvered. This also greatly reduced scattered light without effecting the heat transport.

The KCl bar chosen for the measurements at 5.3 μm was RAP grown, single crystal material prepared by this laboratory. Bulk absorption in this bar was found to be particularly low as may be seen from the β_B values listed in Table 1. The value at 10.6 μm is intrinsic[5] while those at the chemical laser wavelengths, although not intrinsic, are quite low when compared to most materials studied at the DF(3.8 μm) and HF(2.7 μm) wavelengths.[6] The dimensions of the bar were 2 x 2 x 13 cm which, as discussed in Sec. I,

provided surface heat transit times of approximately 2.5 and 10.1 min for heat to travel from the film to the middle or back thermocouples, respectively. Therefore, this bar of KCl, which exhibited a low bulk absorption and had a favorable aspect ratio for separation of surface and bulk heat, was well suited as a substrate for studying absorption in thin films by these calorimetric techniques.

Thin films evaporated on one end of the bar had optical thicknesses of $\lambda/2$ at 5.3 μm. The fractional power βL absorbed by the films was obtained directly from the temperature-time curves, using a three-slope calculation.[7] Using this fractional power, the absorption index k, defined by $N=n-ik$ where N is the complex index of refraction, is computed for the film.[8] Finally, β_F is obtained from $k = \frac{\beta\lambda}{4\pi}$.

III. RESULTS AND DISCUSSION

Four different materials were used for single layer thin film coatings. These materials, which are listed in Table II, are common constituents of multilayer stacks used as antireflection and enhanced reflection coatings. The temperature-time curves for

one of these films, PbF_2, on the KCl bar are shown in Fig. 2. Three thermocouples situated at the front (1), middle (2), and back (3) of the bar were employed in an attempt to obtain heating curves similar to those indicated in Fig. 1.

The front thermocouple nearest the PbF_2 film clearly displays the rapid temperature rise expected from its position near a hot film. A preliminary attempt has been made to extract β_F from this data by fitting the curve to a solution of the heat flow equation. At the present time, however, a successful fit has not been achieved. This is due, in part, to the neglect of scattered light and to the finite response time of the thermocouple. Work is continuing to fit all the temperature-time curves and therefore no β_F has been obtained from the front thermocouple.

The middle thermocouple exhibits the two slope behavior characteristic of bulk (first slope) and bulk plus surface (second slope) heating. After an initial jump lasting about 45 sec, (due to scattered light), an essentially flat temperature response occurs up to 3.5 min. This bulk slope, which is not measurable on this temperature scale, indicates

negligible bulk absorption and, thus, for purposes of calculation of β_F from the second slope, we can assume $\beta_B \approx 0$. The second slope, which begins after the characteristic surface heat transit time τ_1 of 2.5 min., is a combination of $\beta_B + \beta_F + \beta_S$ or for this case $\beta_F + \beta_S$ since $\beta_B \approx o$. A calculation of the fractional power absorbed using this slope yields

$$(\beta_F + \beta_S)L = 3.1 \times 10^{-3}.$$

The back thermocouple response shown in Fig. 2 displays a heating curve with a strong, rapid temperature rise due to surface heat from the uncoated surface. The amount of this surface heat has varied from sample to sample with this particular film-bar combination exhibiting the largest amount of uncoated surface heat. The bulk heating regime then follows for about 6 min. This is shorter than the characteristic 10.1 min film heat transit time τ_2. The reason for this is that heat losses and the magnitude of surface heat compared to bulk heat influence the onset of the bulk-plus-surface second slope. In an exact calculation these transit times are correctly predicted and thus τ_1 and τ_2 as calculated from $\tau \sim (L)^2/6\kappa$

should only be considered as an approximate indication of the film heat transit time.[2] The flat bulk heating regime contains the uncoated surface heat plus the bulk heat. Since this slope is essentially zero, we can assume that β_B is negligible at least in comparison to the second slope which contains β_F. Thus, in agreement with bulk absorption obtained from the middle thermocouple, we assume $\beta_B \approx 0$. It is also obvious from Fig. 2 that the surface heat from the uncoated surface is balanced by the heat losses beyond the first minute and therefore one can also assume for purposes of the calorimetric calculation using the second slope and the back thermocouple that $\beta_S \approx 0$.

The final (second)slope of the back thermocouple represents $\beta_F + \beta_B + \beta_S$ which, in view of the above approximation, reduces to only β_F. The calculation of the fractional power absorbed using this slope yields

$$\beta_F L = 0.9 \times 10^{-3}.$$

This is seen to be less than the fractional power absorbed obtained from the second slope of the middle thermocouple as expected.

A summary of the results for β_F of all films studied appears in Table 2. From the data in this table it can be seen that the middle and back thermocouples sometimes yield the same fractional power (CaF_2) while at other times they yield different values (PbF_2). This implies that the CaF_2 film-bar combination had a β_S that was essentially negligible while the PbF_2 film-bar combination happened to have a β_S that was significant. This discrepancy is due to surface contamination of the uncoated end.

IV. CONCLUSIONS

The film-bar technique described in this paper has enabled us to directly obtain the absorption coefficient of a thin dielectric film deposited on a long-rod shaped substrate. The success of this method depends both on having a good quality bar substrate (ideally $\beta_B \approx \beta_S \approx 0$) and on careful calorimetric techniques in order to effect easy separation of bulk and surface heating. When these conditions are met, the values of β_F can be easily calculated directly from the heating curves and thus the necessity of comparing coated and uncoated substrate β's to obtain

β_F is eliminated. The β_F's listed in Table 2 indicate that the method is at least as sensitive as the older comparison method although the ultimate sensitivity has not been tested since these absorption coefficients do not represent the lowest values for transparent coatings.

It should also be possible to adapt this technique to the measurement of the absorption and reflectivity of highly reflecting films. Since the bar in these experiments is merely acting as a heat pipe for surface heat, an enhanced dielectric reflector facing the laser beam would radiate surface heat down the rod in a manner analogous to a transparent film and thus similar calculations of film absorption could be made.

ACKNOWLEDGMENTS

The authors are grateful to J. Bowers and B. Garcia for their assistance in depositing the dielectric and silver films. This work has been supported by the Office of Naval Research and the Defense Advanced Research Projects Agency; DARPA support monitored by RADC/ETSO Hanscom Air Force Base, Massachusetts, 07131.

REFERENCES

1. M. Hass, J.W. Davisson, H.B. Rosenstock, J.A. Slinkman, and J. Babiskin, in Optical Properties of Highly Transparent Solids, S.S. Mitra and B. Bendow, Eds. (Plenum, New York, 1975).

2. H.B. Rosenstock, M. Hass, D.A. Gregory, and J.A. Harrington, Appl. Opt., [this issue-add specifics].

3. H.B. Rosenstock, D.A. Gregory, and J.A. Harrington, Appl. Opt. 15, 2075 (1976).

4. D.A. Pinnow and T.C. Rich, Appl. Opt. 12, 984 (1973).

5. T.F. Deutsch, J.Electron. Mater. 4, 663 (1975).

6. J.A. Harrington, D.A. Gregory, and W.F. Otto, Jr., Appl. Opt. 15, 1953 (1976).

7. M. Hass, J.W. Davisson, P.H. Klein, and L.L. Boyer, J. Appl. Phys. 45, 3959 (1974).

8. P.P. Burning in Physics of Thin Films, Vol. 1, Academic, New York, NY 1963.

TABLE I - Bulk Absorption Coefficients for RAP-grown KCl Bar at Infrared Laser Wavelengths.

$\lambda(\mu m)$	$\beta_B(cm^{-1})$
10.6	7×10^{-5}
5.3	$\sim 5 \times 10^{-6}$
3.8	6×10^{-5}
2.7	7×10^{-5}

TABLE 2 - Absorption Coe .icients of Single Layer Films on KCl Bar. Film Thickness is $\lambda/2$ at 5.3 μm and $\bar{\beta}L$ is the Average Fractional Power Absorbed.

Film	$\bar{\beta}L$ Middle TC	$\bar{\beta}L$ Back TC	k	$\beta_F(cm^{-1})$
AS_2S_3	5.6×10^{-4}	--	2.0×10^{-4}	4.7
CaF_2	1.5×10^{-3}	1.5×10^{-3}	3.1×10^{-4}	7.3
ThF_4	1.6×10^{-3}	1.1×10^{-3}	4.0×10^{-4}	9.5
PbF_2	3.1×10^{-3}	0.9×10^{-3}	2.5×10^{-4}	5.9

FIGURE CAPTIONS

Figure 1 - Schematic representation of temperature time curves expected from different thermocouple positions on a KCl bar.

Figure 2 - Calorimetric data PbF_2 film on KCl bar for front (1), middle (2), and back (3) thermocouples. Ordinate scale is the same for each temperature-time curve.

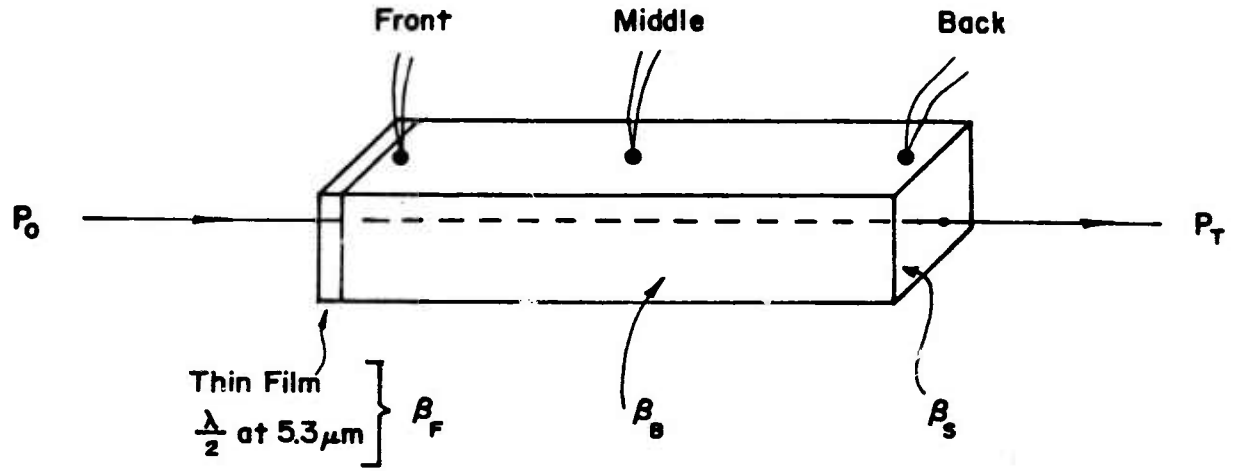
Front
Middle
Back
P_0
P_T
Thin Film
$\frac{\lambda}{2}$ at 5.3μm
β_F
β_B
β_S

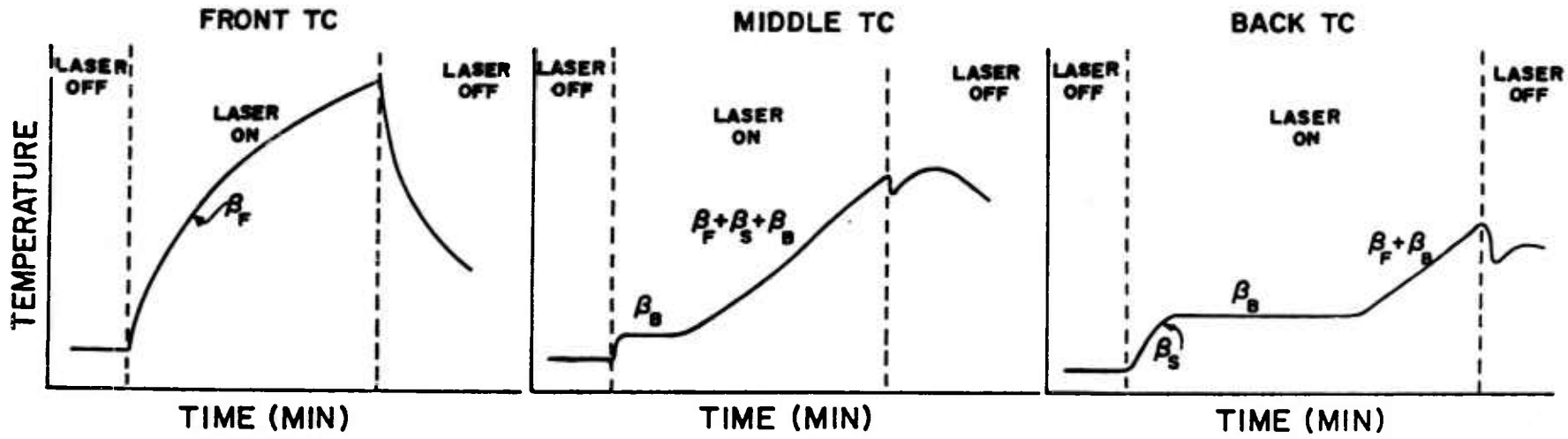
FRONT TC
MIDDLE TC
BACK TC
TEMPERATURE
LASER OFF
LASER ON
LASER OFF
β_F
β_B
$\beta_F+\beta_S+\beta_B$
β_S
$\beta_F+\beta_B$
TIME (MIN)
TIME (MIN)
TIME (MIN)

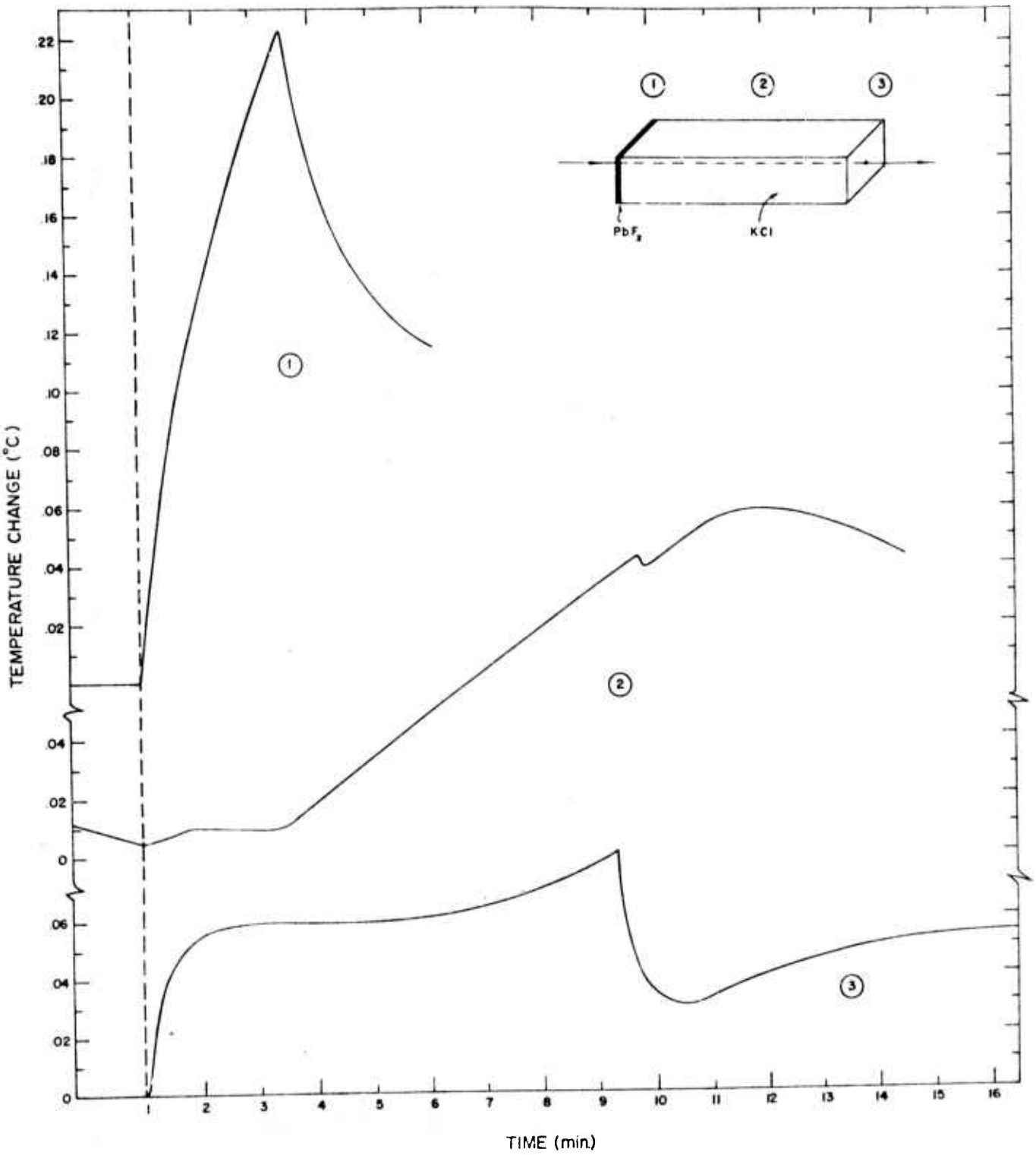
TEMPERATURE CHANGE (°C)
TIME (min)
1
2
3
PbF2
KCl

METRIC SYSTEM

BASE UNITS:

Quantity	Unit	SI Symbol	Formula
length	metre	m	...
mass	kilogram	kg	...
time	second	s	...
electric current	ampere	A	...
thermodynamic temperature	kelvin	K	...
amount of substance	mole	mol	...
luminous intensity	candela	cd	...

SUPPLEMENTARY UNITS:

plane angle	radian	rad	...
solid angle	steradian	sr	...

DERIVED UNITS:

Acceleration	metre per second squared	...	m/s
activity (of a radioactive source)	disintegration per second	...	(disintegration)/s
angular acceleration	radian per second squared	...	rad/s
angular velocity	radian per second	...	rad/s
area	square metre	...	m
density	kilogram per cubic metre	...	kg/m
electric capacitance	farad	F	A·s/V
electrical conductance	siemens	S	A/V
electric field strength	volt per metre	...	V/m
electric inductance	henry	H	V·s/A
electric potential difference	volt	V	W/A
electric resistance	ohm		V/A
electromotive force	volt	V	W/A
energy	joule	J	N·m
entropy	joule per kelvin	...	J/K
force	newton	N	kg·m/s
frequency	hertz	Hz	(cycle)/s
illuminance	lux	lx	lm/m
luminance	candela per square metre	...	cd/m
luminous flux	lumen	lm	cd·sr
magnetic field strength	ampere per metre	...	A/m
magnetic flux	weber	Wb	V·s
magnetic flux density	tesla	T	Wb/m
magnetomotive force	ampere	A	...
power	watt	W	J/s
pressure	pascal	Pa	N/m
quantity of electricity	coulomb	C	A·s
quantity of heat	joule	J	N·m
radiant intensity	watt per steradian	...	W/sr
specific heat	joule per kilogram-kelvin	...	J/kg·K
stress	pascal	Pa	N/m
thermal conductivity	watt per metre-kelvin	...	W/m·K
velocity	metre per second	...	m/s
viscosity, dynamic	pascal-second	...	Pa·s
viscosity, kinematic	square metre per second	...	m/s
voltage	volt	V	W/A
volume	cubic metre	...	m
wavenumber	reciprocal metre	...	(wave)/m
work	joule	J	N·m

SI PREFIXES:

Multiplication Factor	Prefix	SI Symbol
1 000 000 000 000 = 10^{12}	tera	T
1 000 000 000 = 10^{9}	giga	G
1 000 000 = 10^{6}	mega	M
1 000 = 10^{3}	kilo	k
100 = 10^{2}	hecto*	h
10 = 10^{1}	deka*	da
0.1 = 10^{-1}	deci*	d
0.01 = 10^{-2}	centi*	c
0.001 = 10^{-3}	milli	m
0.000 001 = 10^{-6}	micro	μ
0.000 000 001 = 10^{-9}	nano	n
0.000 000 000 001 = 10^{-12}	pico	p
0.000 000 000 000 001 = 10^{-15}	femto	f
0.000 000 000 000 000 001 = 10^{-18}	atto	a

* To be avoided where possible.

MISSION
of
Rome Air Development Center

RADC plans and conducts research, exploratory and advanced development programs in command, control, and communications (C^3) activities, and in the C^3 areas of information sciences and intelligence. The principal technical mission areas are communications, electromagnetic guidance and control, surveillance of ground and aerospace objects, intelligence data collection and handling, information system technology, ionospheric propagation, solid state sciences, microwave physics and electronic reliability, maintainability and compatibility.

Printed by
United States Air Force
Hanscom AFB, Mass. 01731